UNIVERSITY OF CRETE

Departments of Mathematics & Applied Mathematics

VARIATION OF ACOUSTIC ARRIVAL PATTERNS IN THE TIME DOMAIN DUE TO SOUND-SPEED PERTURBATIONS

Author: George Piperakis

Supervisor: Emmanuel Skarsoulis

Readers: Emmanuel Skarsoulis, George Makrakis,
Michael Taroudakis

SUBMITTED IN PARTIAL FULFILLMENT OF THE REQUIREMENTS FOR THE DEGREE
OF MASTER OF SCIENCE AT UNIVERSITY OF CRETE, HERAKLION
FEBRUARY 2005

To Hara and my children.

Table of Contents

Abstract

The feasibility and efficiency of inversions in ocean acoustic travel-time tomography critically relies on the ability to accurately model and predict the reception of an acoustic source at a distant receiver in the time domain (arrival pattern), as well as its perturbations due to changes in the sound-speed distribution. The present work introduces an approximation method for wave-theoretic arrival-pattern predictions in general range-dependent ocean environments based on Born and Rytov approximations of the second order. The range-dependent ocean environment is considered as a perturbation of a range-independent reference state, for which the acoustic field of a point source in the frequency domain, i.e. the Greens function, is modelled using normal-mode theory. Then using the Born and Rytov approximations the perturbed Greens function, corresponding to the perturbed ocean environment, is expressed in terms of the unperturbed Greens function and the medium (sound-speed) perturbation for each frequency within the source bandwidth. Using the normal-mode representation for the unperturbed Greens function, closed-form expressions for the first and second Born and Rytov approximations are derived, generalizing previous results for Green's function perturbations in range-independent environments, and indicating that the effects of range dependence on the acoustic field in the time domain are of second order. To cope with the multi-modal nature of ocean acoustic propagation, a variation of the standard Rytov method is applied, proposed by J. Keller, according to which the Rytov approximation is applied to each modal component independently. Having calculated the perturbed Greens function in the frequency domain, the corresponding arrival pattern in the time domain is obtained through

the inverse Fourier transform. A number of numerical examples demonstrate an advantage of the Rytov approximation (over the Born approximation) for time-domain and arrival-time calculations.

Acknowledgements

The author would like to thank his supervisor, Emmanuel Skarsoulis, Research Director at the Institute of Applied and Computational Mathematics, Foundation for Research and Technology Hellas, for his support to this work.

Also he would like to thank George Makrakis, Associate Professor at the Department of Applied Mathematics, University of Crete, and Michael Taroudakis, Associate Professor at the Department of Mathematics, University of Crete, for their advice.

This work was carried out at the Institute of Applied and Computational Mathematics, Foundation for Research and Technology – Hellas. In this connection the author would like to thank Professor J. Papadakis and Professor V. Dougalis, former and present Director of IACM, respectively, for the permission to join the postgraduate program as well as for the facilities made available for the completion of this work.

Introduction

The problem of ocean acoustic tomography is to infer from precise measurements of travel time, or other properties of acoustic propagation, the state of the ocean traversed by a sound field [41]. Tomography takes advantage of two facts: that the speed of sound is a function of temperature, and that the ocean is virtually transparent to low-frequency sound, so that signals can be transmitted over distances of thousands of kilometers.

The spatial variability of temperature (sound speed) in the ocean gives rise to refraction which in turn causes multi-path propagation. This means that there is a multitude of acoustic paths connecting a source with a distant receiver. Each path traverses different water masses with different temperature and sound-speed values. Thus a pulsed acoustic signal emitted by the source will reach the receiver at different time instants depending on the path it is travelling along. This leads to a sequence of arrivals at the receiver in the time domain conveying information about different water layers.

Ocean acoustic travel-time tomography was introduced by Munk and Wunsch [37], as a remote-sensing technique for monitoring the ocean interior over large sea areas using low-frequency sound waves. Measuring the travel times of pulsed acoustic signals propagating through the water mass over different paths, and exploiting the knowledge about how travel times are affected by the sound-speed (temperature) distribution in the water, the latter can be obtained by inversion.

For long-range acoustic transmissions in deep-water environments the early arrivals at the receiver can be sufficiently described using ray theory, in terms of individual acoustic rays (ray arrivals) which exhibit large deviations from the channel axis – steep rays [38]. The late arrival pattern, on the other hand, is the result of interference of a large number of near-axial (shallow) rays. In terms of normal-mode theory [2], late arrivals can be described by a few low-order modes, whereas early arrivals result from the interference of a large number of high-order modes [38]. Thus, a good strategy for arrival pattern calculations and modelling is to use ray theory for the early arrivals and normal-mode theory for the intermediate and late ones.

Even though the late arrival pattern can be represented by a few low-order modes, the identification of individual modes in the arrival pattern in the time domain (modal arrivals) is not always possible. The modes may interfere with each other, especially in cases of strong dispersion, and may give rise to complicated patterns with unstable arrivals which fade in and out as the environment undergoes small perturbations, such that individual modes cannot be associated with individual arrivals. A way to retrieve information about the modes in such cases is to perform mode filtering using a vertical receiving array [6], [23].

In cases where information about individual modes is difficult to extract from the late arrival pattern (e.g. cases of strong dispersion, absence of vertical array) full-field waveform inversion [5], [12], [11] could be an alternative for analysing tomography data. Nevertheless, waveform inversions are associated with a large number of forward calculations and thus with a heavy computational burden. Several methods have been proposed for accelerating the computation of arrival patterns, such as narrowband normal-mode approximations, relying on Taylor expansion of eigenvalues and eigenfunctions with respect to frequency [17], [26], [27], and frequency-interpolation methods associated with normal modes [1] and the parabolic approximation [15].

A waveform perturbation method is proposed here for the calculation of arrival patterns corresponding to ocean states in the vicinity of a background (reference) state. No approximation (expansion or interpolation) is performed with respect to frequency. Instead, a second-order approximation is used for the perturbation of the Green's function with respect to sound-speed perturbations at each frequency, based on the Rytov approximation [30], [36]. A waveform perturbation approach assuming a range-independent ocean environment, both background and perturbed, was introduced recently [28]. The present approach is general and applies to any kind of reference (background) and perturbed ocean environment, either range independent or range dependent.

Range-dependent features of the ocean such as internal waves [29], [33], [13], mesoscale eddies and large-scale variations [14], [32], [39], [40] can be considered as range-dependent perturbations of a range-independent background state. In this connection, the background state is considered in this work as range independent, such that the efficient normal-mode theory can be applied, whereas the perturbations are taken of a general range-dependent nature. For these range-dependent states the arrival pattern is obtained as a perturbation of the range-independent normal-mode prediction. This approximation offers a computationally efficient alternative to the cumbersome exact range-dependent calculations at each frequency, based on adiabatic/coupled modes or the parabolic approximation [8].

The contents of this work are organized as follows: Chapter 1 is an introduction to wave propagation theory. The time-domain wave equation and the frequency-domain Helmholtz equation as well as the boundary, interface and radiation conditions governing ocean acoustic propagation are introduced. Further, the Green's function of the ocean acoustic waveguide in the frequency domain, as well as the arrival pattern at the receiver in the time domain are introduced and interrelated. Chapter 2 deals

with perturbations of the Green's function caused by perturbations of the sound-speed distribution (medium perturbations). In particular, the first- and second-order Born and Rytov approximations of the perturbed Green's function, as well as the relations between the two approximations (Born and Rytov), are derived. The two approximations are closely related such that one can obtain the Rytov approximation it terms of the Born approximation and vice versa. In chapter 3 using the normal-mode representation for the background acoustic field closed-form expressions for the first and second Born and Rytov approximations are derived. Chapter 4 presents some numerical results from the application of the various approximations for the calculation of time-domain arrival patterns in range-dependent ocean environments, as well as comparisons with exact adiabatic and coupled mode results. Chapter 5 summarizes the main conclusions from this study.

Chapter 1

Wave Propagation Theory

1.1 The wave equation

The wave equation in an ideal fluid can be derived from hydrodynamics and the adiabatic relation between pressure and density [8]. The equations for conservation of mass, Euler's equation, and the adiabatic equation of state are respectively:

$$\begin{aligned} \frac{\partial \rho}{\partial t} + \nabla \cdot \rho \mathbf{v} &= 0, \\ \frac{\partial \mathbf{v}}{\partial t} + \mathbf{v} \cdot \nabla \mathbf{v} &= -\frac{1}{\rho} \nabla p, \\ p = p_0 + \rho' \left[\frac{\partial p}{\partial \rho}\right]_E &+ \frac{1}{2} (\rho')^2 \left[\frac{\partial^2 p}{\partial \rho^2}\right]_E + ... \end{aligned} \tag{1.1.1}$$

In the above equations, ρ is the density, $\mathbf{v}$ the particle velocity, p the pressure, and the subscript E denotes that the thermodynamic partial derivatives are taken at constant entropy. We use small perturbations for the pressure and density, $p = p_0 + p'$, $\rho = \rho_0 + \rho'$, and note that $\mathbf{v}$ is also small quantity. The speed of sound c for an ideal fluid is defined as

$$c^2 = \left[\frac{\partial p}{\partial \rho}\right]_E . \tag{1.1.2}$$

The linear approximations, which lead to the acoustic wave equation, involve retaining only first-order terms in the hydrodynamic equations. To lowest order, equations (1.1.1) become

$$\frac{\partial \rho'}{\partial t} = -\rho_0 \nabla \cdot \mathbf{v}, \tag{1.1.3}$$

$$\frac{\partial \mathbf{v}}{\partial t} = -\frac{1}{\rho_0} \nabla p', \tag{1.1.4}$$

$$p' = \rho' c^2. \tag{1.1.5}$$

Considering that the time scale of oceanographic changes is much longer than the time scale of acoustic propagation, we will assume that the material properties ρ_0 and c^2 are independent of time, take the partial derivative of (1.1.3) with respect to time and the divergence of (1.1.4), interchange the derivative operations and use (1.1.5) to obtain a wave equation for pressure:

$$\nabla^2 p' - \frac{1}{c^2} \frac{\partial^2 p'}{\partial t^2} = 0. \tag{1.1.6}$$

This is a hyperbolic partial differential equation for the pressure perturbation (acoustic pressure) p', and is known as the wave equation.

Sound is produced by natural or artificial phenomena through forced mass injection. Such forcing terms were neglected in the mass conservation equation (1.1.3), and therefore also in the derived wave equation. The consideration of such terms leads to the inhomogeneous wave equations

$$\nabla^2 p' - \frac{1}{c^2} \frac{\partial^2 p'}{\partial t^2} = f(\mathbf{x}, t), \tag{1.1.7}$$

where $\mathbf{x}$ represents the position vector and $f(\mathbf{x}, t)$ represents the volume injection as a function of space and time. In the above equations p' is considered as a function of $\mathbf{x}$ and t whereas c ia a function of $\mathbf{x}$. In the following the primes are omitted for convenience.

1.2 The Helmholtz equation

The wave equation involves four dimensions (three spatial and one temporal). By applying the Fourier transform to eq. (1.1.7) with respect to time we obtain a new partial differential equation

$$\nabla^2 P(\mathbf{x},\omega) + \frac{\omega^2}{c^2(\mathbf{x})} P(\mathbf{x},\omega) = F(\mathbf{x},\omega), \tag{1.2.1}$$

where $P(\mathbf{x},\omega)$ is the Fourier transform of the acoustic pressure

$$P(\mathbf{x},\omega) = \int_{-\infty}^{+\infty} p(\mathbf{x},t) e^{-j\omega t} dt,$$

and $F(\mathbf{x},\omega)$ the transform of the source term $f(\mathbf{x},t)$

$$F(\mathbf{x},\omega) = \int_{-\infty}^{+\infty} f(\mathbf{x},t) e^{-j\omega t} dt.$$

Equation (1.2.1) is known as the Helmholtz equation. It is a partial differential equation of elliptic type. A significant advantage of the Helmholtz equation over the wave equation is the lower dimensionality, the time variable t has been replaced by the parameter ω, the circular frequency. In this connection the majority of wave-theoretic solutions to the acoustic propagation problem are given in the frequency domain.

1.3 Boundary conditions

The ocean is bounded by the free surface and the sea bed. The top of the sea bed consists in general of a number of sediment layers followed by a harder subbottom. In order to obtain unique, physically meaningful solutions of the Helmholtz equation, we must in general impose constraints on the spatial behavior of the wave field, in the form of boundary, interface and radiation conditions.

a) Soft boundary

For a soft or pressure-release boundary S, such as the free surface, the acoustic pressure is assumed to vanish at all positions on the boundary (Dirichlet condition)

$$P(\mathbf{x},\omega) = 0 \quad \mathbf{x}\epsilon S.$$

b) Hard boundary

For a hard boundary S, such as a rigid bottom, the velocity of the acoustic field normal to the boundary vanishes at all positions on the boundary. By applying the Fourier transform to (1.1.4) we obtain $V = j(\omega\rho_0)^{-1}\nabla P$ and $V_n = j(\omega\rho_0)^{-1}\partial P \backslash \partial n$ where n measures distance normal to the boundary. Thus the hard boundary condition becomes (Neuman condition)

$$\frac{\partial P(\mathbf{x},\omega)}{\partial n} = 0 \quad \mathbf{x}\epsilon S.$$

c) Interface conditions

At the interface S between two fluid layers we must have continuity of pressure

$$P_+(\mathbf{x},\omega) = P_-(\mathbf{x},\omega) \quad \mathbf{x}\epsilon S,$$

where the subscript $(+)$ and $(-)$ indicates the two sides of the interface, as well as continuity of particle velocity normal to the interface which can be expressed in terms of the acoustic pressure as follows (see previous relation between velocity and pressure)

$$\frac{1}{\rho_{(+)}}\frac{\partial P_{(+)}}{\partial n} = \frac{1}{\rho_{(-)}}\frac{\partial P_{(-)}}{\partial n}.$$

d) Sommerfeld radiation condition

The Sommerfeld radiation condition [31] quantifies the notion stemming from our physical intuition that sources confined to a finite spatial domain produce outgoing,

radiating wave fields at infinity. Specifically, for homogeneous media $c = const.$ the radiation condition in d dimensions is expressed as

$$\lim_{r\to\infty} r^{\frac{d-1}{2}} \left[\frac{\partial P}{\partial r} + jkP\right] = 0, \tag{1.3.1}$$

where r is the distance from the location of the source, and $k = \omega/c$. The above condition leads to the following asymptotic behavior:

One dimension ($d = 1$):

$$P(r,k) \sim A(k)e^{-jkr}.$$

Two dimensions ($d = 2$):

$$P(r,k) \sim \frac{A(k)e^{-jkr}}{\sqrt{r}}.$$

Three dimensions ($d = 3$):

$$P(r,k) \sim \frac{A(k)e^{-jkr}}{r}.$$

1.4 The Green's function

Of particular importance for the solution of the inhomogeneous Helmholtz equation with arbitrary forcing F is the consideration of point sources represented by the Dirac delta function $\delta(\mathbf{x} - \mathbf{x}_s)$ where $\mathbf{x}_s$ is the source location. In Cartesian coordinates (x, y, z) this function becomes

$$\delta(\mathbf{x} - \mathbf{x}_s) = \delta(x - x_s)\,\delta(y - y_s)\,\delta(z - z_s),$$

whereas in cylindrical coordinates (r, z, θ) it takes the form [4]

$$\delta(\mathbf{x} - \mathbf{x}_s) = \frac{1}{2\pi r}\delta(r)\,\delta(z - z_s),$$

assuming that the point source lies on the z-axis at depth z_s.

The solution of the inhomogeneous Helmholtz equation with point source forcing supplemented by the boundary, interface and radiation conditions described in the previous section is called the Green's function of the acoustic waveguide and is denoted by $G(\mathbf{x}|\mathbf{x}_s)$

$$\left[\nabla^2 + k^2(\mathbf{x})\right] G(\mathbf{x}|\mathbf{x}_s) = -\delta(\mathbf{x} - \mathbf{x}_s), \tag{1.4.1}$$

where $k(\mathbf{x}) = \omega/c(\mathbf{x})$. Thus the Green's function describes the acoustic field of a harmonic point source located at $\mathbf{x}_s$.

If the Green's function of an acoustic waveguide is known, then the acoustic field of any arbitrary distributed source $F(\mathbf{x}, \omega)$ can be represented by the integral

$$P(\mathbf{x}, \omega) = -\iiint_V G(\mathbf{x}|\mathbf{x}')F(\mathbf{x}')dV(\mathbf{x}'), \tag{1.4.2}$$

where V spans the volume (support) of the distributed source F [24].

1.5 Arrival pattern

The acoustic pressure in the time domain can be obtained from the acoustic pressure in the frequency domain through the inverse Fourier transform

$$p(\mathbf{x}, t) = \frac{1}{2\pi} \int_{-\infty}^{+\infty} P(\mathbf{x}, \omega)e^{j\omega t}d\omega. \tag{1.5.1}$$

In ocean acoustic travel-time tomography we are interested in the acoustic pressure p_r at the receiver (location $\mathbf{x}_r$) in the time domain due to a point source at location $\mathbf{x}_s$. Exploiting the Green's function of the waveguide the pressure p_r can be written

$$p_r(t) = \frac{1}{2\pi} \int_{-\infty}^{+\infty} P_r(\omega)e^{j\omega t}d\omega = \frac{1}{2\pi} \int_{-\infty}^{+\infty} P_s(\omega)G(\mathbf{x}_r, \mathbf{x}_s; \omega)e^{j\omega t}d\omega, \tag{1.5.2}$$

where $P_s(\omega)$ denotes the signal emitted by the source in the frequency domain.

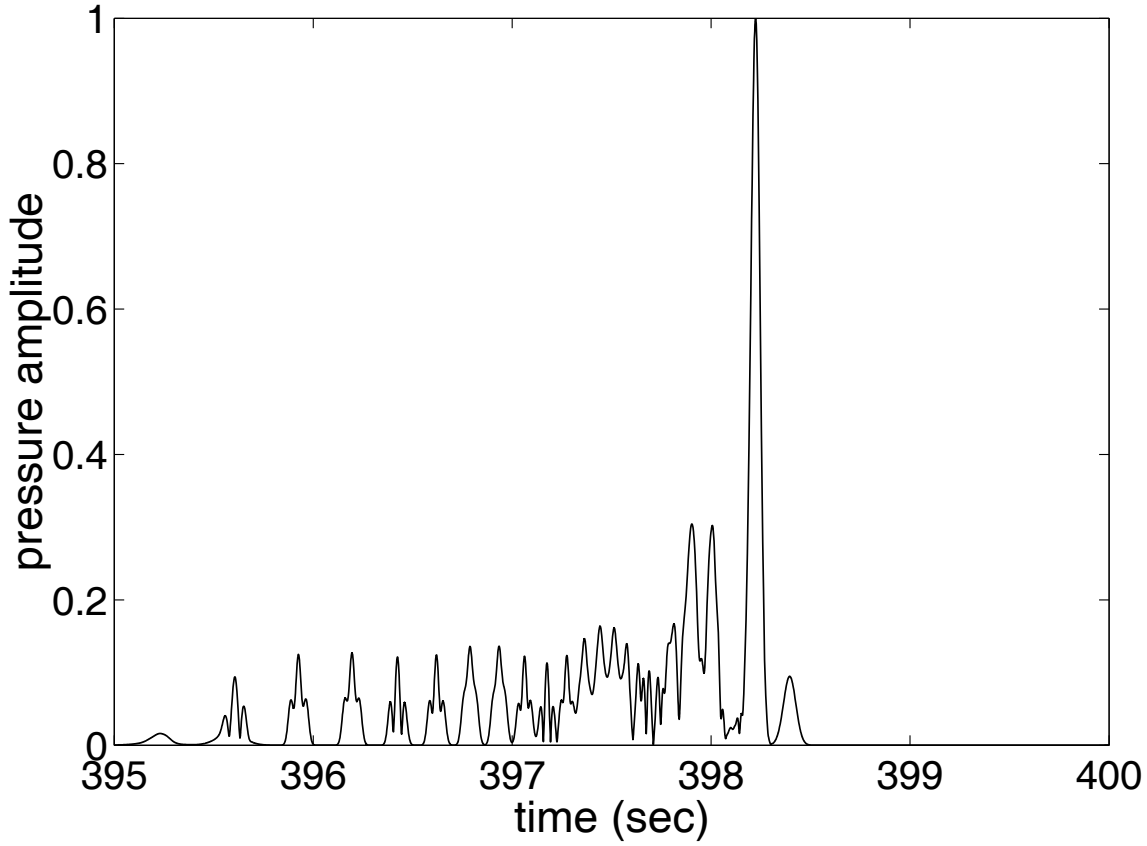

Figure 1.1: Arrival pattern.

The arrival pattern is defined as the absolute value of the complex pressure at the receiver in the time domain

$$\alpha(t) = |p_r(t)| \,.$$

Figure 1.1 shows an arrival pattern calculated 600 km away from a point source in a range-independent ocean environment characterized by a linear sound speed profile with water depth 2500 m and source/receiver depth 150 m. The different arrivals correspond to different acoustic paths sampling different water layers. Variations in the sound-speed (temperature) distribution will cause variations in the arrival times.

Tomography uses measurements of the latter and tries to infer on the underlying sound-speed (temperature) changes by applying inverse methods. The calculation of arrival patterns for general range-dependent environments is a heavy computational task since the range-dependent Green's function has to be evaluated for a large number of frequencies in order to evaluate the integral (1.5.2) by using the discrete Fourier transform (FFT) and avoid aliasing effects [21].

The present work proposes a computationally efficient method for the calculation of the arrival pattern, based on the Rytov approximation of the Green's function at each frequency assuming perturbations about a background ocean state. Thus only one set of exact calculations of the Green's function, those corresponding to the background state, are required. For all other ocean states (perturbations of the background state) the Green's function is obtained by the Rytov approximation formulas derived in the following chapters.

Chapter 2

Perturbations of the Green's function

In this chapter we will explore how small perturbations of the sound-speed distribution influence the Green's function.The Born and Rytov approximations are introduced relating the perturbations of the Green's function with the underlying sound-speed perturbations. There is a relation between the two approximations, in the sense that the terms of the Rytov approximation can be expressed through the corresponding terms of the Born approximation and vice versa.

2.1 First and second Born approximation

Let a background (reference) state be characterized by a sound-speed distribution $c_0(\mathbf{x})$ with corresponding Green's function $G_0(\mathbf{x}|\mathbf{x}_s)$ satisfying the inhomogeneous Helmholtz equation

$$\left[\nabla^2 + \frac{\omega^2}{c_0^2(\mathbf{x})}\right] G_0(\mathbf{x}|\mathbf{x}_s) = -\delta(\mathbf{x} - \mathbf{x}_s), \tag{2.1.1}$$

supplemented by the boundary, interface and radiation conditions described in section 1.3.

A small perturbation of the reference sound-speed by $\epsilon\Delta c$, where ϵ is a small parameter, will cause a perturbation ΔG in the Green's function. The perturbed Green's function $G = G_0 + \Delta G$ satisfies the inhomogeneous Helmholtz equation

$$\left[\nabla^2 + \frac{\omega^2}{[c_0(\mathbf{x}) + \epsilon\Delta c(\mathbf{x})]^2}\right][G_0(\mathbf{x}|\mathbf{x}_s) + \Delta G(\mathbf{x}|\mathbf{x}_s)] = -\delta(\mathbf{x} - \mathbf{x}_s), \tag{2.1.2}$$

and the same additional conditions as the unperturbed Green's function G_0. In the following we consider an expansion of the Green's function perturbation ΔG with respect to ϵ

$$\Delta G\left(\mathbf{x}|\mathbf{x}_s\right) = \epsilon\Delta G_1(\mathbf{x}|\mathbf{x}_s) + \epsilon^2\Delta G_2\left(\mathbf{x}|\mathbf{x}_s\right) + O\left(\epsilon^3\right). \tag{2.1.3}$$

By subtracting Eq. (2.1.1) from Eq. (2.1.2) and adding the term $\omega^2\Delta G/c^2$ to both sides, the following equation is obtained:

$$\left[\nabla^2 + \frac{\omega^2}{c_0^2(\mathbf{x})}\right]\Delta G(\mathbf{x}|\mathbf{x}_s) = -\left[\frac{\omega^2}{[c_0(\mathbf{x}) + \epsilon\Delta c(\mathbf{x})]^2} - \frac{\omega^2}{c_0^2(\mathbf{x})}\right][G_0(\mathbf{x}|\mathbf{x}_s) + \Delta G(\mathbf{x}|\mathbf{x}_s)]. \tag{2.1.4}$$

The perturbation ΔG satisfies the same boundary, interface and radiation conditions as the unperturbed Green's function G_0, whereas the operators on the left hand side of equations (2.1.1) and (2.1.4) are identical ($\nabla^2 + \omega^2/c_0^2$). In this connection, by considering the right-had side of Eq. (2.1.4), as a function of $\mathbf{x}$, to be a distributed source term, the integral representation (1.4.2) can be used to express the solution of (2.1.4) as follows

$$\begin{aligned}\Delta G(\mathbf{x}|\mathbf{x}_s) = \iiint_V G_0(\mathbf{x}|\mathbf{x}')\left[\frac{\omega^2}{[c_0(\mathbf{x}') + \epsilon\Delta c(\mathbf{x}')]^2} - \frac{\omega^2}{c_0^2(\mathbf{x}')}\right] \\ \times [G_0(\mathbf{x}'|\mathbf{x}_s) + \Delta G(\mathbf{x}'|\mathbf{x}_s)]\, dV(\mathbf{x}').\end{aligned} \tag{2.1.5}$$

This is an integral equation for the perturbation of the Green's function. Expanding the expression in brackets up to the second order with respect to ϵ

$$\frac{\omega^2}{[c_0 + \epsilon\Delta c]^2} - \frac{\omega^2}{c_0^2} = \omega^2\left(-\frac{2\epsilon}{c_0^3}\Delta c + \frac{3\epsilon^2}{c_0^4}\Delta c^2 + O\left(\epsilon^3\right)\right),$$

and using the expansion (2.1.3), eq. (2.1.5) can be written in the form (up to the second order):

$$\epsilon\Delta G_1(\mathbf{x}|\mathbf{x}_s) + \epsilon^2\Delta G_2\left(\mathbf{x}|\mathbf{x}_s\right) = \omega^2 \iiint_V G_0(\mathbf{x}|\mathbf{x}') \left[-\frac{2\Delta c(\mathbf{x}')}{c_0^3(\mathbf{x}')}\epsilon + \frac{3\Delta c^2(\mathbf{x}')}{c_0^4(\mathbf{x}')}\epsilon^2\right] \times \left[G_0(\mathbf{x}'|\mathbf{x}_s) + \epsilon\Delta G_1(\mathbf{x}'|\mathbf{x}_s) + \epsilon^2\Delta G_2(\mathbf{x}'|\mathbf{x}_s)\right] dV(\mathbf{x}'). \tag{2.1.6}$$

Equating terms of equal order, expressions can be obtained for the terms in the expansion (2.1.3) of the Green's function perturbation.

A. First order (ϵ):

$$\Delta G_1(\mathbf{x}|\mathbf{x}_s) = -2\omega^2 \iiint_V G_0(\mathbf{x}'|\mathbf{x}_s) G_0(\mathbf{x}|\mathbf{x}') \frac{\Delta c(\mathbf{x}')}{c_0^3(\mathbf{x}')} dV(\mathbf{x}'). \tag{2.1.7}$$

This is the first Born approximation [19], [36] expressing the first-order perturbation ΔG_1 of the Green's function through a linear integral operator applied on the underlying sound-speed perturbation Δc. The kernel $G_0(\mathbf{x}'|\mathbf{x}_s)G_0(\mathbf{x}|\mathbf{x}')$ represents a single scattering mechanism, in which a scatterer (sound-speed perturbation) at the position $\mathbf{x}'$, stimulated by the primary source at position $\mathbf{x}_s$, with stimulation magnitude $G_0(\mathbf{x}'|\mathbf{x}_s)$ acts as a secondary source whose acoustic field $G_0(\cdot|\mathbf{x}')$ is observed at the point $\mathbf{x}$. In this connection the first Born approximation is also called single-scattering approximation, see Fig. 2.1. The approximation (2.1.7) represents efficiently the perturbations caused by very weak scatterers and due to this it is alternatively called weak-scattering approximation. The volume V in (2.1.7) spans the support of the sound-speed perturbation δc.

B. Second order (ϵ^2):

$$\begin{aligned}\Delta G_2(\mathbf{x}|\mathbf{x}_s) = &-2\omega^2 \iiint_V \Delta G_1(\mathbf{x}'|\mathbf{x}_s) G_0(\mathbf{x}|\mathbf{x}') \frac{\Delta c(\mathbf{x}')}{c_0^3(\mathbf{x}')} dV(\mathbf{x}') \\ &+3\omega^2 \iiint_V G_0(\mathbf{x}'|\mathbf{x}_s) G_0(\mathbf{x}|\mathbf{x}') \frac{\Delta c^2(\mathbf{x}')}{c_0^4(\mathbf{x}')} dV(\mathbf{x}').\end{aligned} \tag{2.1.8}$$

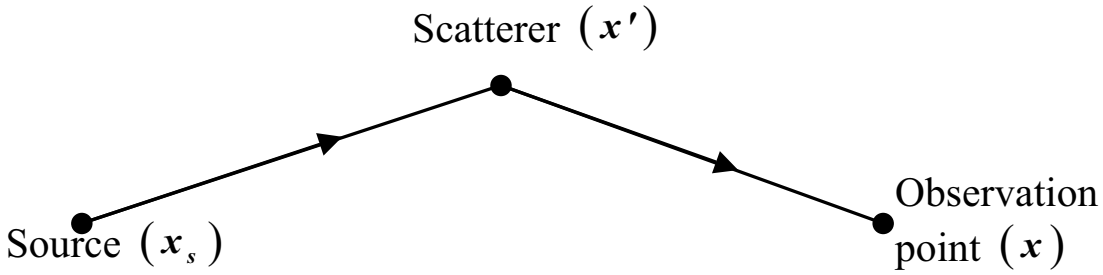

Figure 2.1: Single-scattering approximation.

This is the second Born approximation [19] expressing the second-order perturbation ΔG_2 through two quadratic integral operators applied on the underlying sound-speed perturbation. While the second integral represents a single-scattering mechanism applying on Δc^2 the kernel of the first integral

$$\Delta G_1(\mathbf{x}'|\mathbf{x}_s)G_0(\mathbf{x}|\mathbf{x}') = -2\omega^2 \iiint_V G_0(\mathbf{x}''|\mathbf{x}_s)G_0(\mathbf{x}'|\mathbf{x}'')G_0(\mathbf{x}|\mathbf{x}')\frac{\Delta c(\mathbf{x}'')}{c^3(\mathbf{x}'')}dV(\mathbf{x}''), \tag{2.1.9}$$

represents a double-scattering mechanism: the primary source stimulates a scatterer at position $\mathbf{x}''$ which stimulates, a scatterer at position $\mathbf{x}'$ which is finally received at position $\mathbf{x}$, see Fig 2.2. In this connection the second Born approximation is also called double-scattering approximation.

2.2 Rytov approximation

An alternative representation of the perturbed Green's function was introduced by Rytov [30] in the form

$$G = G_0 e^{\Delta\Psi}. \tag{2.2.1}$$

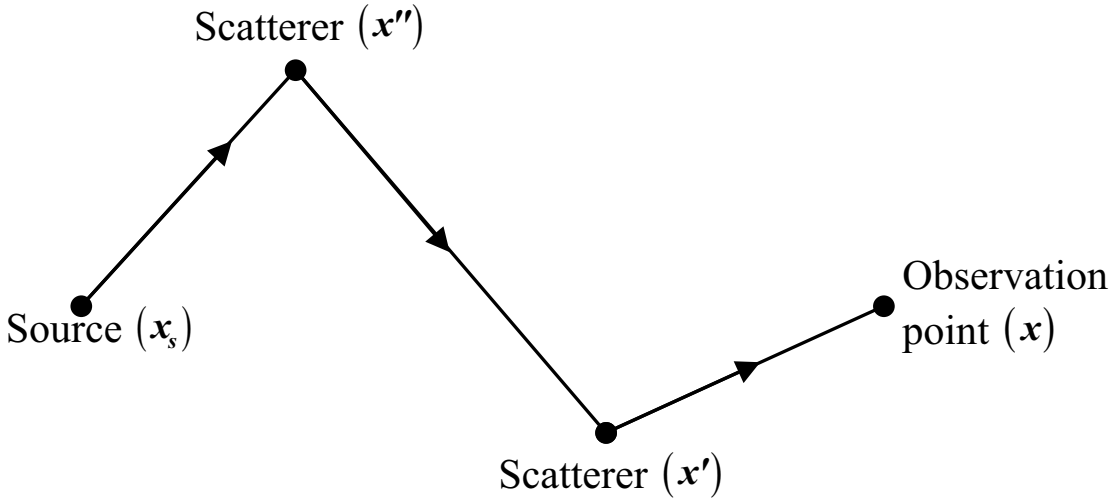

Figure 2.2: Double-scattering approximation.

This representation emphasizes on the phase perturbation $\Delta\Psi$. Taking into account that phase perturbations in the frequency domain reflect in waveform shifts in the time domain [25], i.e. in arrival-time perturbations, the Rytov approximation is expected to be particularly suitable for time-domain (arrival-time) calculations. Expanding the phase perturbation with respect to ϵ

$$\Delta\Psi = \epsilon\Delta\Psi_1 + \epsilon^2\Delta\Psi_2 + O\left(\epsilon^3\right), \tag{2.2.2}$$

and using a Taylor expansion of (2.2.1) in the neighborhood of the unperturbed state ($\epsilon = 0$) the perturbed Green's function can be written in the form

$$\begin{aligned} G =& G_0\left(1 + \epsilon\Delta\Psi_1 + \epsilon^2\Delta\Psi_2 + \frac{1}{2}\left(\epsilon\Delta\Psi_1 + \epsilon^2\Delta\Psi_2 + O\left(\epsilon^3\right)\right)^2 + O\left(\epsilon^3\right)\right) \\ =& G_0 + \epsilon G_0\Delta\Psi_1 + \epsilon^2\left(G_0\Delta\Psi_2 + G_0\frac{\Delta\Psi_1^2}{2}\right) + O\left(\epsilon^3\right). \end{aligned} \tag{2.2.3}$$

Equating the factors of corresponding orders in ϵ between (2.2.3) and (2.1.3) the following relations can be obtained between corresponding terms of the Born and

Rytov approximation

$$\begin{aligned} \Delta G_1 =& G_0 \Delta \Psi_1, \\ \Delta G_2 =& G_0 \left(\Delta \Psi_2 + \frac{\Delta \Psi_1^2}{2} \right). \end{aligned} \tag{2.2.4}$$

Thus, if the terms of the Rytov approximation are known the corresponding terms of the Born approximation can be calculated and vice versa [20], [22], [10]:

$$\begin{aligned} \Delta \Psi_1 =& \frac{\Delta G_1}{G_0}, \\ \Delta \Psi_2 =& \frac{\Delta G_2}{G_0} - \frac{1}{2} \left(\frac{\Delta G_1}{G_0} \right)^2. \end{aligned} \tag{2.2.5}$$

Thus from the expressions (2.1.7) and (2.1.8) for the Born approximation, expressions for the corresponding terms of the Rytov approximation can be obtained though eq. (2.2.5). In this sense the two approximations are closely related to each other. Nevertheless, the two approximations are not equally efficient, as will become clear in the results section, and this is due to the different functional form (representation) of each approximation: The Born approximation focuses on amplitude variations, whereas the Rytov approximation focuses on variations in the phase.

Chapter 3

Normal Modes

In the following we assume the background ocean state to be range independent and we use the normal-mode representation of the background Green's function to obtain closed-form expressions for the first and second Born approximations. The derivation is based: *a*) on analytical integration in the neighborhood of the source and the receiver, taking into account the singularity of the Green's function at the source and receiver location, and *b*) on application of the method of stationary phase for the remaining integration domain (far field). Finally expressions for the first and second Rytov approximations are derived based on the relations (2.2.5) and applying a mode-by-mode approch suggested by Keller [16].

3.1 Normal-mode representation

In the case of a horizontally stratified (range-independent) background environment, normal-mode theory can be used to represent the Green's function [2], [8] which is axisymmetric about the vertical axis through the source. In this connection a cylindrical coordinate system (r, z, θ) is adapted with is origin at the sea surface and the source located on the vertical z-axis (positive downwards) at depth $z = z_s$. Since the environment is horizontally stratified the sound-speed is a function of depth only,

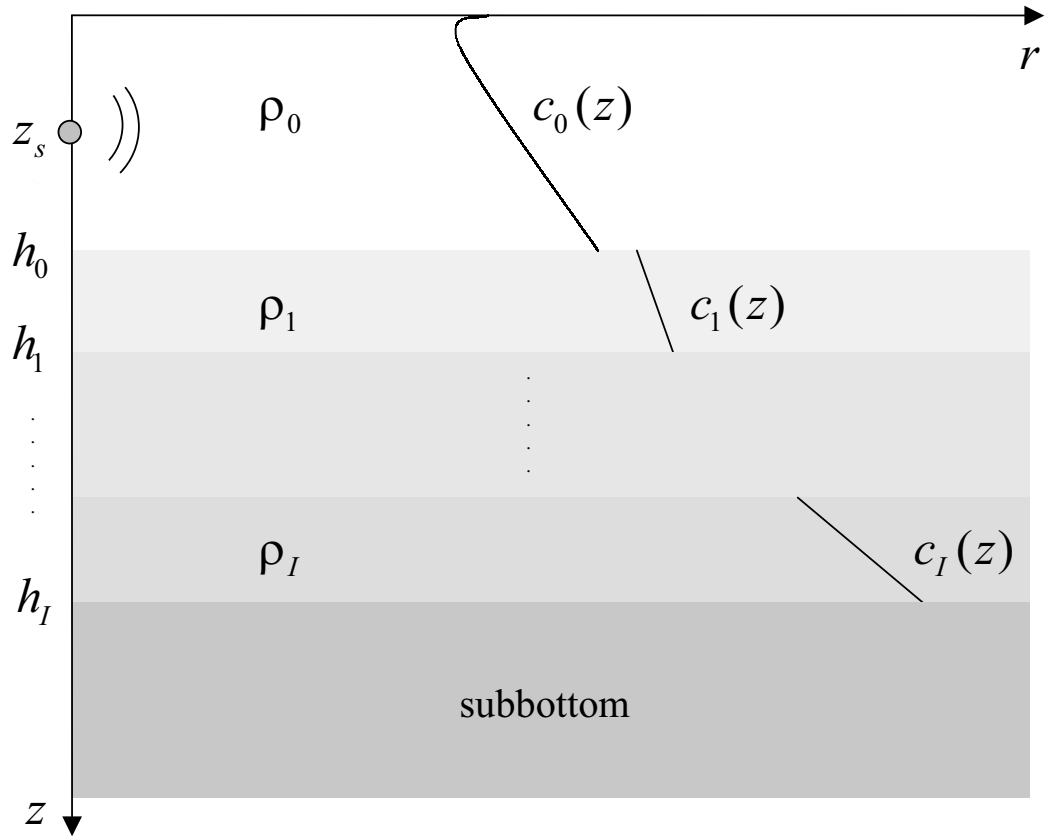

Figure 3.1: Schematic of the range-independent environmental scenario.

$c = c(z)$, and the various interfaces are surfaces of constant depth $z = h_i$, $i = 0, 1, ..., I$, where i denotes the layer from top to bottom ($i = 0$ denotes the water layer). The density in each layer is considered constant (see Fig. 3.1).

The Helmholtz equation for the Green's function in each layer takes the following form in cylindrical coordinates (assuming axial symmetry $\partial/\partial\theta = 0$)

$$\frac{\partial^2 G_i}{\partial r^2} + \frac{1}{r}\frac{\partial G_i}{\partial r} + \frac{\partial^2 G_i}{\partial z^2} + \frac{\omega^2}{c_i^2(z)} G_i = \frac{-\delta(z - z_s)\,\delta(r)}{2\pi r}. \tag{3.1.1}$$

At the free surface the soft-boundary (pressure-release) condition holds

$$G_0 = 0 \quad at \quad z = 0.$$

At the interfaces we have the conditions for continuity of the pressure

$$G_i = G_{i+1} \quad at \quad z = h_i \quad i = 0, 1, ..., I-1,$$

and normal (vertical) velocity

$$\frac{1}{\rho_i}\frac{\partial G_i}{\partial z} = \frac{1}{\rho_{i+1}}\frac{\partial G_{i+1}}{\partial z} \quad at \quad z = h_i \quad i = 0, 1, ..., I-1.$$

The Green's function will satisfy the radiation condition, eq. (1.3.1). Finally, the condition at $z = h_i$ depends on the characteristics of the subbottom. Two cases are considered in the following: rigid subbottom and acoustic subbottom (acoustic halfspace).

3.1.1 Rigid subbottom

In the case of rigid subbottom the Neumann boundary conditions applies at $z = h_I$

$$\frac{\partial G_i}{\partial z} = 0 \quad at \quad z = h_I.$$

In this case the Green's function can be represented in the form [8]

$$G(r, z|z_s) = \frac{-j}{4\rho_0}\sum_{n=1}^{\infty}\phi_n(z_s)\phi_n(z)H_0^{(2)}(k_n r), \tag{3.1.2}$$

where the quantities $\lambda_n = k_n^2$ and $\phi_n(z)$ are the eigenvalues and the eigenfunctions of the following Sturm-Liouville problem

$$\frac{d^2\phi}{dz^2} + \left[\frac{\omega^2}{c^2(z)} - \lambda\right]\phi = 0, \tag{3.1.3}$$

supplemented with the conditions that $\phi = 0$ at the sea surface ($z = 0$), ϕ and $\rho^{-1}d\phi/dz$ are continuous across the interfaces ($z = h_i$, $i = 0, 1, ..., I-1$) and $d\phi/dz = 0$ at $z = h_I$. This is a proper Sturm-Liouville problem [9] which has an infinite

countable set of eigenvalues and eigenfunctions. Some basic properties of eigenvalues and eigenfunctions for this case are described below.

The eigenvalues λ_n are discrete, real and less than ω^2/c_{min}^2, where c_{min} is the minimum sound speed value.

The eigenfunctions are orthogonal

$$\int_0^{h_I} \frac{\phi_n(z)\phi_m(z)}{\rho(z)} dz = 0, \quad for \quad m \neq n. \tag{3.1.4}$$

The eigenfunctions appearing in the normal-mode expansion are normalized

$$\int_0^{h_I} \frac{\phi_n^2(z)}{\rho(z)} dz = 1. \tag{3.1.5}$$

Furthermore, the eigenfunctions $\{\phi_n\}$ constitute a complete set in $L_2\left[0, h_I\right]$ such that any square integrable function in $[0, h_I)$ can be expanded in a series of eigenfunctions. There is no lower bound for the eigenvalues, and in fact they are contained in the interval $(-\infty, \omega^2/c_{min}^2]$. While the positive eigenvalues correspond to positive values for $k_n = \sqrt{\lambda_n}$ in $[0, \omega/c_{min}]$ the negative eigenvalues give rise to imaginary values for k_n in the interval $[0, j\infty)$. Taking into account the far-field asymptotic form of the Hankel function $H_0^{(2)}(k_n r)$ (Appendix D) we see that the positive k_n's are associated with outgoing waves whereas the contribution of the imaginary k_n's is exponentially decaying with increasing range. In this connection the eigenfunctions (modes) corresponding to the positive eigenvalues are called propagating modes. The remaining eigenfunctions (corresponding to negative eigenvalues – imaginary k_n values) are called evanescent modes and their contribution away from the source is negligible.

Thus the normal mode expansion in this case can be written as

$$G(r, z|z_s) = \frac{-j}{4\rho_0} \sum_{n=1}^{M} \phi_n(z_s)\phi_n(z) H_0^{(2)}(k_n r) + \sum_{n=M+1}^{\infty} \mathrm{A}(k_n) H_0^{(2)}(k_n r), \tag{3.1.6}$$

where the first sum represents the propagating modes and the second sum the evanescent modes.

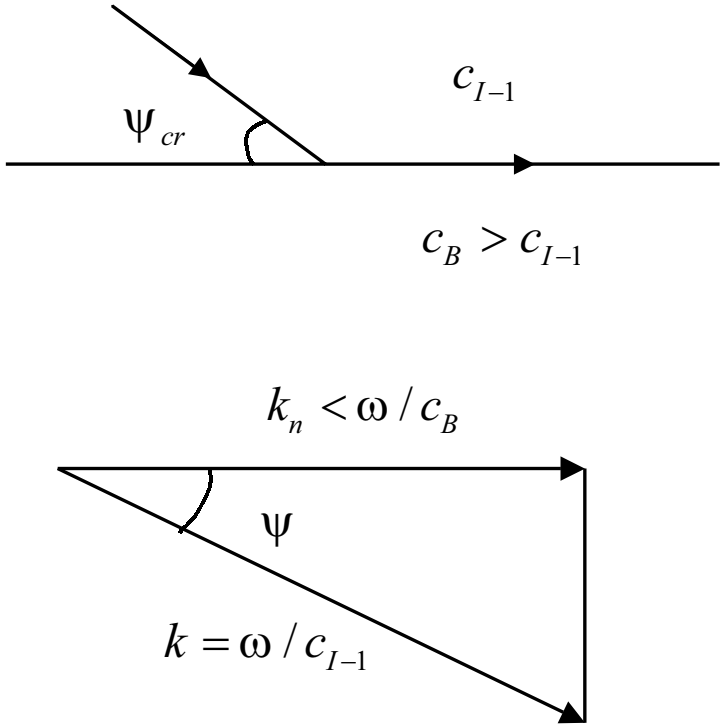

Figure 3.2: The positive eigenvalues smaller than ω^2/c_B^2 correspond to modes propagating with grazing angle ψ greater than the critical ψ_{cr}, since $\psi = \cos^{-1}(k_n/k) > \cos^{-1}(c_{I-1}/c_B) = \psi_{cr}$.

3.1.2 Acoustic subbottom

The case of the acoustic bottom (acoustic halfspace) can be considered as the limit of the previous case with the thickness of the lowermost layer ($i = I$) going to infinity ($h_I - h_{I-1} \to \infty$). We assume that the sound speed in this layer (halfspace) is constant ($c_I(z) = c_B$) and larger than the sound speed at any other depth. As the thickness of the bottom layer increases the eigenvalues λ_n smaller than ω^2/c_B^2 increase in number and their separation decreases such that at the limit they form a continuum (see appendix A).

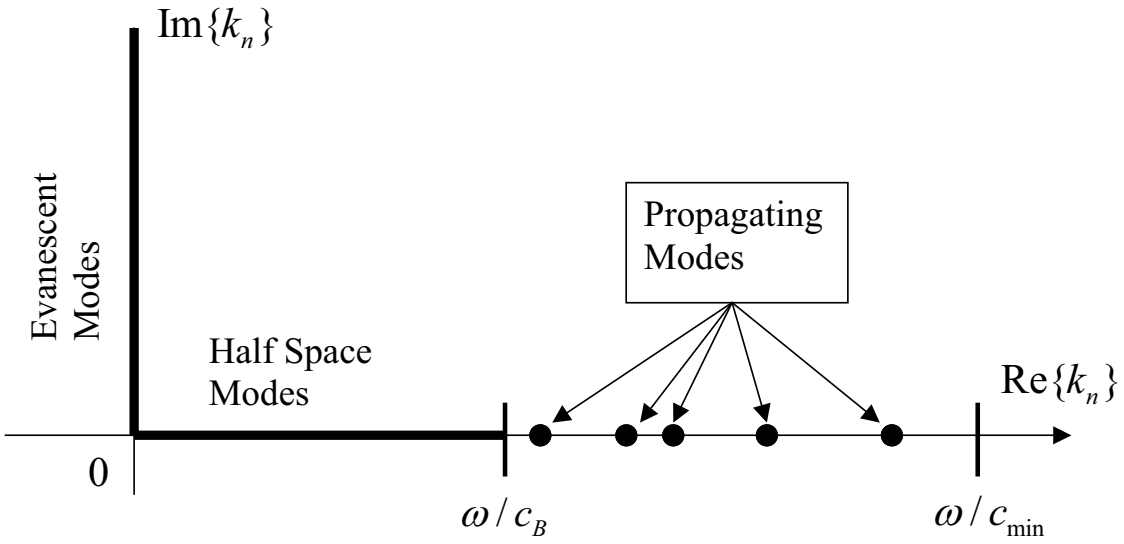

Figure 3.3: Location of eigenvalues k_n for the problem with homogenous acoustic bottom.

While the negative eigenvalues (imaginary k_n values) correspond to evanescent modes (evanescent spectrum), the positive eigenvalues smaller than ω^2/c_B^2 correspond to modes propagating with grazing angle greater than the critical [2], see Fig. 3.2. These modes enter the bottom halfspace and thus they are strongly attenuated in the higher layers. In this connection, they are called half-space modes and their contribution to the acoustic field in the water layer away from the source is negligible. In conclusion, the Green's function for the case with acoustic subbottom can be written in the form (see also Fig. 3.3)

$$G(r,z|z_s) = \frac{-j}{4\rho_0}\sum_{n=1}^{M}\phi_n(z_s)\phi_n(z)H_0^{(2)}(k_n r) + \int_0^{\omega/c_B}\mathcal{A}(k)dk + \int_0^{j\infty}\mathcal{B}(k)dk, \qquad (3.1.7)$$

where the sum represents the finite set of the propagating modes with $\omega/c_B < k_n < \omega/c_{min}$, $n = 1, 2, ..., M$, the first integral represents the half-space modes and the second integral spans the evanescent spectrum. Both integrals are negligible in the

water layer away from the source.

In the following we focus on the effect of sound speed perturbations on the late part of the arrival pattern represented in general by low-order propagating modes, corresponding to eigenvalues λ_n close to ω^2/c_{min}^2. As we will see in the next section the perturbation behavior of a particular mode can be described in terms of the full set of modes, with the nearby modes (closest in terms of eigenvalues) playing the dominant role. Since our interest is in the perturbation behavior of the low-order modes, the influence of the high-order propagating modes, as well as that of half-space and evanescent modes is negligible. Because of this, we keep only the propagating modes for the representation of the Green's function.

3.2 First Born approximation

In this section we obtain a closed-form expression for the first Born approximation by substituting the normal-mode representation for the background Green's function in the right hand side of eq. (2.1.7), assuming a range independent background environment.

Using a cylindrical coordinate system (r, z, θ) with the source on the z-axis the Green's function $G(\mathbf{x}|\mathbf{x}_s)$ can be written in terms of the propagating modes as follows

$$G(\mathbf{x}|\mathbf{x}_s) = -\frac{j}{4\rho_w}\sum_{n=1}^{M}\phi_n(z)\phi_n(z_s)H_0^{(2)}(k_n r), \tag{3.2.1}$$

where ρ_w is the water density. Similarly the Green's function $G(\mathbf{x}|\mathbf{x}_r)$ has the form

$$G(\mathbf{x}|\mathbf{x}_r) = -\frac{j}{4\rho_w}\sum_{m=1}^{M}\phi_m(z)\phi_m(z_r)H_0^{(2)}(k_m \gamma), \tag{3.2.2}$$

where $\gamma = \sqrt{r^2 + R^2 - 2Rr\cos\theta}$ is the horizontal distance from the receiver – R is the horizontal distance between source and receiver (see Fig. 3.4). The sound-

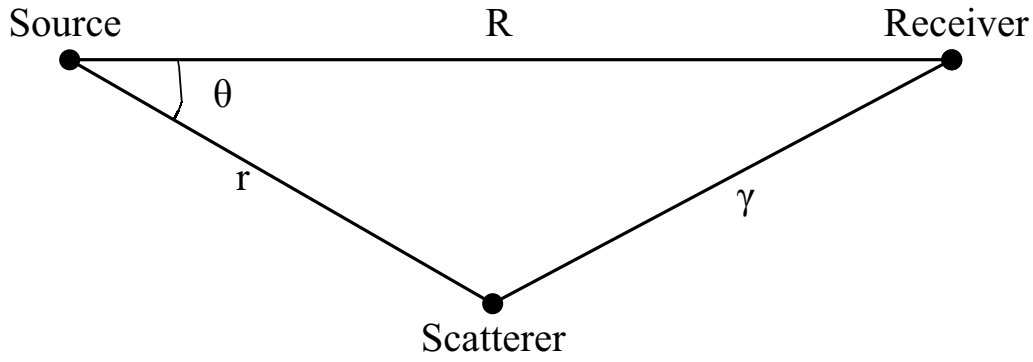

Figure 3.4: Geometry of the problem (top view).

speed perturbations are confined in the water column and for convenience they are considered to be of separable form

$$\Delta c(\mathbf{x}) = \Delta c_r(r)\Delta c_z(z)\Delta c_\theta(\theta), \tag{3.2.3}$$

where Δc_r, Δc_z and Δc_θ are smooth, slowly varying functions of r, z and θ, respectively.

Substituting the expressions (3.2.1), (3.2.2) and (3.2.3) in (2.1.7) we obtain

$$\begin{aligned}\Delta G_1(\mathbf{x}|\mathbf{x}_s) = &\left(\frac{2\omega^2}{16\rho_w^2}\right)\int_0^h\int_0^{2\pi}\int_0^\infty \sum_{n=1}^{M}\sum_{m=1}^{M}\phi_n(z_s)\phi_m(z_r)\phi_n(z)\phi_m(z)\\ &\times\frac{\Delta c_z(z)}{c_0^3(z)}\Delta c_\theta(\theta)\Delta c_r(r)H_0^{(2)}(k_n r)H_0^{(2)}(k_m\gamma)r dr d\theta dz,\end{aligned}$$

where h is the water depth. Separating the integration with respect to z from that with respect to (r,θ) this expression can be written as

$$\begin{aligned}\Delta G_1(\mathbf{x}|\mathbf{x}_s) =&\frac{\omega^2}{8\rho_w^2}\sum_{n=1}^{M}\sum_{m=1}^{M}\phi_n(z_s)\phi_m(z_r)\int_0^h\phi_n(z)\phi_m(z)\frac{\Delta c_z(z)}{c_0^3(z)}dz\\ &\times\int_0^{2\pi}\int_0^\infty\Delta c_\theta(\theta)\Delta c_r(r)H_0^{(2)}(k_n r)H_0^{(2)}(k_m\gamma)r dr d\theta.\end{aligned} \tag{3.2.4}$$

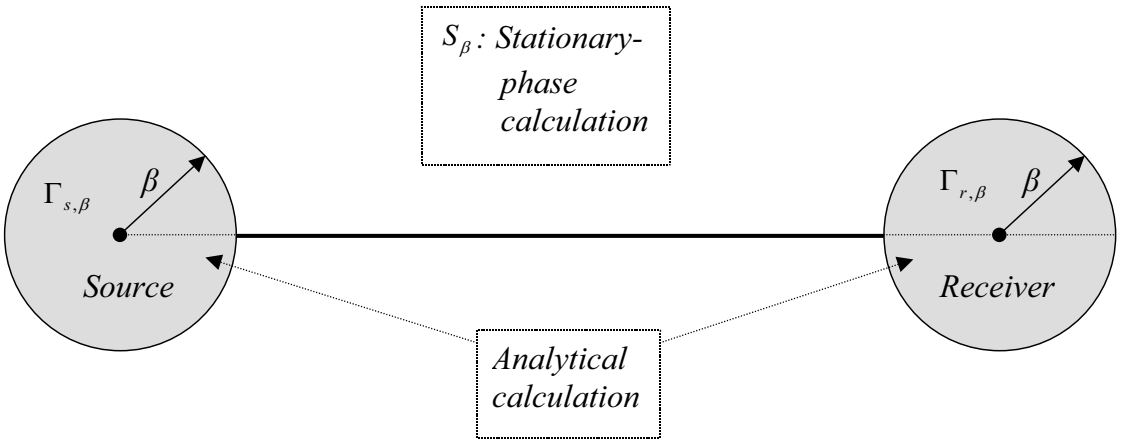

Figure 3.5: Decomposition of the calculation domain into subdomains $\Gamma_{s,\beta}$, $\Gamma_{r,\beta}$ and S_β.

In the following we evaluate the integral

$$I_{nm} = \int_0^{2\pi} \int_0^{\infty} \Delta c_\theta(\theta) \Delta c_r(r) H_0^{(2)}(k_n r) H_0^{(2)}(k_m \gamma) r dr d\theta. \tag{3.2.5}$$

Since the Hankel functions are singular for $r = 0$ and $\gamma = 0$, i.e. at the location of the source and the receiver, respectively, we chose to evaluate the integral I_{nm} analytically in the vicinity $\Gamma_{s,\beta}$ and $\Gamma_{r,\beta}$ of the source and receiver (disks of radius β), see Fig. 3.5. Assuming that the radius β is large enough we use the asymptotic form of the Hankel functions (see Appendix D) at the remaining domain S_β which is the domain outside the above two areas.[1] Further, exploiting the fact that they are rapidly oscillating functions with respect to (r, θ) we apply the method of stationary phase for the evaluation of I_{nm} in this domain.

`STEP 1:` *Analytical calculation of I_{nm} in the vicinity of the source/receiver*

In the vicinity of the source we can assume that $\Delta c_\theta(\theta)$ and $\Delta c_r(r)$ are constants,

[1] $S_\beta = [\beta, \infty) \times [0, 2\pi) \setminus \Gamma_{r,\beta}$.

such that $I_{nm}(\Gamma_{s,\beta}) = \Delta c_\theta \Delta c_r I_{\beta,nm}$ where Δc_θ, Δc_r are taken at the source and

$$I_{\beta,nm} = \int_0^{2\pi} d\theta \left[\int_0^{\beta} r dr H_0^{(2)}(k_n r) H_0^{(2)}(k_m \gamma) \right]. \tag{3.2.6}$$

The Hankel function $H_0^{(2)}(k_m\gamma)$ can be expressed in terms of cylindrical functions of the argument $(k_m r)$ as follows [see M. Abramowitz and I. A. Stegun [18] form. [9.1.79]][2]

$$H_0^{(2)}(k_m\gamma) = J_0(k_m r) H_0^{(2)}(k_m R) + 2\sum_{\ell=1}^{\infty} J_\ell(k_m r) H_\ell^{(2)}(k_m R) cos(\ell\theta).$$

Substituting this expression into (3.2.6), and since $\int_0^{2\pi} cos\ell\theta d\theta = 0$, $\ell = 1, 2, ...,$ $I_{\beta,nm}$ becomes:

$$I_{\beta,nm} = 2\pi H_0^{(2)}(k_m R) I'_{\beta,nm}, \tag{3.2.7}$$

where

$$I'_{\beta,nm} = \int_0^{\beta} J_0(k_m r) H_0^{(2)}(k_n r) r dr.$$

a) For $m \neq n$ the integral $I'_{\beta,nm}$ can be evaluated as follows [Watson [35] form. [134(8)]]

$$I'_{\beta,nm} = \left[\frac{k_m r J_1(k_m r) H_0^{(2)}(k_n r) - k_n r J_0(k_m r) H_1^{(2)}(k_n r)}{k_m^2 - k_n^2} \right]_{r=\alpha\to 0}^{\beta}.$$

Using the asymptotic expressions for small (α) and large (β) arguments given in Appendix D we obtain

$$\begin{aligned} I'_{\beta,nm} =& \frac{2k_m}{(k_m^2 - k_n^2)\,\pi\sqrt{k_m k_n}} \cos\left(k_m\beta - \frac{3\pi}{4}\right) e^{-j\left(k_n\beta - \frac{\pi}{4}\right)} \\ &- \frac{2k_n}{(k_m^2 - k_n^2)\,\pi\sqrt{k_m k_n}} \cos\left(k_m\beta - \frac{\pi}{4}\right) e^{-j\left(k_n\beta - \frac{3\pi}{4}\right)} \\ &- \lim_{\alpha\to 0} \frac{\frac{(k_m\alpha)^2}{2}\left(1 - j\frac{2}{\pi}\ln(k_n\alpha)\right) - k_n\alpha\left(\frac{k_n\alpha}{2} + \frac{2}{k_n\alpha\pi}j\right)}{k_m^2 - k_n^2} \end{aligned}$$

[2]This expansion holds for $r < R$. For $r > R$ the expansion is different.

and finally

$$I'_{\beta,nm} = \frac{2}{\pi\left(k_m^2 - k_n^2\right)} j + o.t., \tag{3.2.8}$$

where *o.t.* stands for an oscillating term with respect to β averaging to zero.

b) For $m = n$ the integral $I'_{\beta,nm}$ becomes

$$\begin{aligned} I'_{\beta,nn} &= \int_0^\beta J_0\left(k_n r\right)\left[J_0\left(k_n r\right) - jY\left(k_n r\right)\right] r dr \\ &= \int_0^\beta \left[\left(J_0(k_n r)\right)^2 r dr - j\int_0^\beta J_0\left(k_n r\right) Y\left(k_n r\right)\right] r dr. \end{aligned}$$

Using form. [135(11)] from Watson [35] we obtain

$$\begin{aligned} I'_{\beta,nn} =& \left[\frac{r^2}{2}\left(\left(J_0\left(k_n r\right)\right)^2 + \left(J_1\left(k_n r\right)\right)^2\right) - j\frac{r^2}{2}\left(J_0\left(k_n r\right) Y_0\left(k_n r\right) + J_1\left(k_n r\right) Y_1\left(k_n r\right)\right)\right]_{r=\alpha\to 0}^{\beta} \\ =& \frac{\beta^2}{2}\left[\left(J_0\left(k_n\beta\right)\right)^2 + \left(J_1\left(k_n\beta\right)\right)^2 - j\left(J_0\left(k_n\alpha\right) Y_0\left(k_n\alpha\right) + J_1\left(k_n\beta\right) Y_1\left(k_n\beta\right)\right)\right] \\ & - \lim_{\alpha\to 0}\frac{\alpha^2}{2}\left[\left(J_0\left(k_n\alpha\right)\right)^2 + \left(J_1\left(k_n\alpha\right)\right)^2 - j\left(J_0\left(k_n\alpha\right) Y_0\left(k_n\alpha\right) + J_1\left(k_n\alpha\right) Y_1\left(k_n\alpha\right)\right)\right]. \end{aligned}$$

Using the asymptotic expressions for small (α) and large (β) arguments (Appendix D) we obtain

$$\begin{aligned} I'_{\beta,nn} =& \left[\cos^2\left(k_n\beta - \frac{\pi}{4}\right) + \cos^2\left(k_n\beta - \frac{3\pi}{4}\right) - j\left[\cos\left(k_n\beta - \frac{\pi}{4}\right)\sin\left(k_n\beta - \frac{\pi}{4}\right)\right.\right. \\ & \left.\left. + \cos\left(k_n\beta - \frac{3\pi}{4}\right)\sin\left(k_n\beta - \frac{3\pi}{4}\right)\right]\right]\frac{\beta^2}{2}\frac{2}{k_n\beta\pi} \\ & - \lim_{\alpha\to 0}\left[1 + \left(\frac{k_n\alpha}{2}\right)^2 - j\left(\frac{2}{\pi}\left(\ln\left(\frac{k_n\alpha}{2}\right)\right) - \frac{k_n\alpha}{2}\left(-\frac{2}{k_n\alpha\pi}\right)\right)\right]\frac{\alpha^2}{2} \\ =& \frac{\beta}{k_n\pi}\left[cos^2\left(k_n\beta - \frac{\pi}{4}\right) + cos^2\left(k_n\beta - \frac{3\pi}{4}\right)\right] = \frac{\beta}{k_n\pi}. \end{aligned} \tag{3.2.9}$$

Consequently the integral I_{nm} calculated in the vicinity $\Gamma_{s,\beta}$ of the source becomes

$$I_{nm}(\Gamma_{s,\beta}) = 2\Delta c_r \Delta c_\theta H_0^{(2)}(k_m R)\cdot\begin{cases} \dfrac{\beta}{k_n} & for \quad n = m \\ \dfrac{2j}{k_m^2 - k_n^2} + o.t. & for \quad n \neq m \end{cases} \tag{3.2.10}$$

where Δc_r and Δc_θ are taken at the source location. Similar expressions can be derived for $I_{nm}(\Gamma_{r,\beta})$.

STEP 2: *Calculation of I_{nm} away from the source/receiver*

Assuming that the radius β is large enough we can use the asymptotic expression for the Hankel functions (see Appendix D) outside the disks surrounding the source and the receiver. The integral I_{nm} over the domain S_β takes the form

$$\begin{aligned} I_{nm}(S_\beta) =& \iint_{S_\beta} \Delta c_\theta(\theta)\Delta c_r(r) H_0^{(2)}(k_n r) H_0^{(2)}(k_m \gamma) dS(r,\theta) \\ =& \iint_{S_\beta} \Delta c_\theta(\theta)\Delta c_r(r) \frac{2j e^{-j\left(k_m r + k_n\sqrt{r^2+R^2-2rRcos\theta}\right)}}{\pi\sqrt{k_n k_m}\sqrt{r\sqrt{r^2+R^2-2rR\cos\theta}}} dS(r,\theta) \\ =& \frac{2j}{\pi\sqrt{k_n k_m}} J_{\beta,nm}, \end{aligned}$$

where dS is the differential area and

$$J_{\beta,nm} = \iint_{S_\beta} \Delta c_\theta(\theta)\Delta c_r(r) \frac{e^{-j\left(k_m r + k_n\sqrt{r^2+R^2-2rRcos\theta}\right)}}{\sqrt{r\sqrt{r^2+R^2-2rR\cos\theta}}} dS(r,\theta).$$

The exponential part in the kernel of this integral is a rapidly oscillating function of (r,θ). In this connection we apply the method of stationary phase [see Appendix B] for the evaluation of $J_{\beta,nm}$. The phase of the exponential is

$$\begin{aligned} \Phi =& k_m r + k_n\sqrt{r^2+R^2-2Rr\cos\theta} \\ =& R\left[k_m\eta + k_n\sqrt{\eta^2+1-2\eta\cos\theta}\right], \end{aligned}$$

where $\eta = r/R$. The only contributions to the integral $J_{\beta,nm}$ will come from the stationary points with respect to θ and η. The derivative of Φ with respect to θ

$$\frac{\partial\Phi}{\partial\theta} = \frac{Rk_n\eta\sin\theta}{\sqrt{\eta^2+1-2\eta\cos\theta}},$$

vanishes at $\theta = 0$ and $\theta = \pi$ (stationary points). The derivative of Φ with respect to η is

$$\frac{\partial\Phi}{\partial\eta} = R\left[k_m + k_n\frac{\eta-\cos\theta}{\sqrt{\eta^2+1-2\eta\cos\theta}}\right]. \tag{3.2.11}$$

α) For $\theta = 0$ this derivative takes the form:

$$\begin{aligned}\frac{\partial \Phi}{\partial \eta} =& R\left[k_m + k_n \frac{\eta - 1}{\sqrt{\eta^2 + 1 - 2\eta}}\right] \\ =& R\left[k_m + k_n sign(\eta - 1)\right],\end{aligned}$$

since the square root represents the normalized distance from the receiver and is taken positive. Thus the stationary points for $\theta = 0$ are $\eta < 1$ and $n = m$.

β) For $\theta = \pi$ the derivative (3.2.11) becomes:

$$\begin{aligned}\frac{\partial \Phi}{\partial \eta} =& R\left[k_m + k_n \frac{\eta + 1}{\sqrt{\eta^2 + 1 + 2\eta}}\right] \\ =& R\left[k_m + k_n\right].\end{aligned}$$

This expression will always be positive such that there are no stationary points for $\theta = \pi$.

The expressions for the second derivatives of the phase with respect to η and θ, calculated at the stationary points, are given next.

$$\left.\frac{\partial^2 \Phi}{\partial \eta^2}\right|_{\substack{\theta=0 \\ \eta<1}} = Rk_n \left.\frac{\sqrt{\eta^2 + 1 - 2\eta\cos\theta} - \frac{(\eta - \cos\theta)^2}{\sqrt{\eta^2 + 1 - 2\eta\cos\theta}}}{\eta^2 + 1 - 2\eta\cos\theta}\right|_{\substack{\theta=0 \\ \eta<1}} = 0$$

$$\left.\frac{\partial^2 \Phi}{\partial \theta \partial \eta}\right|_{\substack{\theta=0 \\ \eta<1}} = Rk_n \sin\theta \left.\frac{\sqrt{\eta^2 + 1 - 2\eta\cos\theta} - \eta\frac{\eta - \cos\theta}{\sqrt{\eta^2 + 1 - 2\eta\cos\theta}}}{\eta^2 + 1 - 2\eta\cos\theta}\right|_{\substack{\theta=0 \\ \eta<1}} = 0$$

$$\left.\frac{\partial^2 \Phi}{\partial \theta^2}\right|_{\substack{\theta=0 \\ \eta<1}} = Rk_n \eta \frac{\sqrt{\eta^2 + 1 - 2\eta}}{\eta^2 + 1 - 2\eta} = \frac{Rk_n \eta}{1 - \eta}$$

The first two derivatives are identically equal to zero. Thus expanding the phase $\Phi(\eta, \theta)$ in a two-dimensional Taylor series about the stationary points, and keeping

terms up to the second order we obtain

$$\Phi(\eta,\theta) \approx \Phi(\eta,0) + \frac{1}{2}\frac{\partial^2\Phi}{\partial\theta^2}(\eta,0)\theta^2.$$

Since the stationary points of the phase Φ are $k_n = k_m$, $\theta = 0$, $\beta < r < R - \beta$, the integral $J_{\beta,nm}$, can be expressed in the form

$$\begin{aligned} J_{\beta,nm} =& \iint_{S_\beta} \Delta c_\theta(\theta)\Delta c_r(r)\frac{e^{-j\left(k_m r + k_n\sqrt{r^2+R^2-2rRcos\theta}\right)}}{\sqrt{r\sqrt{r^2+R^2-2rR\cos\theta}}}dS \\ \approx& \Delta c_\theta(0)e^{-jk_nR}\int_\beta^{R-\beta}\frac{\Delta c_r(r)}{\sqrt{r(R-r)}}\left(\int_0^{2\pi} e^{-\frac{j}{2}\frac{\partial^2\Phi}{\partial\theta^2}\Big|_{\substack{\theta=0\\ \eta<1}}\theta^2}d\theta\right)rdr \\ =& \Delta c_\theta(0)e^{-jk_nR}e^{-j\pi/4}\sqrt{\frac{2\pi}{k_nR}}\int_\beta^{R-\beta}\Delta c_r(r)dr. \end{aligned} \tag{3.2.12}$$

Thus the stationary phase method gives for the integral $I_{nm}(S_\beta)$

$$I_{nm}(S_\beta) \approx \delta_{nm}2\Delta c_\theta(0)\frac{H_0^{(2)}(k_nR)}{k_n}\int_\beta^{R-\beta}\Delta c_r(r)dr, \tag{3.2.13}$$

where δ_{nm} is the Kronecker delta. Combining the expressions for $I_{nm}(\Gamma_{s,\beta})$ and $I_{nm}(\Gamma_{r,\beta})$, eq. (3.2.10), with the above expression for $I_{nm}(S_\beta)$ and omitting oscillating terms we finally obtain the following expression for $I_{nm} = I_{nm}(S_\beta) + I_{nm}(\Gamma_{s,\beta}) + I_{nm}(\Gamma_{r,\beta})$

$$I_{nm} = \begin{cases} 2\Delta c_\theta(0)\dfrac{H_0^{(2)}(k_nR)}{k_n}\displaystyle\int_0^R \Delta c_r(r)dr & for \quad \text{n=m} \\ \\ 4j\Delta c_\theta(0)\left[\dfrac{H_0^{(2)}(k_mR)}{k_m^2-k_n^2}\Delta c_r(0) + \dfrac{H_0^{(2)}(k_nR)}{k_n^2-k_m^2}\Delta c_r(R)\right] & for \quad n \neq m \end{cases} \tag{3.2.14}$$

Substituting the above expressions into (3.2.4) the first-order Born approximation

takes the form

$$\begin{aligned}\Delta G_1(\mathbf{x}_r|\mathbf{x}_s) =&\frac{\omega^2}{8\rho_w^2}\sum_{n=1}^{M}\Bigg\{\phi_n(z_s)\phi_n(z_r)\int_0^h \phi_n^2(z)\frac{\Delta c_z(z)}{c_0^3(z)}dz\\ &\times\frac{2\Delta c_\theta(0)}{k_n}\int_0^R \Delta c_r(r)dr\\ &+\sum_{\substack{m=1\\m\neq n}}^{M}\phi_m(z_s)\phi_n(z_r)\int_0^h \phi_m(z)\phi_n(z)\frac{\Delta c_z(z)}{c_0^3(z)}dz\\ &\times\frac{4j}{k_n^2-k_m^2}\Delta c_\theta(0)\Delta c_r(0)\\ &+\sum_{\substack{m=1\\m\neq n}}^{M}\phi_m(z_r)\phi_n(z_s)\int_0^h \phi_m(z)\phi_n(z)\frac{\Delta c_z(z)}{c_0^3(z)}dz\\ &\times\frac{4j}{k_n^2-k_m^2}\Delta c_\theta(0)\Delta c_r(R)\Bigg\}H_0^{(2)}(k_nR).\end{aligned}$$

By rearranging terms we obtain

$$\begin{aligned}\Delta G_1(\mathbf{x}_r|\mathbf{x}_s) =&\frac{\omega^2}{8\rho_w^2}\sum_{n=1}^{M}\Bigg\{\phi_n(z_s)\phi_n(z_r)\frac{2\Delta c_\theta(0)}{k_n}\int_0^h \phi_n^2(z)\frac{\Delta c_z(z)}{c_0^3(z)}dz\int_0^R \Delta c_r(r)dr\\ &+4j\Delta c_\theta(0)\sum_{\substack{m=1\\m\neq n}}^{M}\frac{\Delta c_r(0)\phi_m(z_s)\phi_n(z_r)+\Delta c_r(R)\phi_n(z_s)\phi_m(z_r)}{k_n^2-k_m^2}\\ &\times\int_0^h \phi_n(z)\phi_m(z)\frac{\Delta c_z(z)}{c_0^3(z)}dz\Bigg\}H_0^{(2)}(k_nR).\end{aligned}\tag{3.2.15}$$

Setting

$$\Lambda_{nm} =k_n^2-k_m^2 \tag{3.2.16}$$

$$Q_{nm} =-\frac{2\omega^2}{\rho_w^2}\int_0^h \phi_n(z)\phi_m(z)\frac{\Delta c_z(z)}{c_0^3(z)}dz, \tag{3.2.17}$$

$$U_n =-\phi_n(z_s)\phi_n(z_r)/2, \tag{3.2.18}$$

$$V_{nm} =\phi_m(z_s)\phi_n(z_r)\Delta c_r(0)+\phi_n(z_s)\phi_m(z_r)\Delta c_r(R). \tag{3.2.19}$$

The first Born approximation can be finally written in the compact form

$$\Delta G_1(\mathbf{x}_r|\mathbf{x}_s) = -\frac{j\Delta c_\theta(0)}{4\rho_w}\sum_{n=1}^{M}\left\{\sum_{\substack{m=1\\m\neq n}}^{M}\frac{Q_{nm}V_{nm}}{\Lambda_{nm}} + j\frac{Q_{nn}U_n}{k_n}\int_0^R \Delta c_r(r)dr\right\}H_0^{(2)}(k_nR). \tag{3.2.20}$$

This expression is a generalization of previous results obtained for range-independent perturbations [28]. The more important term in (3.2.20) is the one containing the integral over r, which e.g. for range independent perturbations this will lead to multiplication by a factor R, (the source-receiver range). However in the case of a zero-mean range-dependent perturbation $\left(\int_0^R \Delta c_r(r)dr = 0\right)$ this term will vanish. The first term including the sum over m is in general negligible to the first order. This term will become of importance for the second Born approximation. The more important contribution to this term comes from the elements that are close to the diagonal (small $|n-m|$), for which the denominator Λ_{nm} becomes very small.

At this point we can see why the contribution of the half-space and evanescent modes can be neglected, if we are interested in the perturbation behavior of the low-order modes. The term containing the integral over r evaluates the contribution of the various modes at the receiver's location $\left(H_0^{(2)}(k_nR)\right)$, and for large R the contribution of half-space and evanescent modes will be negligible since these modes are highly attenuated in water. Coming to the term with the sum over m, since we are interested in low-order modes (small n) the half-space modes (large m) will be characterized by large Λ_{nm} values and thus their contribution will be negligible. The contribution of the evanescent modes will be even smaller since k_m will be imaginary and thus the differences Λ_{nm} will become sums of the form $k_n^2 + Im(k_m)^2$.

3.3 Second Born approximation

We continue with the second Born approximation. The expression (2.1.8), can be written in the form $\Delta G_2(\mathbf{x}_r, \mathbf{x}_s) = I_1 + I_2$ where

$$I_1 = \iiint_V G_0(\mathbf{x}_r|\mathbf{x}) \left[-\frac{2\omega^2}{c_0^3(\mathbf{x})} \Delta c(\mathbf{x}) \right] \Delta G_1(\mathbf{x}|\mathbf{x}_s) dV(\mathbf{x}), \tag{3.3.1}$$

$$I_2 = \iiint_V G_0(\mathbf{x}_r|\mathbf{x}) \left[\frac{3\omega^2}{c_0^4(\mathbf{x})} \Delta c^2(\mathbf{x}) \right] G_0(\mathbf{x}|\mathbf{x}_s) dV(\mathbf{x}). \tag{3.3.2}$$

Substituting the normal-mode representation for the background Green's function and the expression (3.2.20) for the first Born approximation into the integral I_1 we obtain

$$\begin{aligned}
I_1 = & \int_0^h \int_0^{2\pi} \int_0^{\infty} \sum_{\ell=1}^{M} \phi_\ell(z)\phi_\ell(z_r) H_0^{(2)}\left(k_\ell \sqrt{r^2 + R^2 - 2rR\cos\theta}\right) \left(-\frac{j}{4\rho_w}\right)^2 \Delta c_\theta(0) \\
& \times \left[-\frac{2\omega^2}{c_0^3(z)} \Delta c_z(z) \Delta c_\theta(\theta) \Delta c_r(r) \right] \sum_{n=1}^{M} \left\{ \sum_{\substack{m=1 \\ m\neq n}}^{M} \frac{Q_{nm} V_{nm}}{\Lambda_{nm}} + j \frac{Q_{nn} U_n}{k_n} \int_0^r \Delta c_r(r') dr' \right\} \\
& \times H_0^{(2)}(k_n r) r dr d\theta dz \\
= & \int_0^h \int_0^{2\pi} \int_0^{\infty} \sum_{\ell=1}^{M} \phi_\ell(z)\phi_\ell(z_r) H_0^{(2)}\left(k_\ell \sqrt{r^2 + R^2 - 2rR\cos\theta}\right) \left(-\frac{\Delta c_\theta(0)}{16\rho_w^2}\right) \\
& \times \left[-\frac{2\omega^2}{c_0^3(z)} \Delta c_z(z) \Delta c_\theta(\theta) \Delta c_r(r) \right] \\
& \times \sum_{n=1}^{M} \left\{ \sum_{\substack{m=1 \\ m\neq n}}^{M} \frac{Q_{nm} \left[\phi_m(z_s)\phi_n(z) \Delta c_r(0) + \phi_m(z)\phi_n(z_s) \Delta c_r(r) \right]}{k_n^2 - k_m^2} \right. \\
& \left. -j \int_0^r \Delta c_r(r') dr' \frac{Q_{nn} \phi_n(z_s)\phi_n(z)}{2k_n} \right\} H_0^{(2)}(k_n r)\, r dr d\theta dz
\end{aligned}$$

$$
\begin{aligned}
=&\frac{\omega^2\Delta c_\theta(0)\Delta c_r(0)}{8\rho_w^2}\sum_{n=1}^{M}\sum_{\substack{m=1\\m\neq n}}^{M}\sum_{\ell=1}^{M}\frac{Q_{nm}\phi_\ell(z_r)\phi_m(z_s)}{k_n^2-k_m^2}\int_0^h\frac{\phi_\ell(z)\phi_n(z)}{c_0^3(z)}\Delta c_z(z)dz\\
&\times\int_0^{2\pi}\int_0^{\infty}H_0^{(2)}(k_nr)H_0^{(2)}\left(k_\ell\sqrt{r^2+R^2-2rR\cos\theta}\right)\Delta c_\theta(\theta)\Delta c_r(r)rdrd\theta\\
&+\frac{\omega^2\Delta c_\theta(0)}{8\rho_w^2}\sum_{n=1}^{M}\sum_{\substack{m=1\\m\neq n}}^{M}\sum_{\ell=1}^{M}\frac{Q_{nm}\phi_\ell(z_r)\phi_n(z_s)}{k_n^2-k_m^2}\int_0^h\frac{\phi_\ell(z)\phi_m(z)}{c_0^3(z)}\Delta c_z(z)dz\\
&\times\int_0^{2\pi}\int_0^{\infty}H_0^{(2)}(k_nr)H_0^{(2)}\left(k_\ell\sqrt{r^2+R^2-2rR\cos\theta}\right)\Delta c_\theta(\theta)\Delta c_r^2(r)rdrd\theta\\
&-\frac{j\omega^2\Delta c_\theta(0)}{8\rho_w^2}\sum_{n=1}^{M}\sum_{\ell=1}^{M}\frac{Q_{nn}\phi_\ell(z_r)\phi_n(z_s)}{2k_n}\int_0^h\frac{\phi_\ell(z)\phi_n(z)}{c_0^3(z)}\Delta c_z(z)dz\\
&\times\int_0^{2\pi}\int_0^{\infty}H_0^{(2)}(k_nr)H_0^{(2)}\left(k_\ell\sqrt{r^2+R^2-2rR\cos\theta}\right)\Delta c_\theta(\theta)\Delta c(r)\int_0^r\Delta c(r')dr'rdrd\theta.
\end{aligned}
\tag{3.3.3}
$$

The integrals with respect to (r,θ) in the above expression are of the general form:

$$
K_{n\ell}=\int_0^{2\pi}\int_0^{\infty}H_0^{(2)}(k_nr)H_0^{(2)}\left(k_\ell\sqrt{r^2+R^2-2rR\cos\theta}\right)\Delta c_\theta(\theta)F(r)rdrd\theta,
$$

where F is a smooth slowly varying function of r. This integral is of the same type as the integral I_{nm}, eq. (3.2.5) that we dealt with in the previous section. Applying the same method (analytical calculation close to the source/receiver, and stationary phase in the far field) this integral can be evaluated

$$
K_{n\ell}=\begin{cases}
2\Delta c_\theta(0)\dfrac{H_0^{(2)}(k_nR)}{k_n}\displaystyle\int_0^R F(r)dr & for\quad k_n=k_\ell\\[2ex]
4j\Delta c_\theta(0)\left[\dfrac{H_0^2(k_\ell R)}{k_\ell^2-k_n^2}F(0)+\dfrac{H_0^2(k_nR)}{k_n^2-k_\ell^2}F(R)\right] & for\quad k_n\neq k_\ell
\end{cases}
\tag{3.3.4}
$$

Using this result, the first term (first two lines) in (3.3.3) denoted by T_1, becomes (for $k_n = k_\ell$)

$$T_1 = \frac{\omega^2 \Delta c_\theta(0) \Delta c_r(0)}{8\rho_w^2} \sum_{n=1}^{M} \sum_{\substack{m=1 \\ m\neq n}}^{M} \frac{Q_{nm}\phi_n(z_r)\phi_m(z_s)}{k_n^2 - k_m^2} \int_0^h \frac{\phi_n^2(z)}{c_0^3(z)} \Delta c_z(z) dz \times \frac{2\Delta c_\theta(0)}{k_n} H_0^{(2)}(k_n R) \int_0^R \Delta c_r(r) dr.$$

Using the definitions (3.2.16)-(3.2.19) T_1 becomes:

$$T_1 = -\frac{\Delta c_\theta^2(0)}{4\rho_w} \sum_{n=1}^{M} \sum_{\substack{m=1 \\ m\neq n}}^{M} \frac{Q_{nm}Q_{nn}\phi_n(z_r)\phi_m(z_s)\Delta c_r(0)}{2k_n\left(k_n^2 - k_m^2\right)} H_0^{(2)}(k_n R) \int_0^R \Delta c_r(r) dr. \quad (3.3.5)$$

Applying (3.3.4) to the second term (3rd and 4th line) of (3.3.3), denoted by T_2, we obtain (for $k_n \neq k_\ell$)

$$T_2 = \frac{\omega^2 \Delta c_\theta(0)}{8\rho_w^2} \sum_{n=1}^{M} \sum_{\substack{m=1 \\ m\neq n}}^{M} \frac{Q_{nm}\phi_n(z_r)\phi_n(z_s)}{k_n^2 - k_m^2} \int_0^h \frac{\phi_n(z)\phi_m(z)}{c_0^3(z)} \Delta c_z(z) dz \times \frac{2\Delta c_\theta(0) H_0^{(2)}(k_n R)}{k_n} \int_0^R \Delta c_r^2(r) dr,$$

and using the abbreviations (3.2.16)-(3.2.19)

$$T_2 = \frac{\Delta c_\theta^2(0)}{4\rho_w} \sum_{n=1}^{M} \sum_{\substack{m=1 \\ m\neq n}}^{M} \frac{|Q_{nm}|^2 U_n}{k_n\left(k_n^2 - k_m^2\right)} H_0^{(2)}(k_n R) \int_0^R \Delta c_r^2(r) dr. \quad (3.3.6)$$

Only the dominating terms including the factors R and R^2 are retained in the second order expressions. The second line in (3.3.4) corresponding to $k_n \neq k_\ell$ is not taken into account for T_1 and T_2; this is not significance for the third order and higher but not for the second order studied here.

The third term (T_3 – last two lines) in (3.3.3) can be written as a sum of two terms. T_{3a} and T_{3b}. In T_{3a} the double sum $\sum_n \sum_\ell$ is considered over the diagonal

($\ell = n$) whereas in (T_{3b}) the rest of the sum ($\ell \neq n$) is considered. Using (3.3.4) the following expression is obtained for T_{3a}

$$T_{3a} = \frac{-j\omega^2 \Delta c_\theta(0)}{8\rho_w^2} \sum_{n=1}^{M} \frac{Q_{nn}\phi_n(z_r)\phi_n(z_s)}{2k_n} \int_0^h \frac{\phi_n^2(z)}{c_0^3(z)} \Delta c_z(z) dz$$
$$\times \frac{2\Delta c_\theta(0)}{k_n} H_0^{(2)}(k_n R) \int_0^R \Delta c_r(r) \int_0^r \Delta c_r(r') dr' dr,$$

and further using (3.2.16)-(3.2.19) we obtain the following expression

$$T_{3a} = \frac{-j\Delta c_\theta^2(0)}{4\rho_w} \sum_{n=1}^{M} \frac{|Q_{nn}|^2 U_n}{2k_n^2} H_0^{(2)}(k_n R) \int_0^R \Delta c_r(r) \int_0^r \Delta c_r(r') dr' dr. \tag{3.3.7}$$

For the term T_{3b} the eq. (3.3.4) will give

$$T_{3b} = \frac{-j\omega^2 \Delta c_\theta(0)}{8\rho_w^2} \sum_{n=1}^{M} \sum_{\substack{\ell=1 \\ \ell \neq n}}^{M} \frac{Q_{nn}\phi_\ell(z_r)\phi_n(z_s)}{2k_n} \int_0^h \frac{\phi_\ell(z)\phi_n(z)}{c_0^3(z)} \Delta c_z(z) dz$$
$$\times \frac{4j\Delta c_\theta(0)\Delta c_r(R)}{k_n^2 - k_\ell^2} H_0^{(2)}(k_n R) \int_0^R \Delta c_r(r) dr.$$

Note in this case that $F(r) = \Delta c_r(r) \int_0^r \Delta c_r(r') dr'$, which vanishes for $r = 0$. Again using definitions (3.2.16)-(3.2.19) this expression can be written as:

$$T_{3b} = \frac{-\Delta c_\theta^2(0)}{4\rho_w^2} \sum_{n=1}^{M} \sum_{\substack{\ell=1 \\ \ell \neq n}}^{M} \frac{Q_{nn}Q_{n\ell}\phi_\ell(z_r)\phi_n(z_s)\Delta c_r(R)}{2k_n\left(k_n^2 - k_\ell^2\right)} H_0^{(2)}(k_n R) \int_0^R \Delta c_r(r) dr. \tag{3.3.8}$$

By adding T_1, T_2, T_{3a} and T_{3b} and noticing that

$$T_1 + T_{3b} = \frac{-\Delta c_\theta^2(0)}{4\rho_w^2} \sum_{n=1}^{M} \sum_{\substack{m=1 \\ m \neq n}}^{M} \frac{Q_{nn}Q_{nm}V_{nm}}{2k_n\left(k_n^2 - k_m^2\right)} H_0^{(2)}(k_n R) \int_0^R \Delta c_r(r) dr. \tag{3.3.9}$$

The following expression is finally obtained for I_1

$$\begin{aligned} I_1 =& \frac{\Delta c_\theta^2(0)}{4\rho_w} \sum_{n=1}^{M} \sum_{\substack{m=1 \\ m\neq n}}^{M} \frac{|Q_{nm}|^2 U_n}{k_n \left(k_n^2 - k_m^2\right)} H_0^{(2)}(k_n R) \int_0^R \Delta c_r^2(r) dr \\ & - \frac{j\Delta c_\theta^2(0)}{4\rho_w} \sum_{n=1}^{M} \frac{|Q_{nn}|^2 U_n}{2k_n^2} H_0^{(2)}(k_n R) \int_0^R \Delta c_r(r) \int_0^r \Delta c_r(r') dr' dr \\ & - \frac{\Delta c_\theta^2(0)}{4\rho_w^2} \sum_{n=1}^{M} \sum_{\substack{m=1 \\ m\neq n}}^{M} \frac{Q_{nn} Q_{nm} V_{nm}}{2k_n \left(k_n^2 - k_m^2\right)} H_0^{(2)}(k_n R) \int_0^R \Delta c_r(r) dr. \end{aligned} \tag{3.3.10}$$

For the integral I_2, eq. (3.3.2), using the normal-mode representation for the background Green's functions we get:

$$\begin{aligned} I_2 =& \frac{j^2}{16\rho_w^2} \int_0^h \int_0^{2\pi} \int_0^{\infty} \sum_{n=1}^{M} \phi_n(z_s)\phi_n(z) H_0^{(2)}(k_n r) \left[\frac{3\omega^2}{c_0^4(z)} \Delta c_r^2(r) \Delta c_\theta^2(\theta) \Delta c_z^2(z)\right] \\ & \times \sum_{m=1}^{M} \phi_m(z)\phi_m(z_r) H_0^{(2)}\left(k_m \sqrt{r^2 + R^2 - 2rR\cos\theta}\right) r dr d\theta dz \\ =& \frac{-1}{16\rho_w} \sum_{n=1}^{M} \sum_{m=1}^{M} \phi_n(z_s)\phi_m(z_r) \frac{3\omega^2}{\rho_w} \int_0^h \phi_n(z)\phi_m(z) \frac{\Delta c_z^2(z)}{c_0^4(z)} dz \\ & \times \int_0^{2\pi} \int_0^{\infty} H_0^{(2)}(k_n r) H_0^{(2)}\left(k_m \sqrt{r^2 + R^2 - 2rR\cos\theta}\right) \Delta c_r^2(r) \Delta c_\theta^2(\theta) r dr d\theta. \end{aligned}$$

Applying eq. (3.3.4) to the integral with respect to (r, θ) we finally obtain the following expression for I_2

$$I_2 = \frac{\Delta c_\theta^2(0)}{4\rho_w} \int_0^R \Delta c_r^2(r) dr \sum_{n=1}^{M} \frac{U_n Q'_n}{k_n} H_0^{(2)}(k_n R), \tag{3.3.11}$$

where

$$Q'_n = \frac{3\omega^2}{\rho_w} \int_0^h \phi_n^2(z) \frac{\Delta c_z^2(z)}{c_0^4(z)} dz,$$

where again we have omitted the sum over the off-diagonal terms ($m \neq n$) since it is not significant for the second order.

Combining the relations (3.3.10) and (3.3.11) we obtain the following expression for the second-order term of the Born approximation

$$\begin{aligned}\Delta G_2(\mathbf{x}_r|\mathbf{x}_s) =& \frac{-j\Delta c_\theta^2(0)}{4\rho_w}\sum_{n=1}^{M}\left\{\frac{-jQ_{nn}}{2k_n}\sum_{\substack{m=1\\m\neq n}}^{M}\frac{Q_{nm}V_{nm}}{\Lambda_{nm}}\int_0^R \Delta c_r(r)dr\right.\\ &+\frac{|Q_{nn}|^2U_n}{2k_n^2}\int_0^R \Delta c_r(r)\int_0^r \Delta c_r(r')dr'dr \qquad (3.3.12)\\ &\left.+\frac{jU_n}{k_n}\left(\sum_{\substack{m=1\\m\neq n}}^{M}\frac{|Q_{nm}|^2}{\Lambda_{nm}}+Q'_n\right)\int_0^R \Delta c_r^2(r)dr\right\}H_0^{(2)}(k_nR).\end{aligned}$$

As in the case of the first Born approximation this is a generalization of previous results obtained for range-independent perturbations [28]. The above expression contains the dominating terms, including the factors R and R^2, where as the remaining terms (not essential for the second-order approximation) have been omitted.

3.4 Rytov-Keller approximation

Once we have obtained expressions for the first and second Born approximations, it is straightforward to obtain the corresponding expressions for the Rytov approximation by applying eq. (2.2.5). The Rytov approximation performs well in the case of single-component waves, but fails in the case of multiple component waves such as the present case [36]. The reason is that each component mode of a multiple-component wave field is characterized by its own phase, with different perturbation behavior. The standard Rytov approximation on the other hand assumes that the whole wave field can be described by a single phase. In such cases the Rytov method must be

applied to each wave component separately and not to the total field as Keller pointed out [16]. This means consider the phase perturbation of each component separately. In this connection the perturbed Green's function (up to the first order) is written as follows:

$$G_{RK} = \sum_{n=1}^{M} G_{0_n} e^{\Delta\Psi_n}, \tag{3.4.1}$$

where G_{0_n} is the $n-th$ mode contribution to the unperturbed Green's function. Based on eq. (2.2.5) and (3.2.20) the first-order term of the Rytov approximation for the $n-th$ mode can be calculated as follows

$$\Delta\Psi_{1_n} = \frac{-j\Delta c_\theta(0)}{4\rho_w G_{0_n}} \left(\sum_{\substack{m=1 \\ m\neq n}}^{M} \frac{Q_{nm}V_{nm}}{\Lambda_{nm}} + j\frac{Q_{nn}U_n}{k_n} \int_0^R \Delta c_r(r)dr \right) H_0^{(2)}(k_n R), \tag{3.4.2}$$

where Q_{nm}, V_{nm}, Λ_{nm}, U_n are the quantities defined in eq. (3.2.16)-(3.2.19).

Using the normal-mode expression (3.1.7) for the background Green's function C_{0_n} finally obtain for the phase perturbation of the $n-th$ mode

$$\Delta\Psi_{1_n} = \frac{-\Delta c_\theta(0)}{2U_n} \sum_{\substack{m=1 \\ m\neq n}}^{M} \frac{Q_{nm}V_{nm}}{\Lambda_{nm}} - j\frac{\Delta c_\theta(0)Q_{nn}}{2k_n} \int_0^R \Delta c_r(r)dr. \tag{3.4.3}$$

The dominating term in this expression with respect to the phase is the second (imaginary) one. The first term is real and represents attenuation effects on the phase).

Taking into account the Born-Rytov relations eq. (2.2.5) and the expression for the

second-order term of the Born approximation the corresponding term of the Rytov-Keller approximation can be written as follows

$$\begin{aligned}\Delta\Psi_{2_n} =& \frac{-j\Delta c_\theta^2(0)}{4G_{0_n}\rho_w}\left\{\frac{-j}{2k_nQ_{nn}}\sum_{\substack{m=1\\m\neq n}}^{M}\frac{Q_{nm}V_{nm}}{\Lambda_{nm}}\int_0^R\Delta c_r(r)dr\right.\\ &+\frac{|Q_{nn}|^2U_n}{2k_n^2}\int_0^R\Delta c_r(r)\int_0^r\Delta c_r(r')dr'dr\\ &\left.+\frac{jU_n}{k_n}\left(\sum_{\substack{m=1\\m\neq n}}^{M}\frac{|Q_{nm}|^2}{\Lambda_{nm}}+Q'_n\right)\int_0^R\Delta c_r^2(r)dr\right\}H_0^{(2)}(k_nR)\\ &-\frac{1}{2}\left(\Delta\Psi_{1_n}\right)^2\end{aligned} \tag{3.4.4}$$

Substituting the modal representation for G_{0n} obtain

$$\begin{aligned}\Delta\Psi_{2_n} =& \frac{j\Delta c_\theta^2(0)}{4U_nk_nQ_{nn}}\sum_{\substack{m=1\\m\neq n}}^{M}\frac{Q_{nm}V_{nm}}{\Lambda_{nm}}\int_0^R\Delta c_r(r)dr\\ &-\frac{\Delta c_\theta^2(0)|Q_{nn}|^2}{4k_n^2}\int_0^R\Delta c_r(r)\int_0^r\Delta c_r(r')dr'dr\\ &-\frac{j\Delta c_\theta^2(0)}{2k_n}\left(\sum_{\substack{m=1\\m\neq n}}^{M}\frac{|Q_{nm}|^2}{\Lambda_{nm}}+Q'_n\right)\int_0^R\Delta c_r^2(r)dr\\ &-\frac{1}{2}\left(\Delta\Psi_{1_n}\right)^2\end{aligned} \tag{3.4.5}$$

The dominating term in this expression in the case of a zero-mean range perturbation is the imaginary term on the third line. All other terms either vanish or they are real, which means that they have no effect on the phase.

In Appendix C it is seen that the second-order Rytov-Keller approximation has strong similarities to the second-order adiabatic approximation of the Green's function. This indicates that Keller's approach of treating each wave component separately is based on the assumption that there is no interaction (energy exchange)

between different modes in the perturbed state.

Chapter 4

Numerical Results

In this chapter some numerical examples for the waveform perturbation approach are presented. Three different range-dependent environments are considered which are perturbations of a range independent environment characterized by a linear sound speed profile shown in Fig. 4.1. The particular profile (1503 m/sec at the surface and 1546.9 m/sec at 2500 m depth) represents a typical average profile for the western Mediterranean sea during winter. The water depth is 2500 m, both source and receiver depths are set to 150 m; the horizontal distance between source and receiver is taken 600 km (these values are motivated from the Thetis-2 tomography experiment conducted from January to October 1994 in the Western Mediterranean [34]). The emitted signal is assumed to be a Gaussian pulse of central frequency 150 Hz and effective bandwidth 60 Hz. Acoustic calculations are performed in the frequency range from 100 to 200 Hz. Fig. 4.2 shows the background arrival pattern corresponding to the reference profile of Fig. 4.1. For the calculation the complex pressure was evaluated at 501 frequencies from 100 Hz to 200 Hz, with a step of 0.2 Hz, using a normal-mode code and then applying FFT. An absorbing bottom is assumed filtering out the bottom-interacting part of the acoustic energy [7].

In the following the calculations will focus on the late part of the arrival pattern

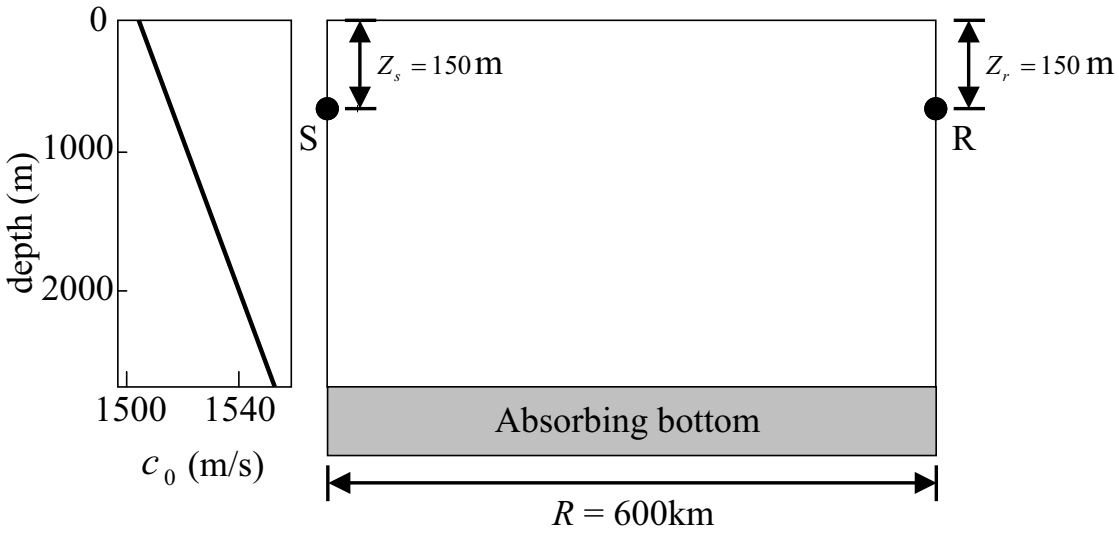

Figure 4.1: Background environment for the three example-cases.

(represented by the low-order modes) – bottom panel in Fig. 4.2 – which is most affected by range dependence.

A velocity perturbation of the form $\Delta c(r, z) = \Delta c_r(r)\Delta c_z(z)$ is considered. Fig. 4.3 shows the depth mode $\Delta c_z(z)$ used in all examples. This mode is confined in the upper 50 m layer (range dependence is more pronounced in the near-surface layer), reaching 1 m/sec at the surface and decreasing linearly to zero at 50 m depth and remains zero thereafter. As regards the range mode $\Delta c_r(r)$ tree cases are considered:

1) Linear zero-mean range dependence.

2) Bilinear zero-mean range dependence.

3) Linear non-zero mean range dependence.

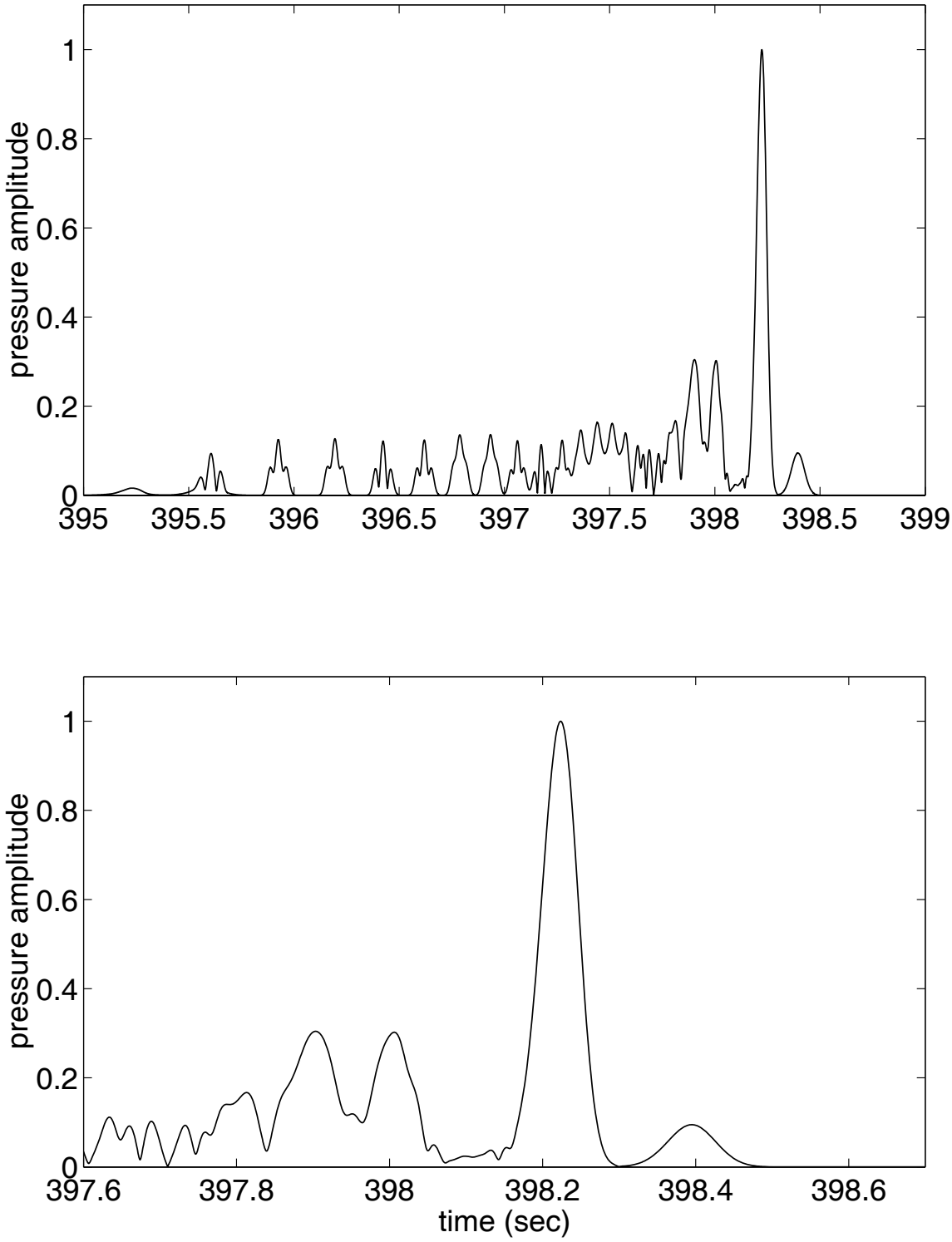

Figure 4.2: Background arrival pattern corresponding to the reference profile. Bottom panel focus on the late arrival pattern represented by the low order modes.

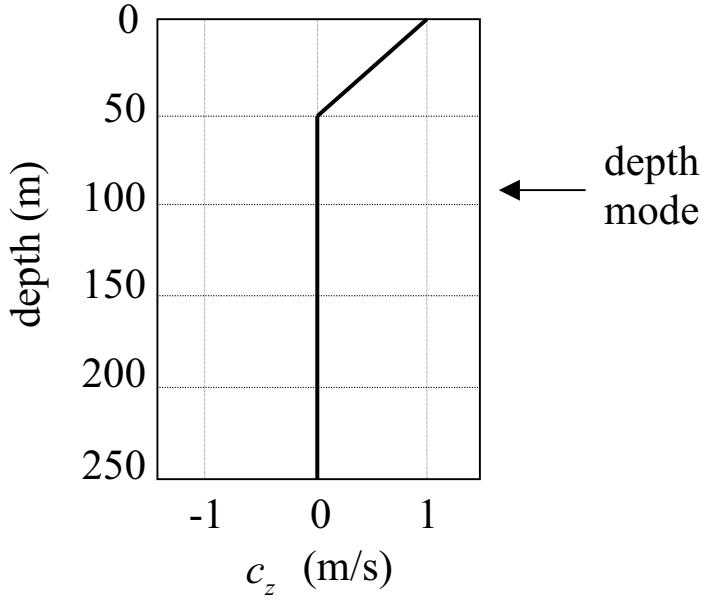

Figure 4.3: The depth mode Δc_z, used in all examples.

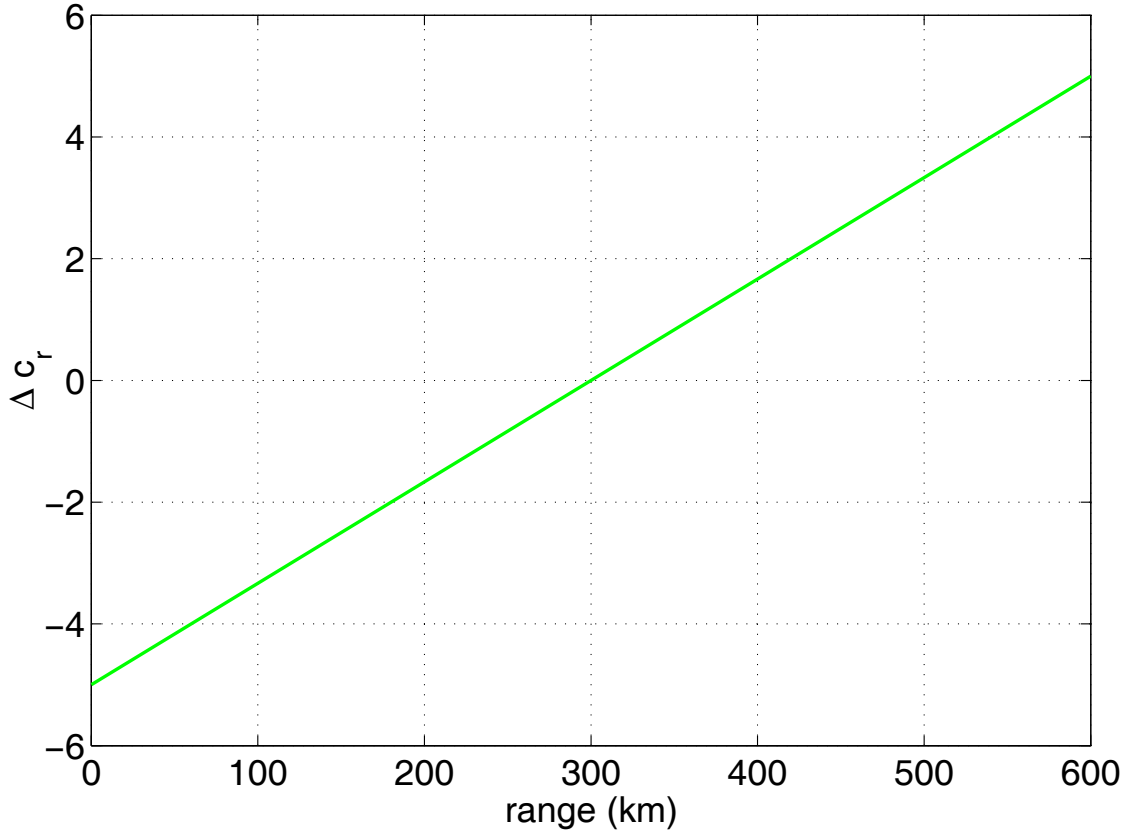

Figure 4.4: The range mode Δc_r of the sound-speed perturbation (linear zero-mean).

4.1 Linear zero-mean range dependence

In the first example the range mode Δc_r of the sound-speed perturbation is linear from -5 at the source to 5 at the receiver, Fig. 4.4. Fig. 4.5 shows the resulting sound speed profiles at various ranges. The 10 m/s difference in the sound speed over the 600 km corresponds to what has been observed in the Western Mediterranean Sea (warming trend from north to south).

Fig. 4.6 shows the result of the exact calculation of the late arrival pattern for the range-dependent perturbed state, based on adiabatic and coupled-mode theory.

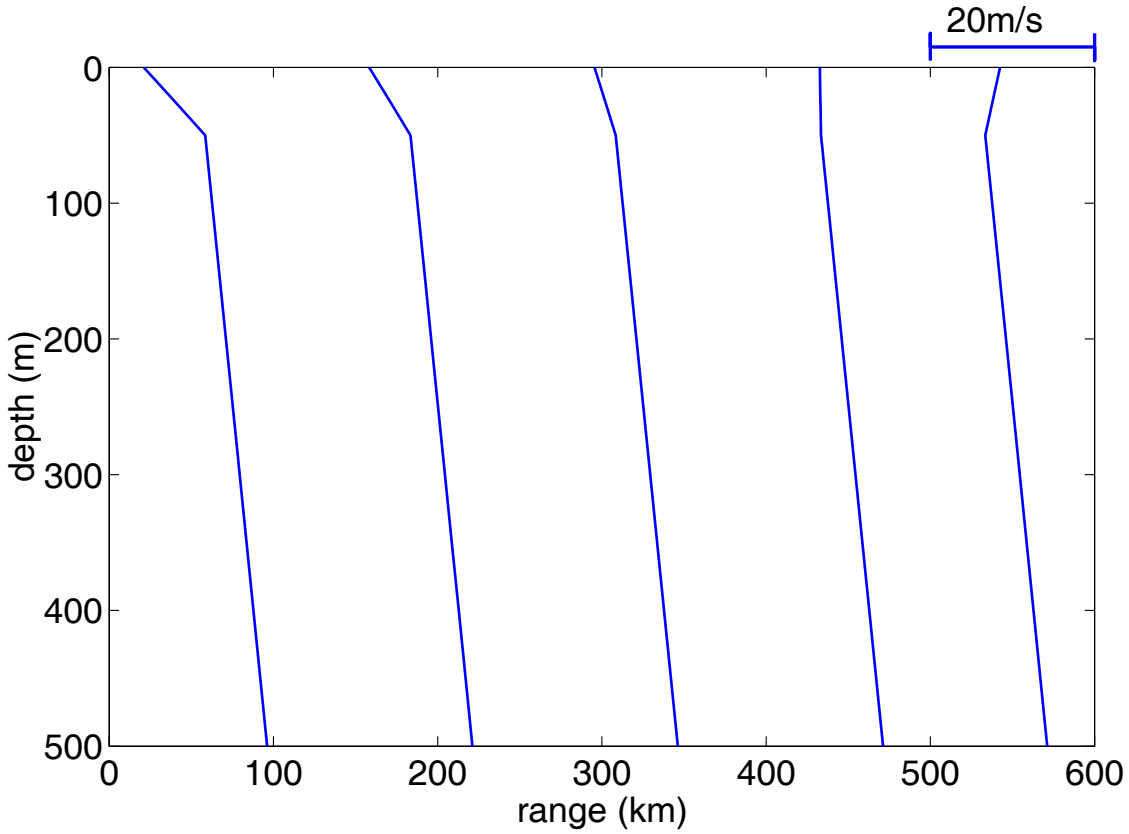

Figure 4.5: Sound speed profiles at various ranges (linear zero-mean RD environment).

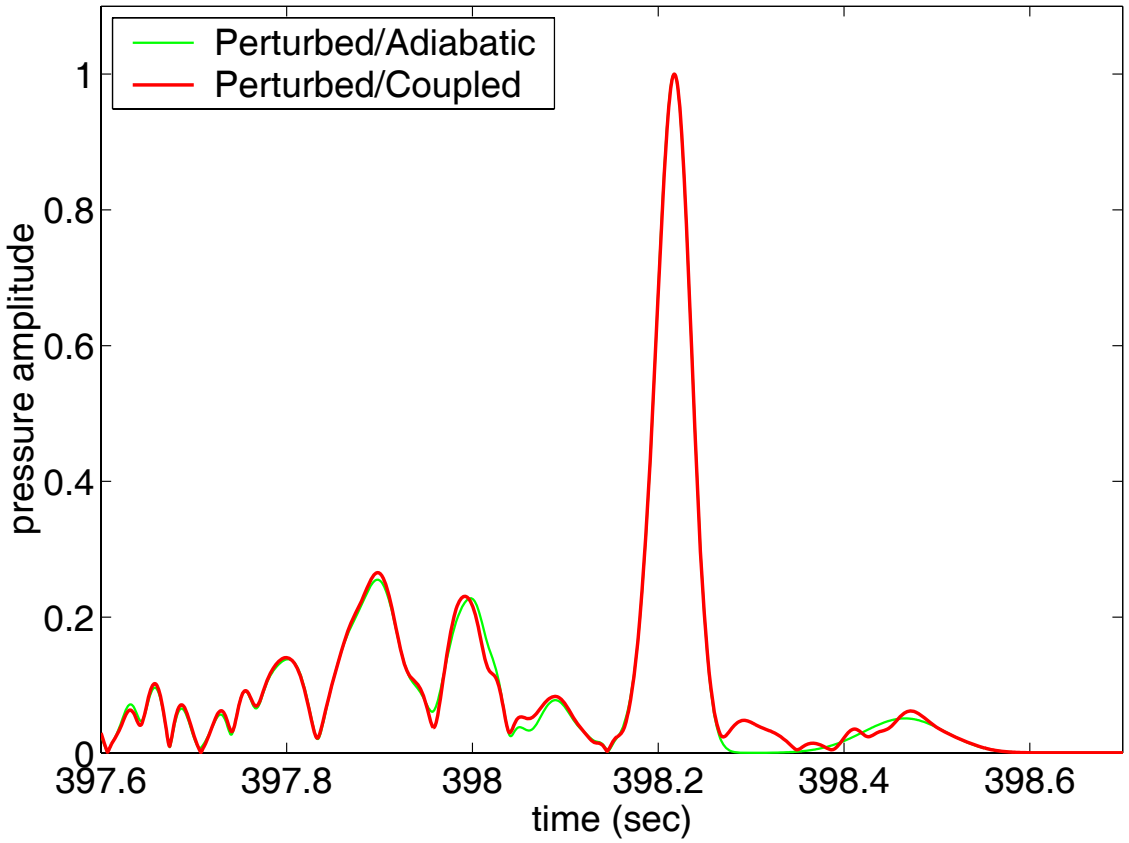

Figure 4.6: Exact calculation of the late arrival pattern (linear zero-mean) for the range-dependent perturbed state.

The small deviation between the two predictions indicates that mode coupling is not significant in this case.

Fig. 4.7 shows the arrival pattern predicted from the second Born approximation together with the exact adiabatic prediction and the background arrival pattern. Since the range mode $\Delta c_r(r)$ of the sound-speed perturbation has zero mean the first Born approximation result is practically the same as the background arrival pattern. From this figure we see that the Born approximation differs from the background arrival pattern in amplitude but hardly as far the arrival times are concerned. In

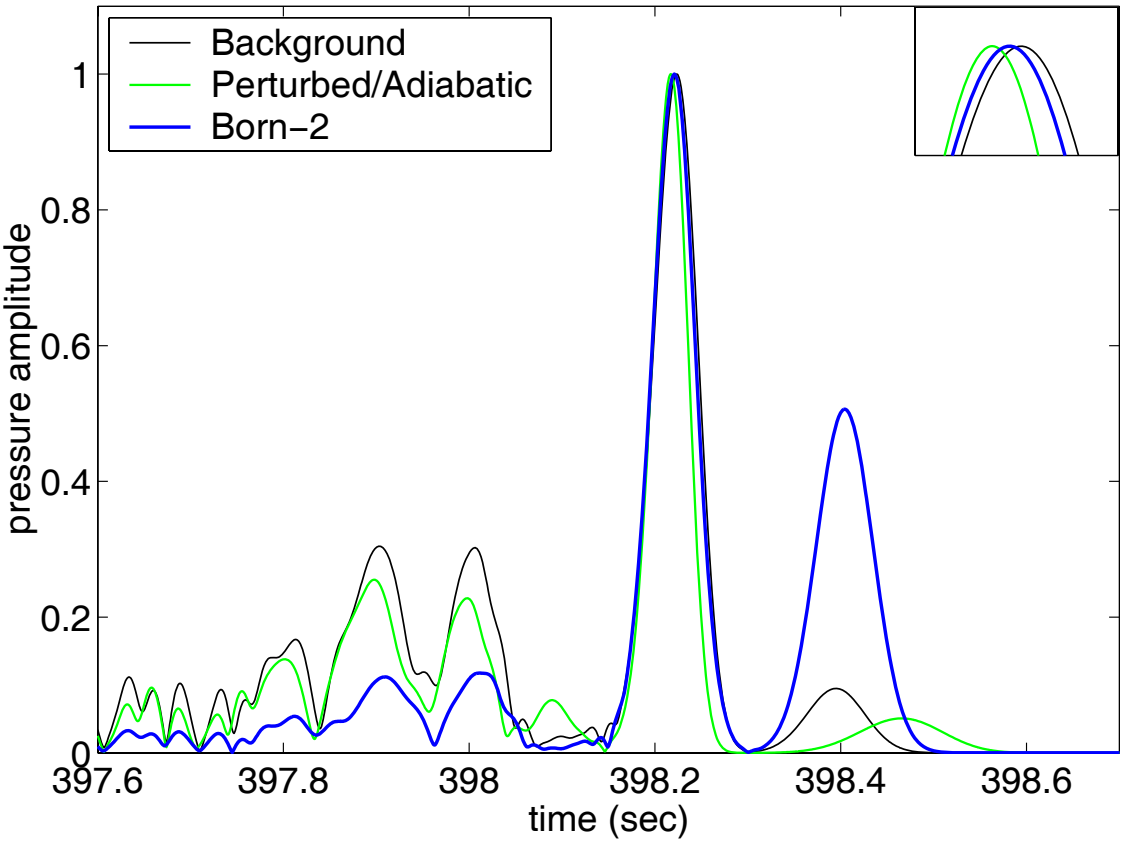

Figure 4.7: Late arrival pattern predicted from the Born approximation, together with the exact adiabatic prediction and the background arrival pattern (linear zero-mean).

the perturbed arrival pattern on the other hand the arrivals, especially the late ones, are significantly displaced by as much as 70 msec with respect to their background locations. Thus, the Born approximation fails to predict correct arrival times in the perturbed state.

Fig. 4.8 shows the arrival pattern predicted from the second Rytov approximation; the exact adiabatic prediction and the background arrival pattern are also show in this figure, as before. Again since the range mode $\Delta c_r(r)$ was zero mean the first Rytov approximation, relying on the first Born approximation, predicts no deviation

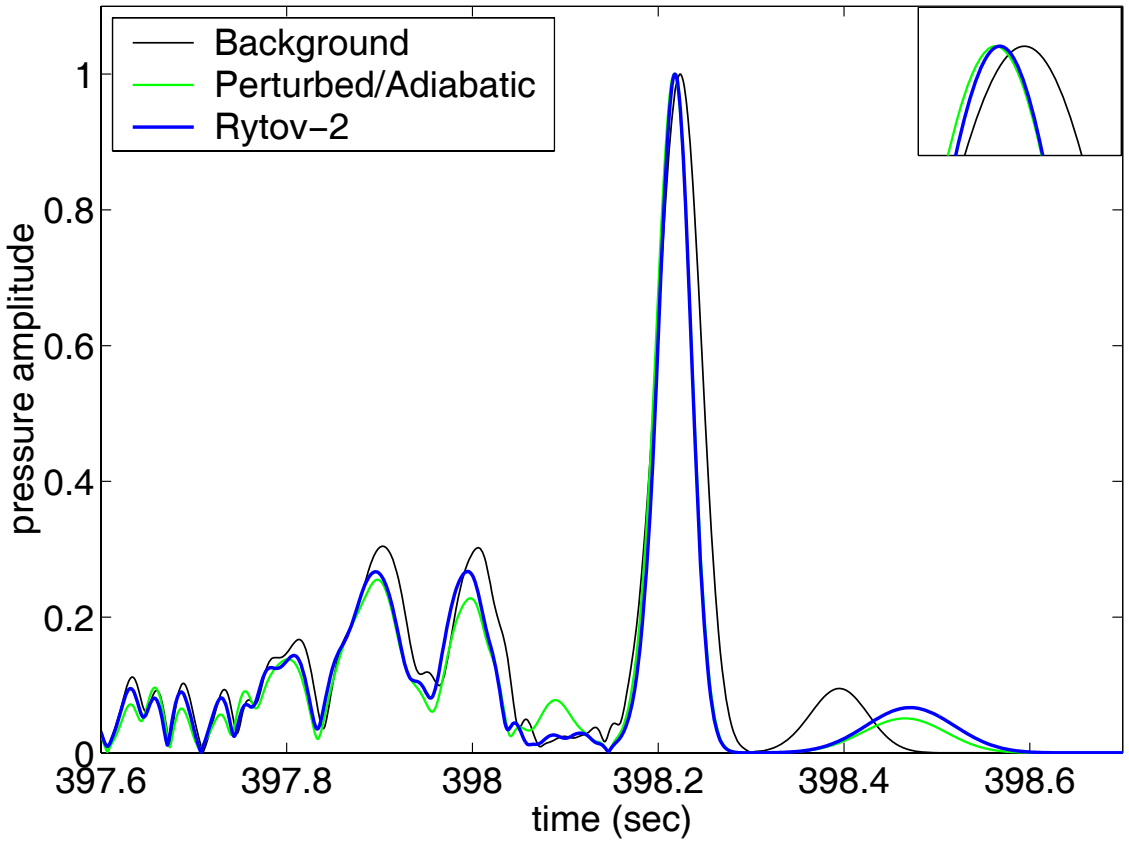

Figure 4.8: Late arrival pattern predicted from the Rytov approximation, together with the exact adiabatic prediction and the background arrival pattern (linear zero-mean).

from the background arrival pattern. We see that the Rytov approximation manages to describe efficiently the arrival shifts in all cases. Thus for the late arrivals it reproduces the delays, with respect to the background state, predicted by the exact calculations. For the earlier arrivals the exact calculations predict advancement of the perturbed arrivals with respect to the background state. This behavior is very well reproduced by the second-order Rytov approximation as well.

Fig. 4.9 presents a more detailed comparison of travel times of the first 10 modes

at the central frequency (150 Hz). The horizontal axis of this figure measures distance from the source whereas the vertical axis measures the equivalent travel time which is defined as the group slowness $s_{g,m}(r)$ of the mode m, which is different from range to range, multiplied by the source-receiver range R. The group slowness is obtained from the relation $s_{g,m}(r) = \partial k_m(r;\omega)/\partial\omega$ by applying numerical differentiation with respect to ω. The adiabatic arrival time at the receiver is given by

$$t_{g,m} = \int_0^R s_{g,m}(r)dr = \frac{1}{R}\int_0^R Rs_{g,m}(r)dr$$

and thus it is just the average of the equivalent travel time.

In Fig. 4.9 the equivalent travel times corresponding to the background and exact adiabatic predictions are shown, as well as the first and second Rytov approximation. The background equivalent travel time for each mode is constant with respect to range and equals the corresponding group travel time. In the first Rytov approximation the phase has a linear dependency on the sound-speed perturbation and since the latter in this case is a linear function of range, the equivalent travel times in the first Rytov approximation are linear functions of range, as we see in Fig. 4.9, fully reflecting the zero-mean property of the range mode $\Delta c_r(r)$. In this connection the first Rytov approximation results in exactly the same group travel times as in the background situation. In the second Rytov approximation the phase is a quadratic functional of the sound-speed perturbation and, since the latter varies linearly with range, the corresponding equivalent travel times are quadratic functions of range, and thus their average will be different than the background group travel times. In this sense the effect of range dependence an travel times is a second-order effect.

We see from Fig. 4.9 that the second Rytov approximation lies very close to the exact adiabatic prediction as far as the equivalent travel times are concerned. This explains the good agreement between the Rytov approximation and the adiabatic prediction in the previous figure.

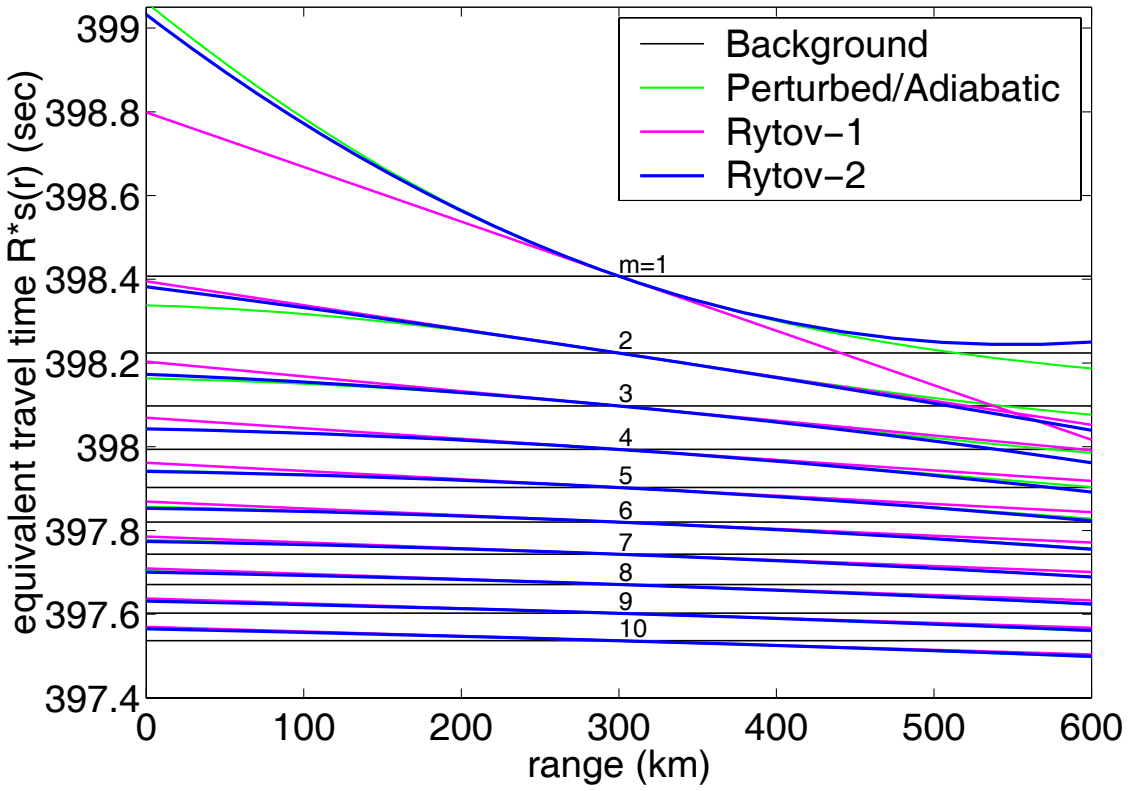

Figure 4.9: Travel-time comparison for modes 1 – 10, at the central frequency (150 Hz).

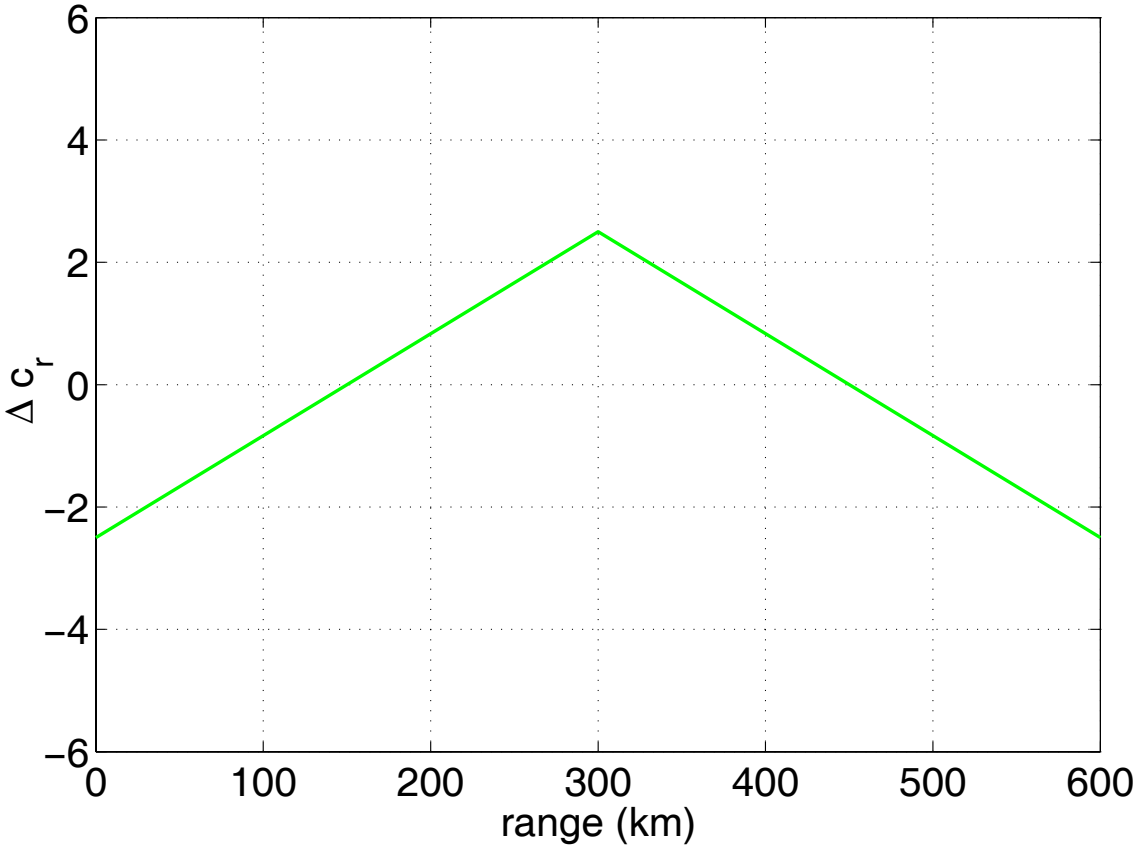

Figure 4.10: Range mode Δc_r of the sound speed perturbation - bilinear (I).

4.2 Bilinear zero-mean range dependence

In the second example the range mode Δc_r is bilinear with zero mean. Two cases are considered with different slopes.

Case I:

In the first case Δc_r increases linearly from -2.5 at the source to 2.5 at 300 km range and then decreases linearly to -2.5 at the receiver, Fig. 4.10. Fig. 4.11 shows the resulting sound-speed profiles, at various ranges.

Fig. 4.12 shows the result of the exact calculation of the late arrival pattern for

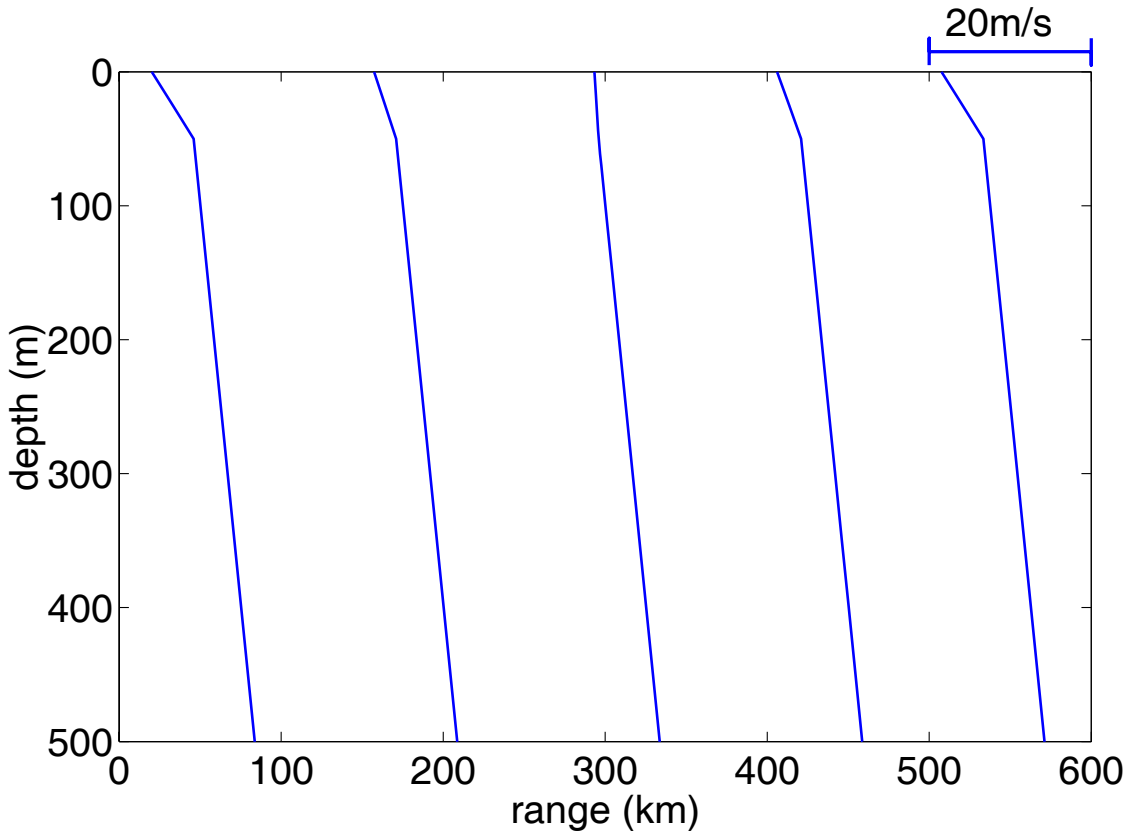

Figure 4.11: Sound speed profiles at various ranges – bilinear (I).

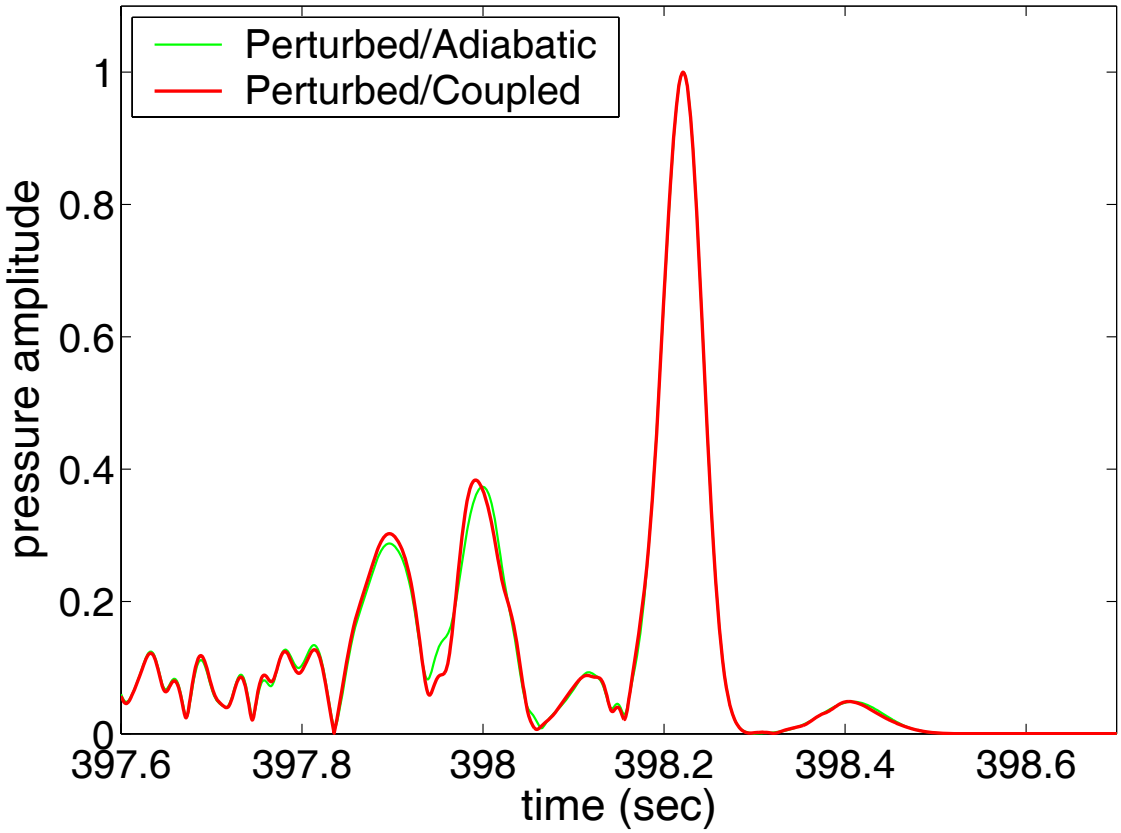

Figure 4.12: Exact calculation of the late part of the arrival pattern (bilinear (I)) for the range dependent perturbed state.

the range-dependent perturbed state, based on adiabatic and coupled-mode theory. The small deviation between the two predictions indicate that mode coupling is not significant in this case.

Fig. 4.13 shows the arrival pattern predicted from the second Born approximation, together with the exact adiabatic prediction and the background arrival pattern. Since the range mode $\Delta c_r(r)$ of the sound-speed perturbation has zero mean the first Born approximation result is practically the same as the background arrival pattern. From this figure we see that the Born approximation cannot describe the travel-time

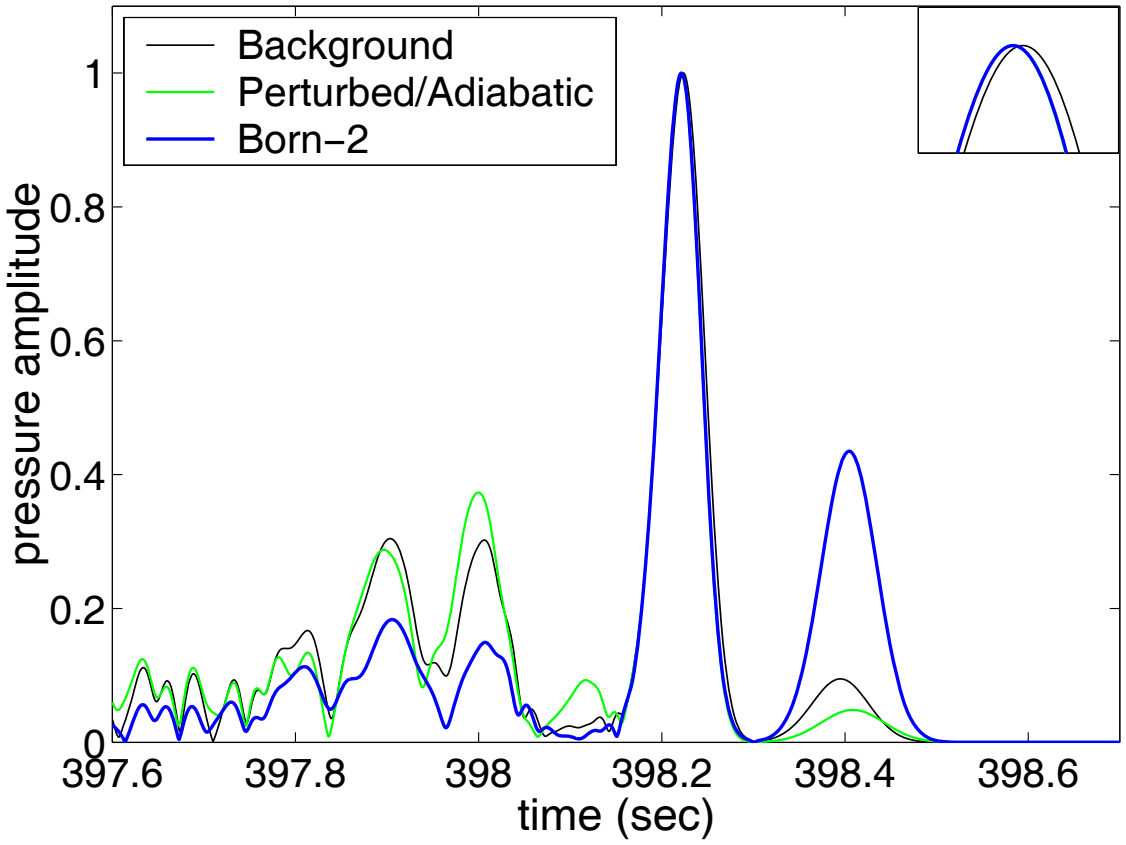

Figure 4.13: Late arrival pattern predicted from the Born approximation, together with the exact adiabatic prediction and the background arrival pattern (bilinear (I)).

and amplitude changes from the background to the perturbed state.

Fig. 4.14 shows the late arrival pattern predicted from the second Rytov approximation together with the exact adiabatic prediction and the background arrival pattern. Since the range mode Δc_r was zero mean the first Rytov approximation, relying on the first Born approximation, predicts no deviation from the background arrival pattern. The Rytov approximation manages to describe efficiently the travel-time amplitude changes in nearly all cases. Thus for the late arrivals it reproduces the delays, with respect to the background state, predicted by the exact calculations.

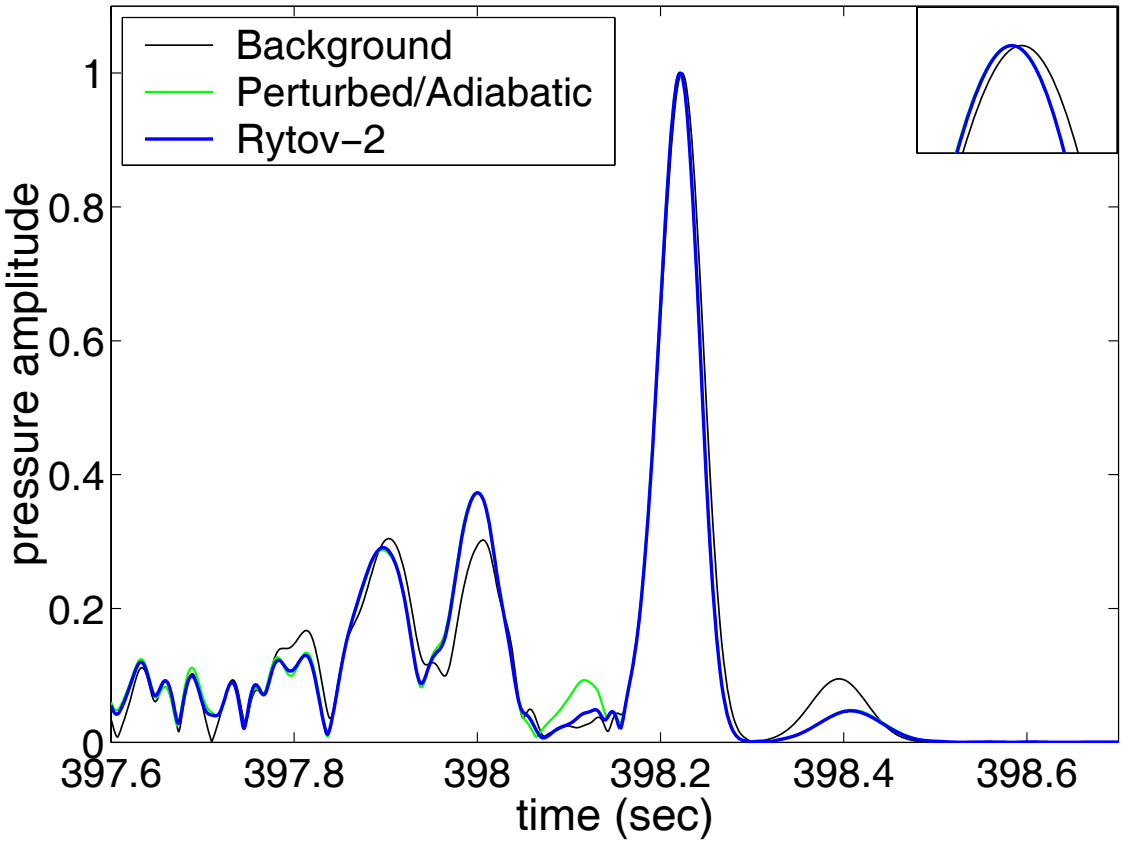

Figure 4.14: Late arrival pattern predicted from the Rytov approximation, together with the exact adiabatic prediction and the background arrival pattern (bilinear (I)).

For the earlier arrivals the exact calculations predict advancement of the perturbed arrivals with respect to the background state. This behavior is very well reproduced by the second-order Rytov approximation.

Case II:

In the second case Δc_r increases linearly from -5 at the source to 5 at 300 km range and then decreases linearly to -5 at the receiver, Fig. 4.15. Fig. 4.16 shows the resulting sound-speed profiles, at various ranges.

Fig. 4.17 shows the result of the exact calculation of the late arrival pattern for

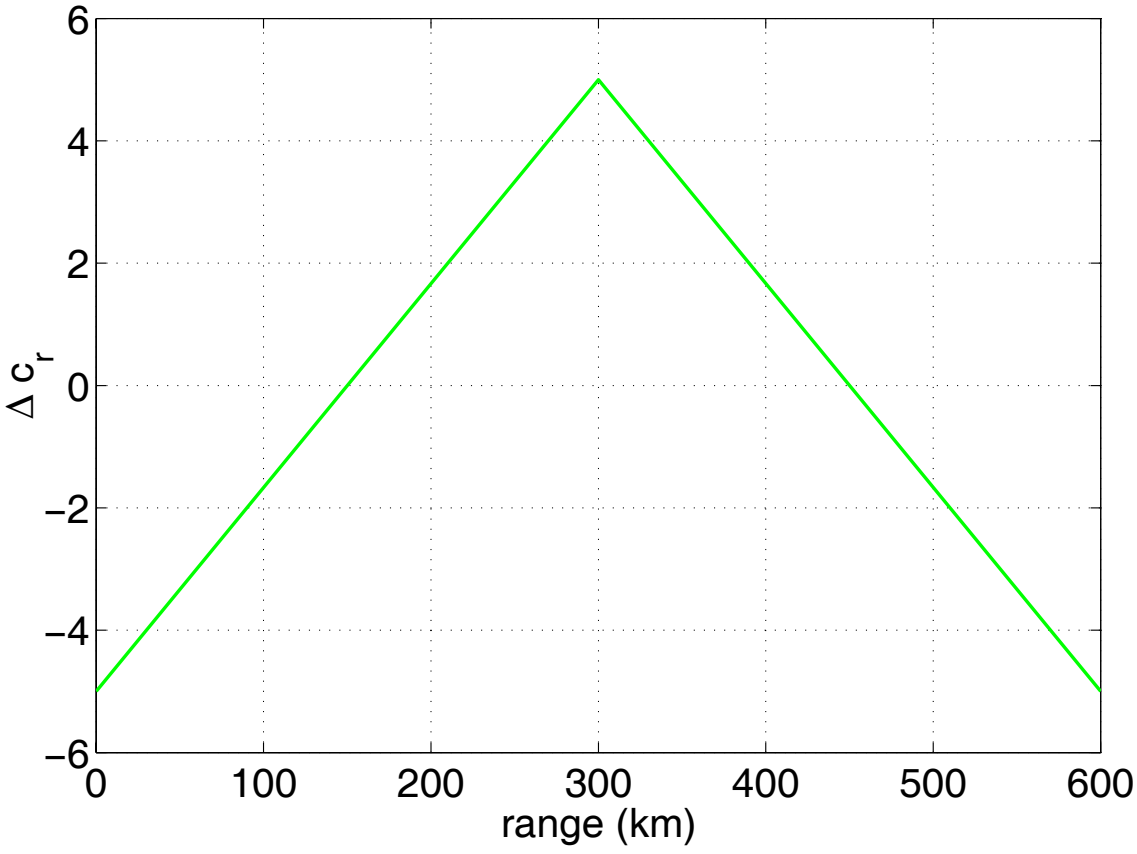

Figure 4.15: Range mode Δc_r of the sound speed perturbation – bilinear (II).

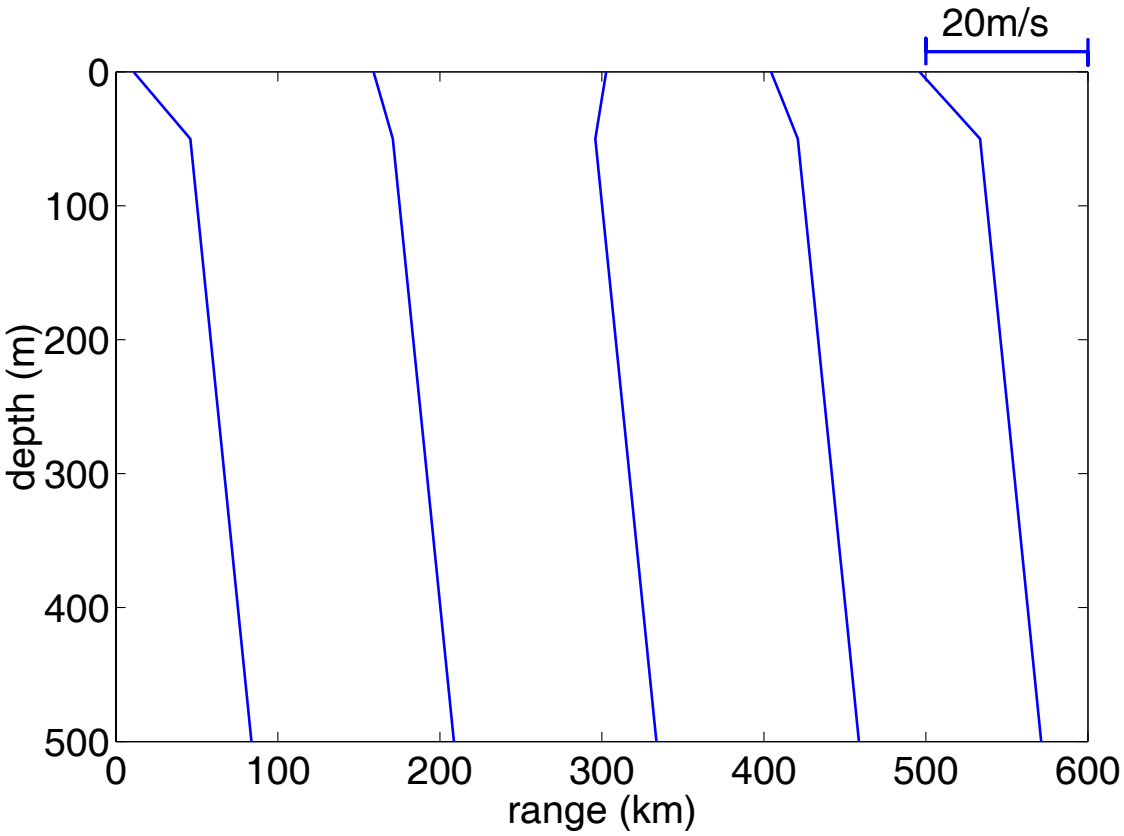

Figure 4.16: Sound speed profiles, at various ranges– bilinear (II).

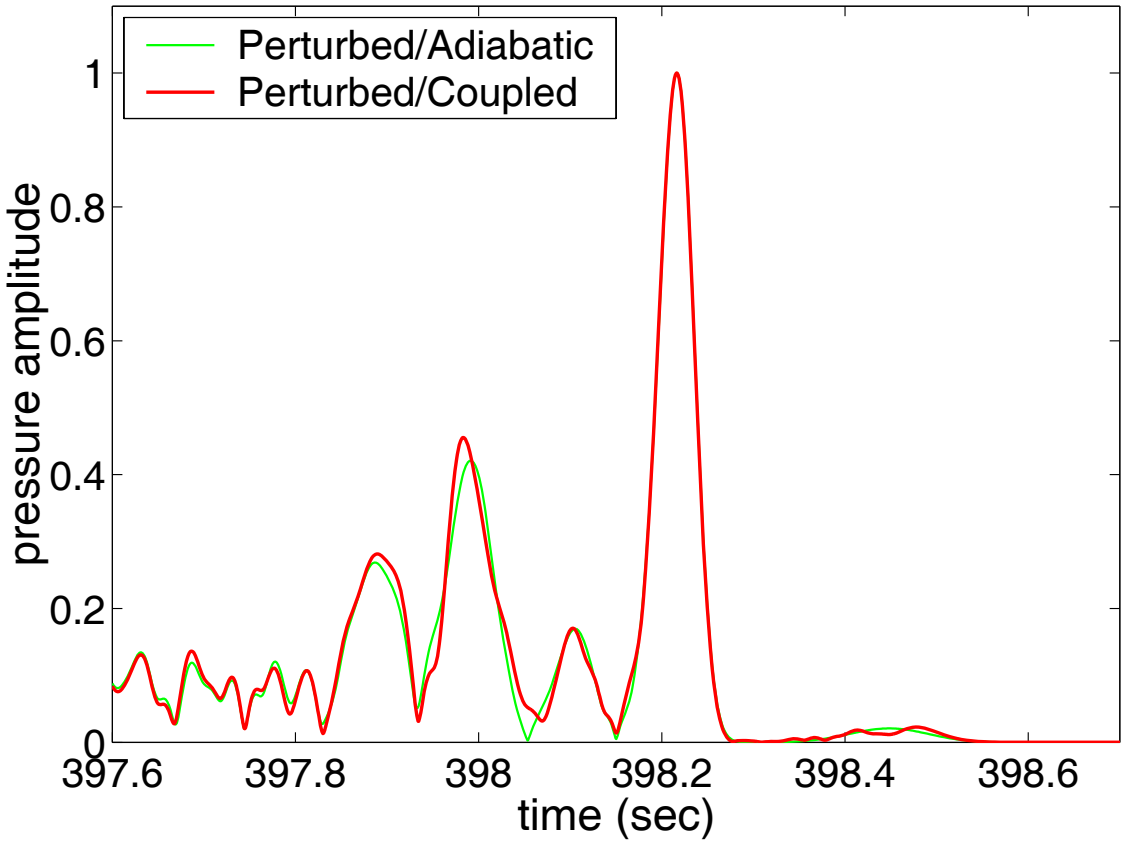

Figure 4.17: Exact calculation of the late arrival pattern (bilinear (II)), for the range dependent perturbed state.

the range-dependent perturbed state, from adiabatic and coupled-mode theory. The deviations between the two predictions indicate that mode coupling starts to become significant in this case.

Fig. 4.18 shows the late arrival pattern predicted from the second Born approximation together with the exact adiabatic prediction and the background arrival pattern. Since the range mode $\Delta c_r(r)$ has zero mean the first Born approximation is practically the same as the background arrival pattern. From this figure we see that the Born approximation fails to describe the travel time and amplitude changes from the

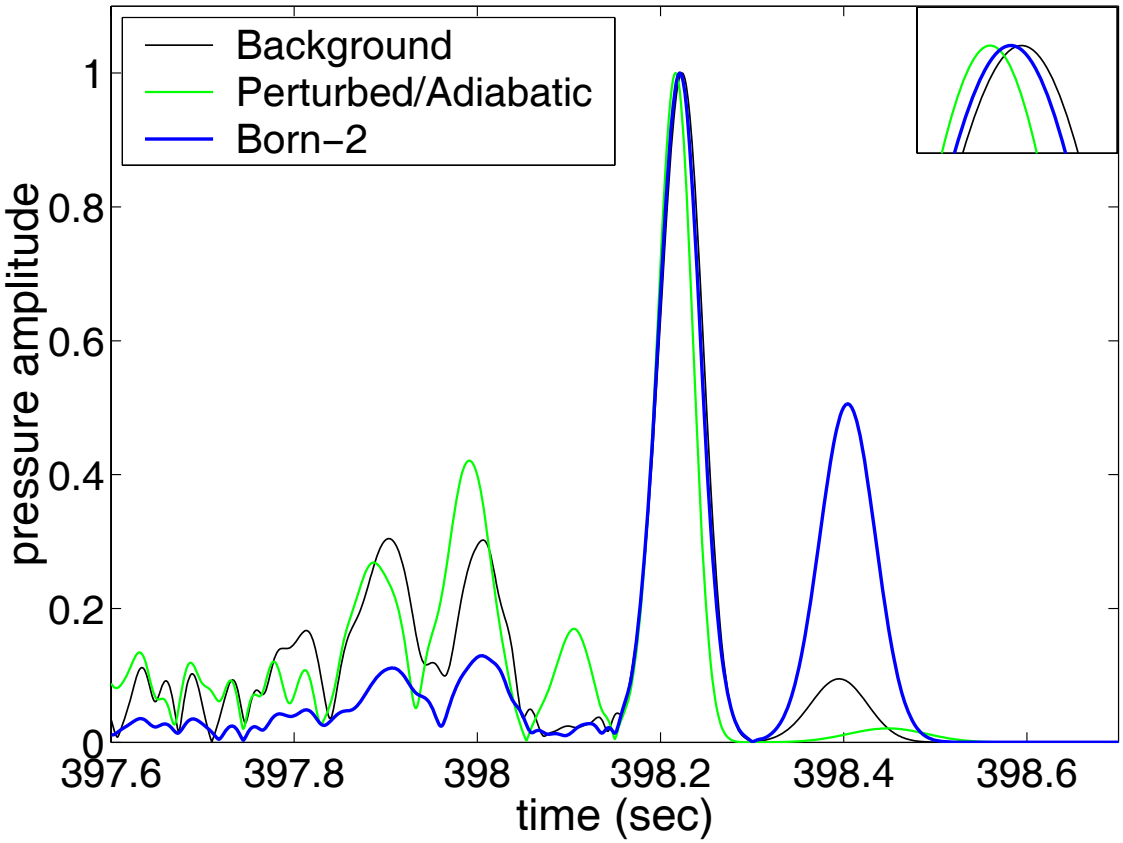

Figure 4.18: Late arrival pattern predicted from the Born approximation, together with the exact adiabatic prediction and the background arrival pattern (bilinear (II)).

background to the perturbed state.

Fig. 4.19 shows the late arrival pattern predicted from the second Rytov approximation. Since the range mode Δc_r was zero mean the first Rytov approximation, relying on the first Born approximation, predicts no deviation from the background and the adiabatic prediction is included in Fig. 4.19 as in the previous figure. In Fig. 4.19 it is confirmed that the results of the second Rytov, they approach very well the perturbed/adiabatic calculations.

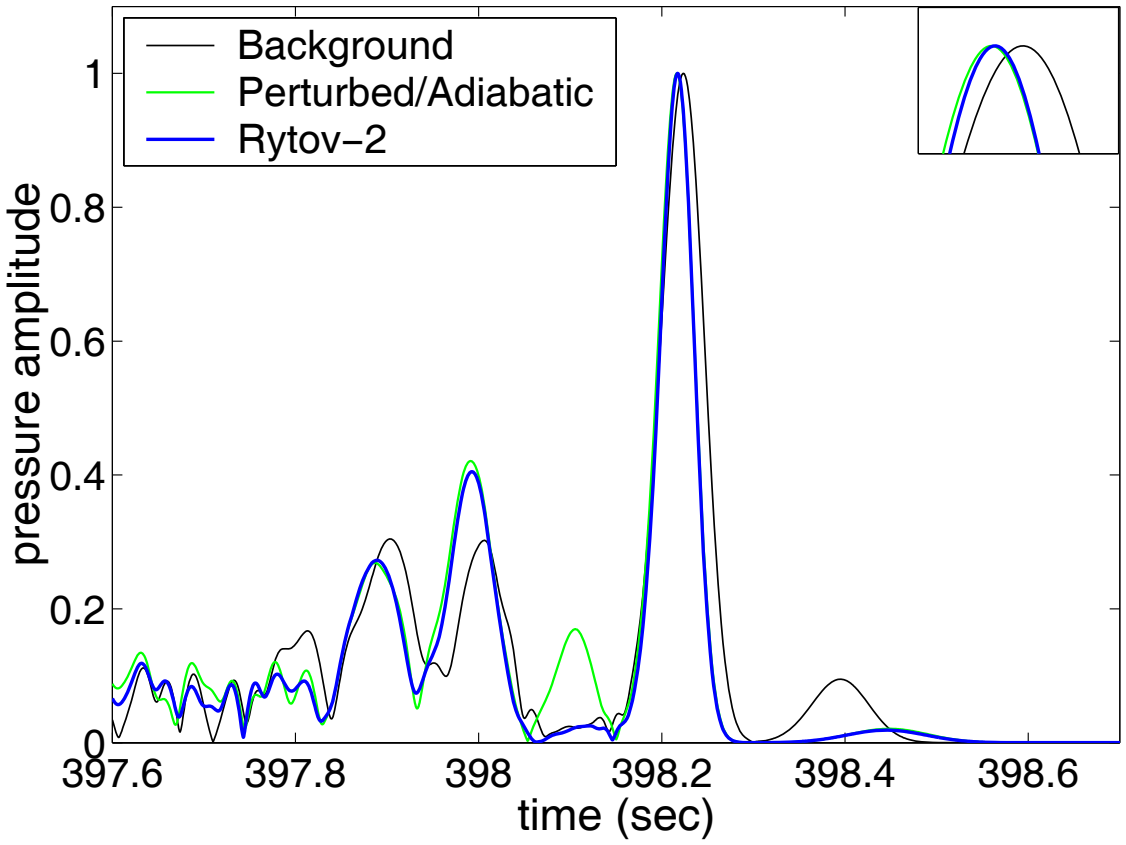

Figure 4.19: Late arrival pattern predicted from the Rytov approximation, together with the exact adiabatic prediction and the background arrival pattern (bilinear (II)).

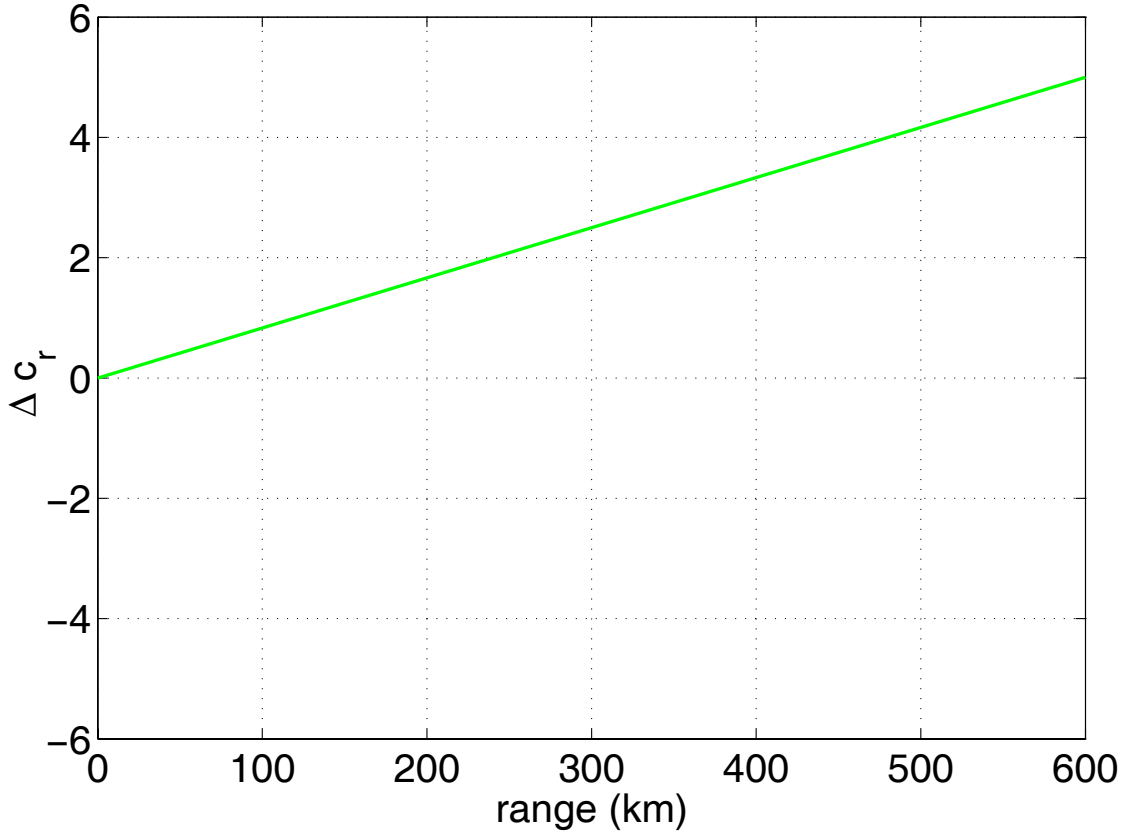

Figure 4.20: Range mode Δc_r of the sound speed perturbation (linear non-zero mean).

4.3 Linear non-zero mean range dependence

In this last case we consider as in the first example, that the range mode Δc_r of the sound-speed perturbation is linear, but not zero mean, from 0 at the source to 5 at the receiver, Fig. 4.20. Fig. 4.21 shows the resulting sound speed profiles, at various ranges.

Fig. 4.22 shows the result of the exact calculation of the late arrival pattern for the range-dependent perturbed state, from adiabatic and coupled-mode theory. The small deviation between the two predictions indicate that mode coupling is not significant

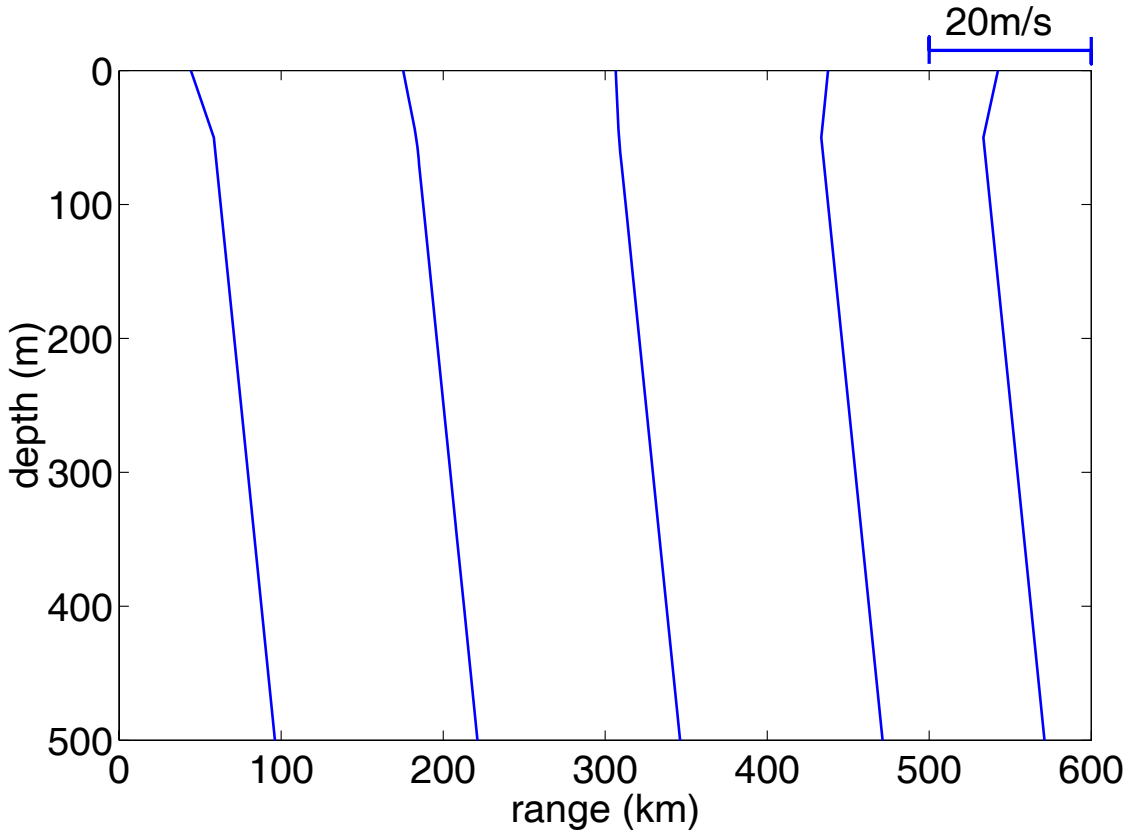

Figure 4.21: Sound speed profiles at various ranges (linear non-zero means RD environment).

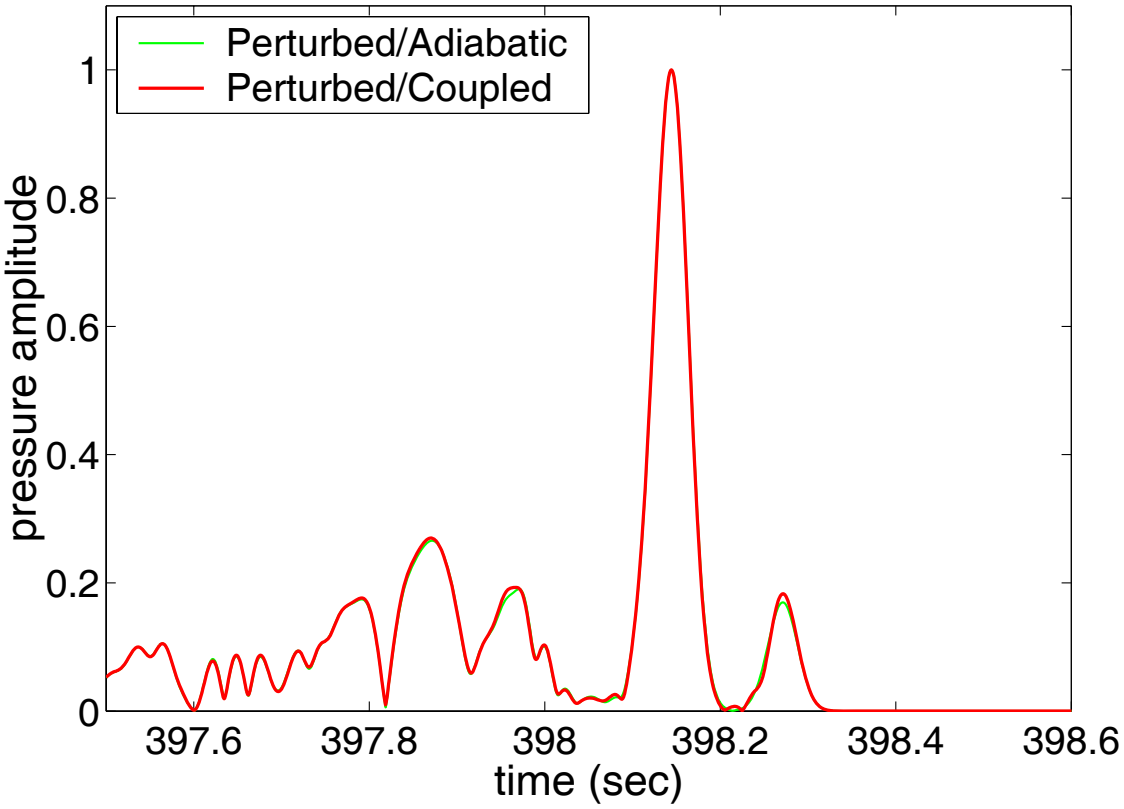

Figure 4.22: Exact calculation of the late part of the arrival pattern (linear non-zero mean), for the range-dependent perturbed state.

in this case.

Fig. 4.23 shows the late arrival pattern predicted from the first and second Born approximations. Since δc_r is non-zero-mean the first Born approximation predicts an arrival pattern different from the background one. The background arrival pattern is also shown on Fig. 4.23 together with the adiabatic prediction (target arrival pattern) for the perturbed state. From this figure we see that the two Born approximations significantly differ from the background arrival pattern in amplitude but hardly as far the arrival times are concerned. In the exact (perturbed) arrival pattern on the other hand the arrivals, especially the late ones, are advanced by more than 100 msec

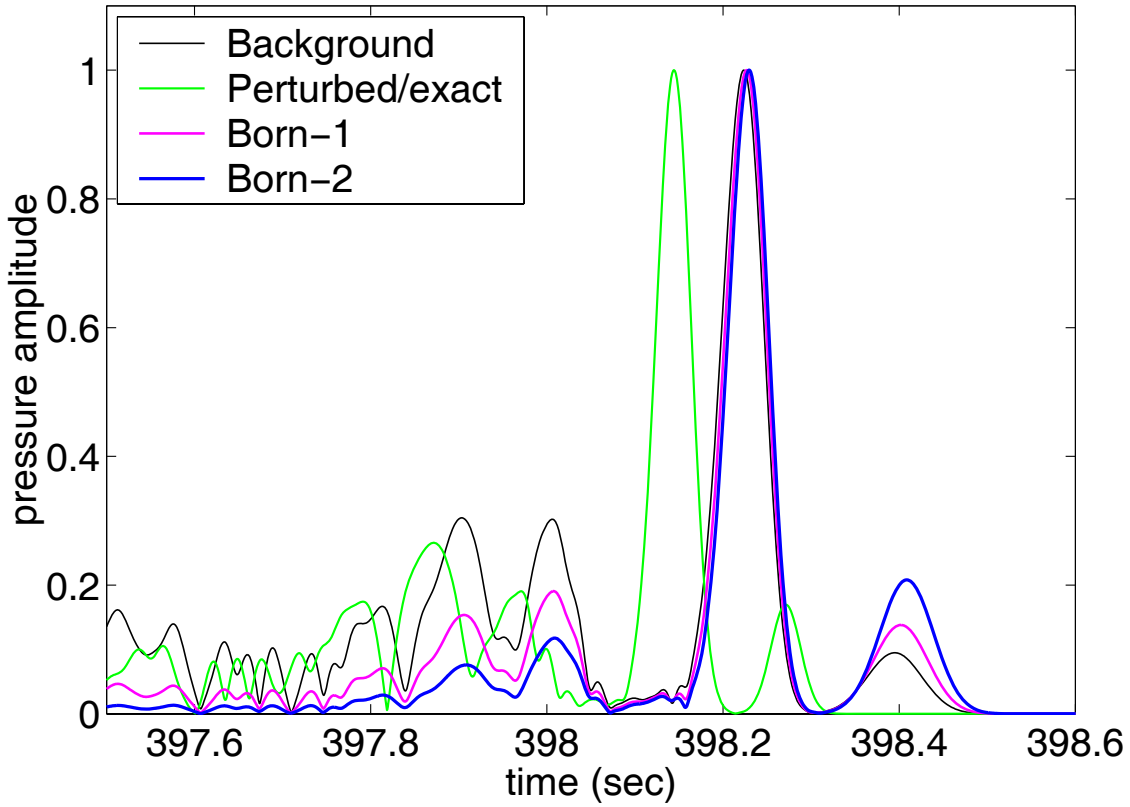

Figure 4.23: Late arrival pattern predicted from the first and second Born approximations, together with the exact adiabatic prediction and the background arrival pattern (linear non-zero mean).

with respect to their background locations. Thus, the Born approximation fails to predict correct arrival times in the perturbed state, whereas there is a remarkable disagreement in the arrival amplitude as well.

Fig. 4.24 shows the arrival pattern predicted from the first and second Rytov approximation. Again due to the non zero average of δc_r the first Rytov approximation differs from the background prediction. The background arrival pattern and the perturbed adiabatic prediction are shown in Fig. 4.24 as in the previous figure. We see that the first Rytov approximation significantly differs from the background arrival

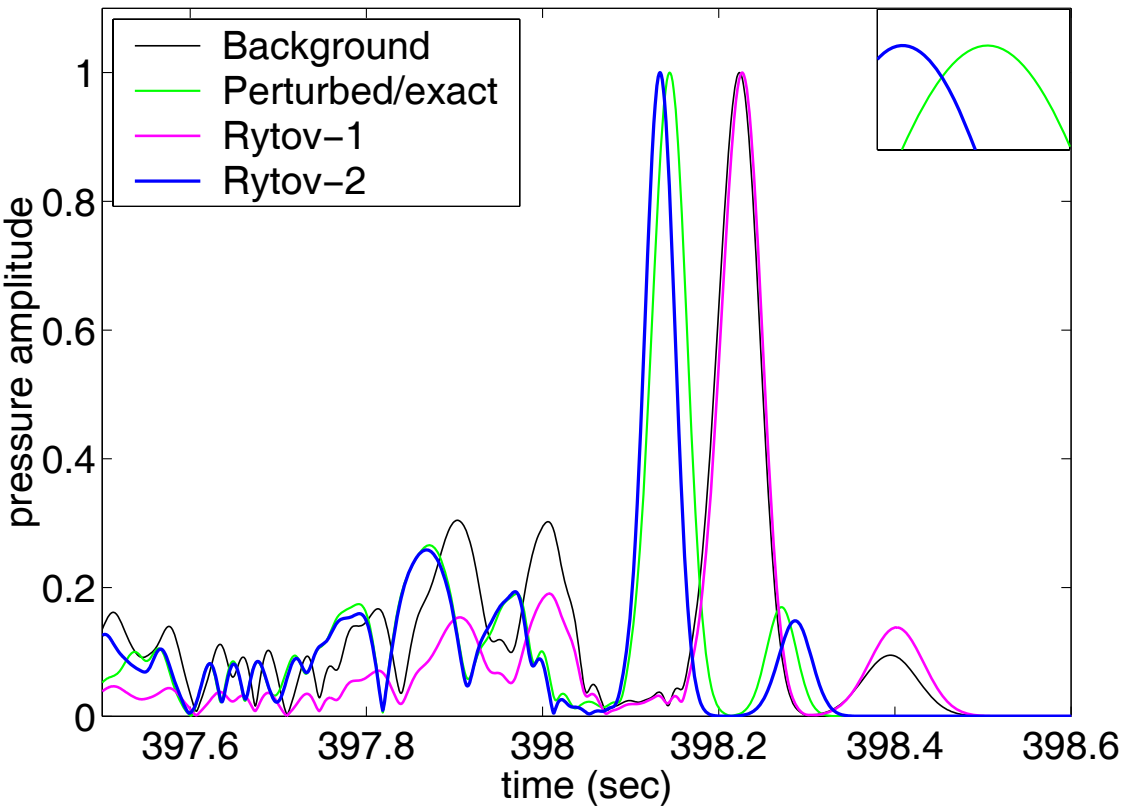

Figure 4.24: Late arrival pattern predicted from the first and second Rytov approximations, together with the exact adiabatic prediction and the background arrival pattern (linear non-zero mean).

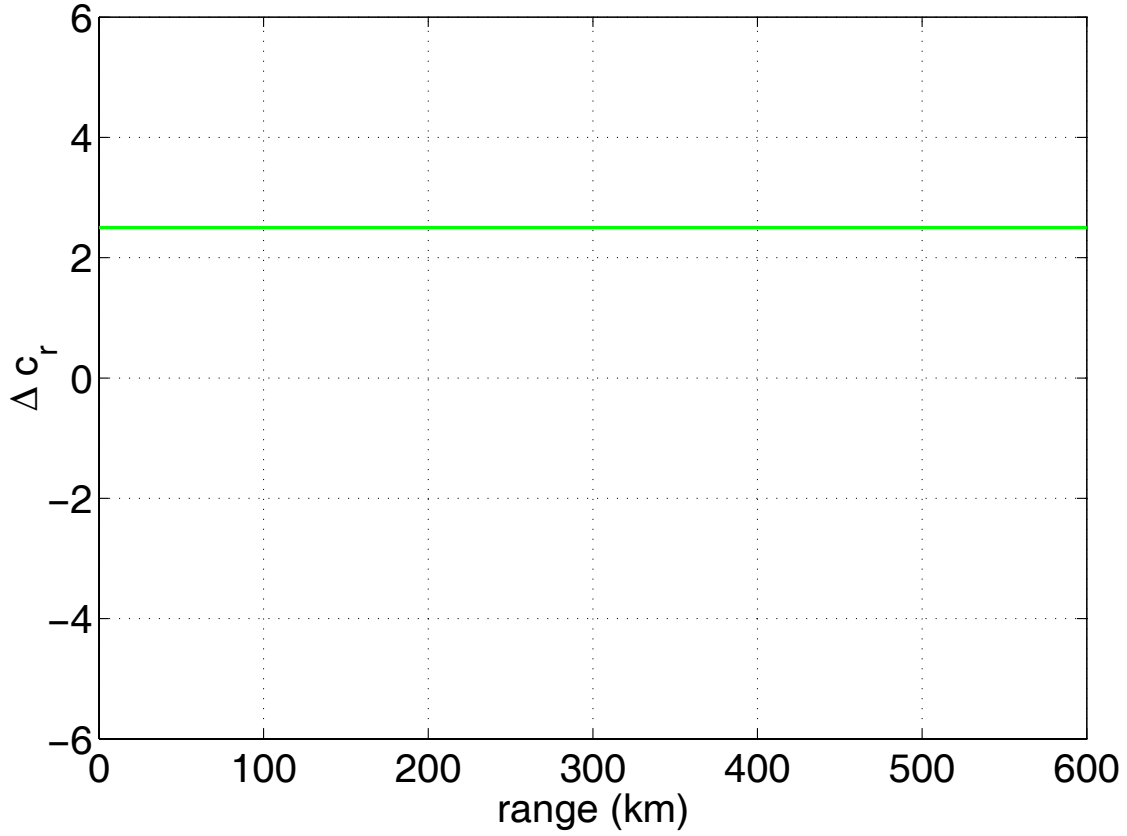

Figure 4.25: Range mode Δc_r of the sound speed perturbation (linear non-zero means RI environment).

pattern and the second Rytov approximation does not describe efficiently the arrival shifts in all cases. In the exact (perturbed) arrival pattern, especially the last arrival, is significantly displaced by as much as 120 msec with respect to its background location, but with the second Rytov the shift is only 100 msec. Thus, the second Rytov approximation fails to predict correct arrival times in the perturbed state.

In Fig. 4.25 present the range mode Δc_r of the sound-speed perturbation, with constant value, at the mean of the range dependence to previous case of the third example. The results we obtain are shown in Fig. 4.26. This figure presents the

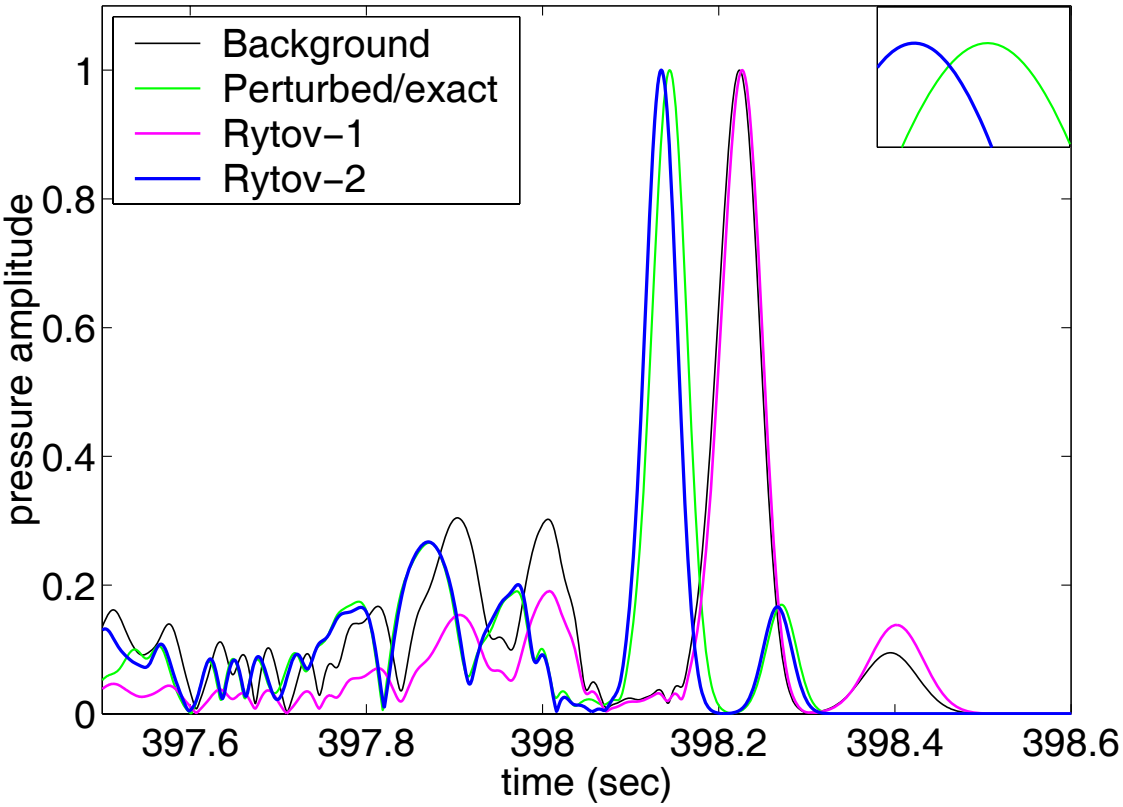

Figure 4.26: Late arrival pattern: Compare linear non-zero means RD environment (Rytov) with linear non-zero means RI environment (Exact).

perturbed exact calculations as in Fig. 4.21, the background arrival pattern, and the first and second Rytov. In this case we tried a range independent perturbation at the mean value of the previous case and the same reference profile. Although it was a range independent example the results were better than the results of the previous case.

Fig. 4.27 shows the range mode Δc_r of the sound-speed perturbation, which is linear from -2.5 at the source to 2.5 at the receiver. Taking into account as reference profile the range independent profile of the previous case and the range dependence of figure 4.27 the perturbed environment is the same as in the first case of the third

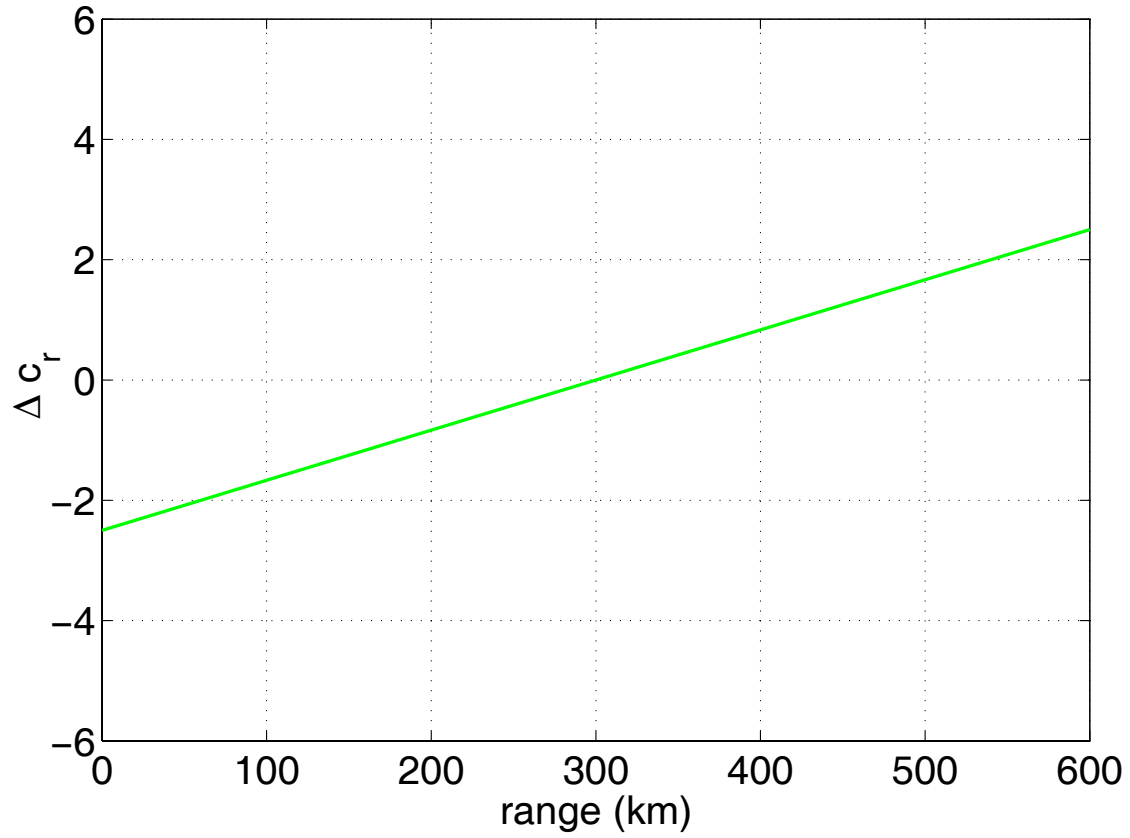

Figure 4.27: Range mode Δc_r of the sound speed perturbation (linear zero means RD environment).

example.

Fig. 4.28 shows, the perturbed exact calculations, the new background arrival pattern which is the perturbed exact in second case of the third example and the second Rytov corresponds to this background. At this case the second Rytov, approaches very well the exact calculations. Conclusively the selection of the reference profile is very important, in order to obtain correct predictions with the second Rytov method.

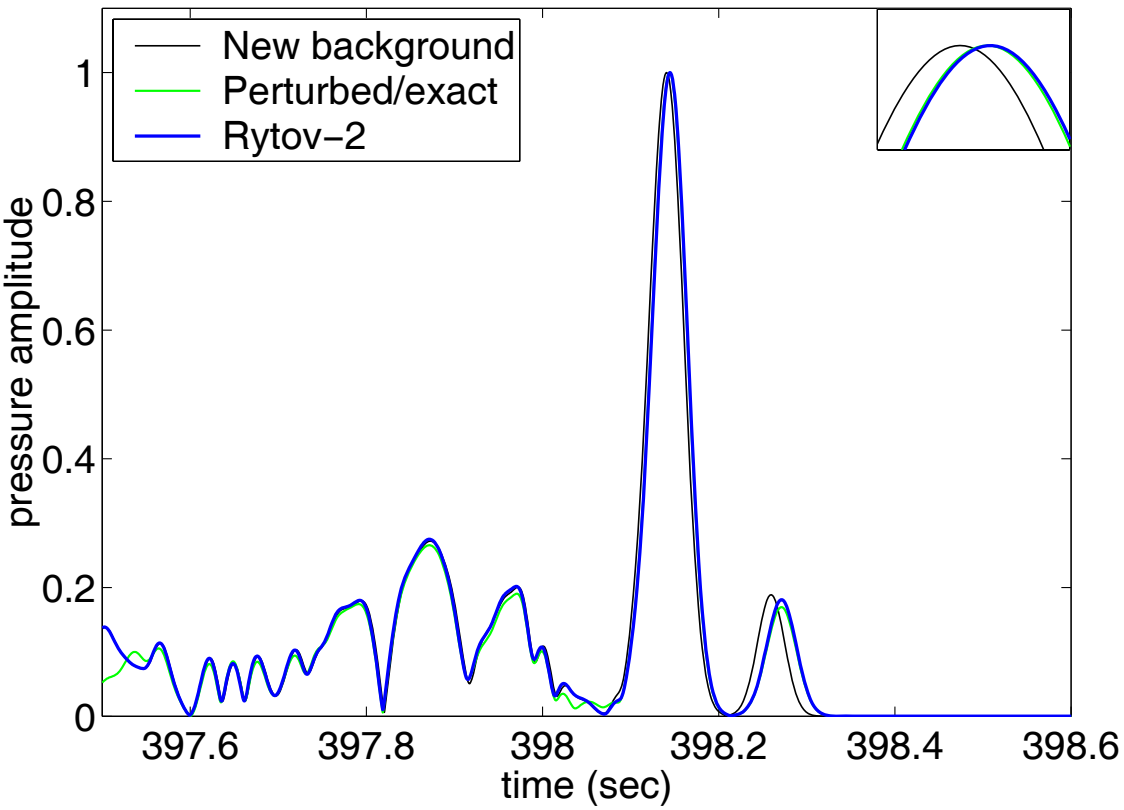

Figure 4.28: Late arrival pattern predicted from the Rytov approximation, together with the exact adiabatic prediction and the new background arrival pattern (linear zero means RD environment).

Conclusions

In this work we examined the possibility of using the Born and Rytov approximation of Green's function perturbations for arrival pattern calculations associated with long-range acoustic propagation modelling in the time domain. Such calculations are particularly important in the context of ocean acoustic travel–time tomography.

The proposed approach is to use first- and second-order Born and Rytov approximations to calculate the perturbations of the frequency-domain Green's function associated with range-dependent sound-speed perturbations about a range-independent background state for a large number of frequencies and then obtain the time-domain acoustic field by applying the inverse Fourier transform. General expressions were obtained for the first- and second-order terms of the Born and Rytov approximation. Further, assuming a range-independent background ocean environment the normal-mode representation of the background Green's function was used to obtain closed-form expressions for the Born and Rytov terms describing the perturbation behavior of the low-order modes. The performance of the various approximations was tested in several cases of range-dependent perturbations of a stratified background environment and long range (600 km) propagation.

The main conclusions from this work are the following:

The Born approximation fails to describe the temporal displacement of arrivals due to the sound-speed perturbations. The reason is that the Born representation is based on a perturbation expansion of the Green's function in the frequency domain

which can hardly be translated in shifts in the time domain (temporal displacements) through the inverse Fourier transform.

The Rytov approximation, on the other hand, is based on a perturbation expansion of the phase in the frequency domain, which is directly associated with shifts in the time domain. In this connection the Rytov approximation is suitable for time domain calculations with emphasis on temporal displacements, as is the case in ocean acoustic travel time tomography.

Since the acoustic field in the ocean is a multi-component wave field, each component (mode) being characterized by a different phase and perturbation behavior the standard Rytov approximation cannot be applied, since it imposes a single phase and phase perturbation to the whole field. To face this problem, a quasi-adiabatic approach preposed by Keller was adopted (Rytov-Keller approximation). According to this approach the Rytov method must be applied to each wave component separately. The Rytov-Keller second-order approximation was shown here to perform very well for the calculation of arrival pattern perturbations in long-range acoustic propagation over hundreds of kilometers in the ocean.

Nevertheless, the "adiabatic" assumption associated with the Rytov-Keller approximation appears to make this approach a good approximation of the exact adiabatic propagation model and thus limits its applications to cases of small/smooth perturbations.

The effect of range dependence on travel times is a second-order effect. In particular, if the range average of the sound-speed perturbation is zero the first-order Rytov approximation fails to predict any travel-time change from the background state. In this case the second-order Rytov approximation (or higher) is required.

Appendices

A. Evanescent modes for homogeneous 2-layer waveguide

In this appendix we study the behavior of propagating, half-space and evanescent modes in a waveguide consisting of two homogeneous layers as the thickness of the lower layer increases. The two layers, denoted by 1 (upper layer) and 2 (lower layer), are characterized by constant density ρ_i and sound velocity c_i and have thickness h_i, $i = 1, 2$. The top boundary of the upper layer is considered a pressure-release surface whereas the bottom boundary of the lower layer is considered a rigid bottom.

Adopting a cylindrical coordinate system (r, z, θ) and assuming that a harmonic point source of circular frequency ω is located on the z-axis at depth z_s the axisymmetric pressure field in the upper layer is given by [2]

$$p(r,z) = \frac{-j}{4\rho_1} \sum_{n=1}^{\infty} N_n^2 \sin(\gamma_{1_n} z_s) \sin(\gamma_{1_n} z) H_0^{(2)}\left(\sqrt{\lambda_n} r\right), \tag{A-1}$$

where

$$\gamma_{i_n} = \sqrt{\frac{\omega^2}{c_i^2} - \lambda_n} \qquad i = 1, 2$$

and λ_n are the eigenvalues of the associated Sturm-Liouville problem. All eigenvalues are real and can be obtained by solving the following characteristic equation [2]

$$\frac{\rho_1}{\rho_2} \frac{\gamma_2}{\gamma_1} \tan(\gamma_1 h_1) \tan(\gamma_2 h_2) = 1. \tag{A-2}$$

The quantity N_n is defined as

$$N_n = \left(\frac{h_1}{2\rho_1} - \frac{\sin\gamma_{1_n} h_1 \cos\gamma_{1_n} h_1}{2\gamma_{1_n}\rho_1} + \frac{1}{2\gamma_{2_n}\rho_2} \sin^2\gamma_{1_n} h_1 \frac{sin\gamma_{2_n} h_2}{\cos\gamma_{2_n} h_2} + \frac{h_2}{2\rho_2} \frac{\sin^2\gamma_{1_n} h_1}{\cos^2\gamma_{2_n} h_2} \right)^{-\frac{1}{2}} \tag{A-3}$$

The use of $H_0^{(2)}$ instead of $H_0^{(1)}$ has to do with the time dependence of the source, assumed here to be of the form $e^{j\omega t}$ cf. eq. (1.5.1). Assuming that $c_1 < c_2$ (we think of the upper layer as water and the lower layer as solid) the eigenvalues are bounded from above by ω^2/c_1^2 whereas there is no lower bound. The eigenvalues in the interval $(\omega^2/c_2^2, \omega^2/c_1^2)$ correspond to modes that propagate in the upper layer. The limit ω^2/c_2^2 corresponds to the critical angle see Fig. 3.2, and the he interval $(0, \omega^2/c_2^2)$ corresponds to modes penetrating the lower layer; as h_2 increases these modes become the half-space modes. Finally the interval $(-\infty, 0)$ corresponds to the evanescent modes with imaginary $\sqrt{\lambda_n}$ values.

In the following we give some results for an environment characterized by a water layer ($\rho_1 = 1$ gr/cm^3, $c_1 = 1500$ m/s, $h_1 = 100$ m) and a bottom layer ($\rho_2 = 1.8$ gr/cm^3, $c_2 = 1800$ m/s,) with different values for its thickness from 0.1 m to 1000 m. The source depth is taken $z_s = 10$ m and the frequency $f = 70$ Hz ($\omega = 2\pi f$).

Fig. A-1 shows the eigenvalues λ_n (measured on the horizontal axis) vs. excitation amplitudes $N_n^2 \sin^2\gamma_{1_n} z_s$ (measured on the vertical axis), assuming $z = z_s$, for different thicknesses of the lower layer, from 0.1 m to 1000 m. The upper bound for the eigenvalues and the value corresponding to the critical angle are also shown an this figure. It is seen from Fig. A-1 that as the thickness h_2 increases the eigenvalues smaller than ω^2/c_2^2 increase in number and get closer to each other and at the limit ($h_2 \to \infty$) they form a continuum. Further, the maximum excitation amplitudes for the propagating $(\omega^2/c_2^2, \omega^2/c_1^2)$, the half-space $(0, \omega^2/c_2^2)$ and the evanescent $(-\infty, 0)$ modes are comparable.

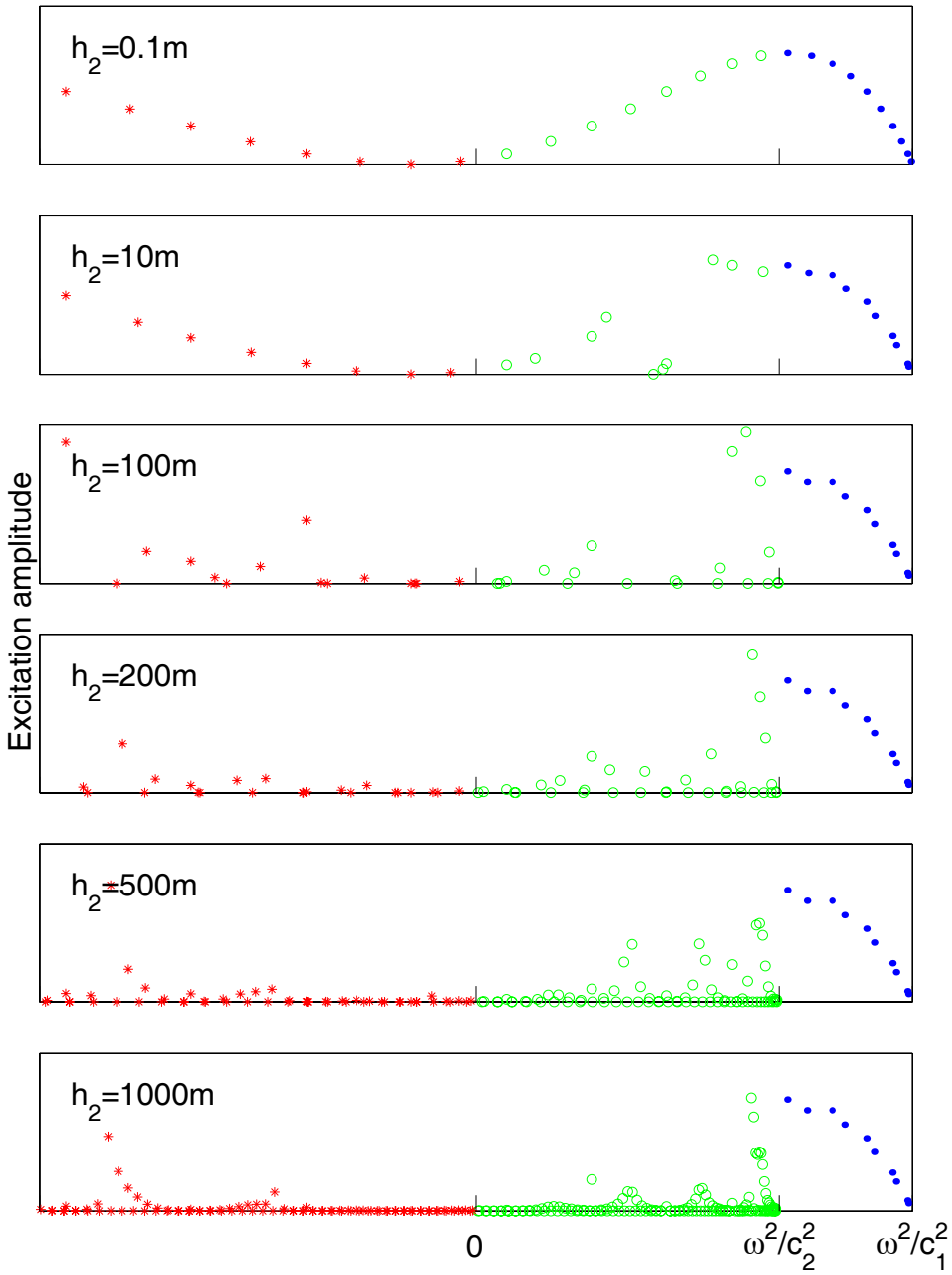

Figure A-1: Eigenvalues and Excitation amplitudes ($z = z_s$) of evanescent (*), half-space (o) and propagating modes (•) modes for different thickness (h_2) of lower layer.

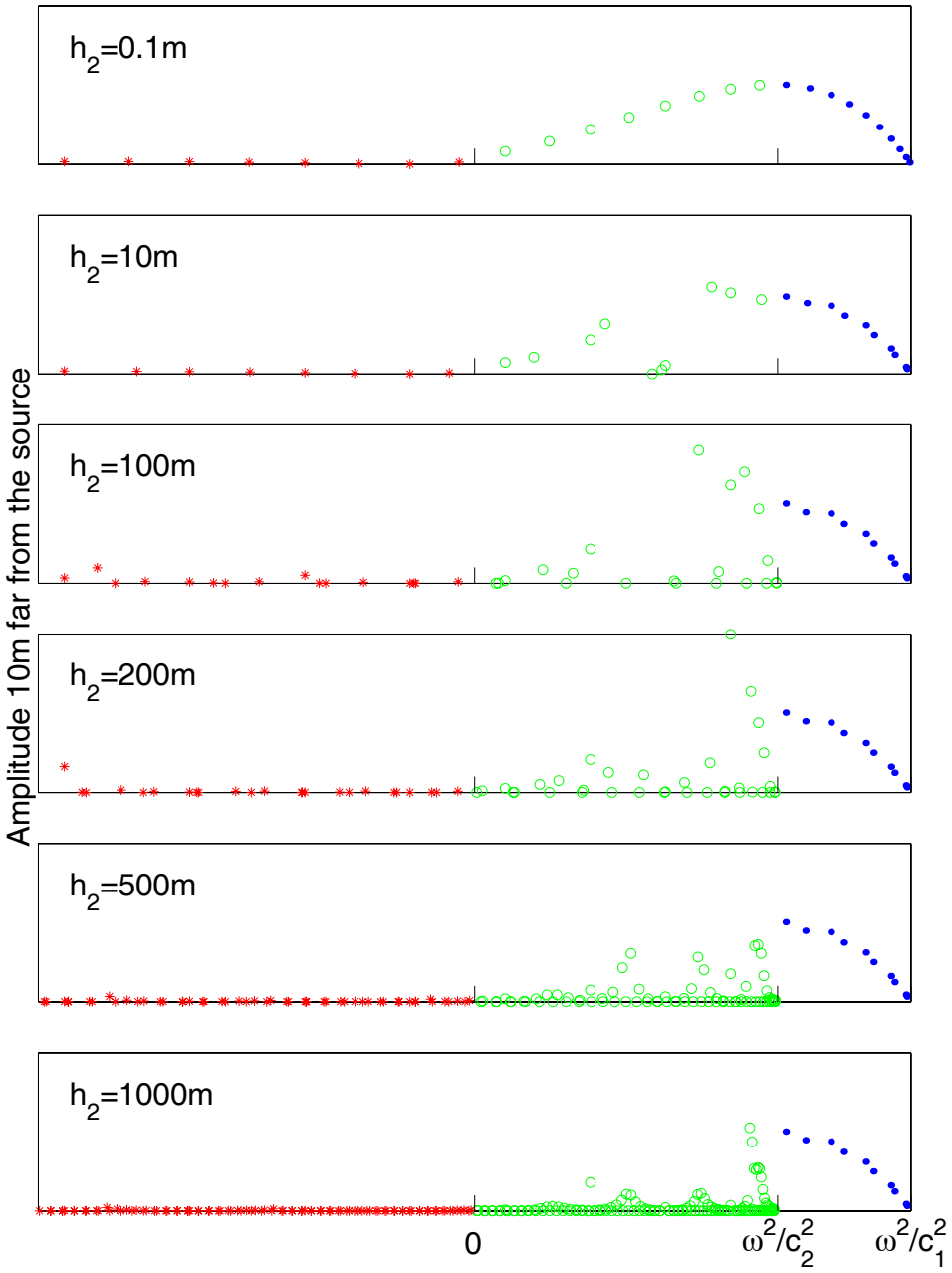

Figure A-2: Eigenvalues and contributions to acoustic field (absolute values) at $r = 10\ m$ and $z = z_s$ of evanescent (*), half-space (o) and propagating modes (•) modes for different thickness (h_2) of lower layer.

The contribution of each mode to the acoustic field 10 m away from the source ($r = 10$ m, $z = z_s$)is shown in Fig. A-2. From this figure we see that the contribution of the evanescent modes is negligible. The distance of 10 m corresponds to about half of the acoustic wavelength in this case. The rapid attenuation of the evanescent modes is due to the exponential decay caused by the imaginary $\sqrt{\lambda_n}$ values in $H_0^{(2)}\left(\sqrt{\lambda_n}r\right)$.

B. Stationary phase method in one and two dimensions

The stationary phase method is an approach for evaluating integrals whose kernel is expressed as a product of a highly oscillating function with a slowly varying function of the integration variable(s) [3].

In one dimension, integrals of the form

$$I(k) = \int_{-\infty}^{\infty} e^{jk\phi(x)} f(x) dx$$

where $f(x)$ is a continuous (slowly varying) function of x, are approximated asymptotically [42] when $k \to \infty$ by

$$I(k) \approx e^{jk\phi(x_s)} f\left(x_s\right) e^{sign(\phi''(x_s))\frac{j\pi}{4}} \left[\frac{2\pi}{k|\phi''\left(x_s\right)|}\right]^{\frac{1}{2}} \tag{B-1}$$

where x_s is the *stationary point* in which the derivative of the phase is zero. The approximation described in equation (B-1) assumes that the second derivative is different from zero at the stationary point.

In the two-dimensional case

$$I = \int\int_{-\infty}^{\infty} f(x,y) e^{-jk\Phi(x,y)} dxdy \tag{B-2}$$

The stationary point (x_s, y_s) is defined as

$$\begin{aligned} \frac{\partial \phi}{\partial x}(x_s, y_s) &= 0, \\ \frac{\partial \phi}{\partial y}(x_s, y_s) &= 0. \end{aligned} \tag{B-3}$$

Expanding $\phi(x, y)$ in a two-dimensional Taylor series about the stationary point, and keeping terms up to the second order we obdain

$$\begin{aligned} \phi(x, y) \approx \phi(x_s, y_s) + \frac{1}{2} \Bigg[& \left. \frac{\partial^2 \phi}{\partial x^2} \right|_{x_s, y_s} (x - x_s)^2 + 2 \left. \frac{\partial^2 \phi}{\partial x \partial y} \right|_{x_s, y_s} (x - x_s)(y - y_s) \\ & + \left. \frac{\partial^2 \phi}{\partial y^2} \right|_{x_s, y_s} (y - y_s)^2 \Bigg] \end{aligned} \tag{B-4}$$

Substituting this into (B-2) gives

$$I \approx f(x_s, y_s)\, e^{-jk\phi(x_s, y_s)} \int \int_{-\infty}^{\infty} e^{-j\frac{k}{2}\left[\left. \frac{\partial^2 \phi}{\partial x^2} \right|_{x_s, y_s} u^2 + 2 \left. \frac{\partial^2 \phi}{\partial x \partial y} \right|_{x_s, y_s} uv + \left. \frac{\partial^2 \phi}{\partial y^2} \right|_{x_s, y_s} v^2 \right]} du dv \tag{B-5}$$

where $u = (x - x_s)$ and $v = (y - y_s)$.

Remark. If the phase has more than one stationary points, then we split the integration domain into subdomains containing only one stationary point, and deal with each one independently.

C. Adiabatic approximation

The axisymmetric acoustic field of a harmonic point source in the adiabatic approximation is given by [8]

$$G'(R, z_r | z_s) = \frac{e^{-j\pi/4}}{\rho_w \sqrt{8\pi R}} \sum_{n=1}^{M} \frac{\phi_n(0, z_s)\phi_n(R, z_r)}{\sqrt{k_n(r)}} e^{-j\int_0^R k_n(r) dr}, \tag{C-1}$$

where z_s is the depth of the source located on the z-axis of the (r, z, θ) cylindrical coordinate system, R and z_r are the receiver range and depth. In the case of a range-dependent environment the quantities ϕ_n and k_n are functions of range as well. The

phase of each modal component is associated with the integral

$$\Psi_n = -j \int_0^R k_n(r) dr. \tag{C-2}$$

Assuming a range-independent background environment, characterized by $c_0(z)$, and an axisymmetric range-dependent sound-speed perturbation of the form $\Delta c_r(r)\Delta c_z(z)$, we can obtain the perturbed phase using a second-order Taylor expansion of k_n with respect to the sound-speed about the background state [28]

$$k_n(r) = k_{n,0} + \frac{Q_{nn}}{2k_{n,0}} \Delta c_r(r) + \frac{1}{2k_{n,0}} \left[Q'_n + \sum_{\substack{m=1 \\ m \neq n}}^{M} \frac{|Q_{nn}|^2}{\Lambda_{nm}} - \frac{|Q_{nn}|^2}{4k_{n,0}^2} \right] \Delta c_r^2(r) \tag{C-3}$$

and substituting this expansion into the above integral we obtain

$$\Psi_n = -jk_{n,0}R - j\frac{Q_{nn}}{2k_{n,0}} \int_0^R \Delta c_r(r) dr - \frac{j}{2k_{n,0}} \left[Q'_n + \sum_{\substack{m=1 \\ m \neq n}}^{M} \frac{|Q_{nn}|^2}{\Lambda_{nm}} - \frac{|Q_{nn}|^2}{4k_{n,0}^2} \right] \int_0^R \Delta c_r^2(r) dr. \tag{C-4}$$

Comparing the right-hand side with the first and second Rytov-Keller approximation eq. (3.4.3), (3.4.5), we note that:

- The first-order adiabatic approximation is equivalent to the dominant part of the first Rytov-Keller approximation.

- In case of zero-mean range dependent perturbations, the second-order adiabatic approximation has the same dominant part as the second Rytov-Keller approximation except for the last term in the bracket in eq. (C-4) which does not appear in the Rytov-Keller approximation – this term is much smaller than the previous term including the sum over m. Thus the Rytov-Keller approximation has strong similarity to the above second order adiabatic approximation, separately is intrinsically of adiabatic nature.

D. Asymptotic approximations of Bessel and Hankel functions

The solutions for the differential equation [18]

$$z^2\frac{d^2w}{dz^2} + z\frac{dw}{dz}\left(z^2 - \nu^2\right)w = 0, \qquad \text{(Abr.–St.–9.1.1)}$$

are the Bessel functions of the first kind $J_{\pm\nu}(z)$ of the second kind $Y_\nu(z)$ (also called Weber's functions) and of the third kind $H_\nu^{(1)}(z)$, $H_\nu^{(2)}(z)$ (also called the Hankel functions, where $z \epsilon \mathbb{C}$.

Relations between solutions

$$H_\nu^{(1)}(z) = J_\nu(z) + jY_\nu(z) \qquad \text{(Abr.–St.–9.1.3)}$$

$$H_\nu^{(2)}(z) = J_\nu(z) - jY_\nu(z) \qquad \text{(Abr.–St.–9.1.4)}$$

$$\begin{aligned} J_{-\nu}(z) &= (-1)^\nu J_\nu(z) \\ Y_{-\nu}(z) &= (-1)^\nu Y_\nu(z) \end{aligned} \qquad \text{(Abr.–St.–9.1.5)}$$

$$\begin{aligned} H_{-\nu}^{(1)}(z) &= e^{\nu\pi j}H_\nu^{(1)}(z) \\ H_{-\nu}^{(2)}(z) &= e^{-\nu\pi j}H_\nu^{(2)}(z) \end{aligned} \qquad \text{(Abr.–St.–9.1.6)}$$

When ν is fixed and $z \to 0$

$$J_\nu(z) = \frac{\left(-\frac{1}{2}z\right)^\nu}{\Gamma(\nu+1)} \quad (\nu \neq -1, -2, -3, ...) \qquad \text{(Abr.–St.–9.1.7)}$$

$$Y_0(z) = \frac{2}{\pi}\ln z \qquad \text{(Abr.–St.–9.1.8)}$$

$$Y_\nu(z) = -\frac{1}{\pi}\Gamma(\nu)\left(\frac{1}{2}z\right)^{-\nu}, \quad (\nu > 0). \qquad \text{(Abr.–St.–9.1.9)}$$

Asymptotic expansions for large arguments, when ν is fixed and $|z| \to \infty$

$$J_\nu(z) \approx \sqrt{\frac{2}{\pi z}}\cos\left(z - \frac{1}{2}\nu\pi - \frac{1}{4}\pi\right) \qquad \text{(Abr.–St.–9.2.1)}$$

$$Y_\nu(z) \approx \sqrt{\frac{2}{\pi z}}\sin\left(z - \frac{1}{2}\nu\pi - \frac{1}{4}\pi\right) \qquad \text{(Abr.–St.–9.2.2)}$$

Bibliography

[1] B.E. McDonald, M.D. Collins, W.A. Kuperman, and K.D. Heaney, *Comparison of data and model predictions for Heard island acoustic transmisions*, J. Acoust. Soc. Am. **96** (1994), 2357–2370.

[2] C.A. Boyles, *Acoustic waveguides. Applications to oceanic science*, J. Wiley & Sons, New York, 1984.

[3] C.M. Bender and S.A. Orszag, *Advanced mathematical methods for scientists and engineers*, Mc-Graw Hill, New York, 1978.

[4] J.A. DeSanto, *Scalar Wave Theory*, Spinger–Verlag, New York, 1992.

[5] D.Y. Mikhin, O.A. Godin, S.V. Burenkov, Yu.A. Chepurin, V.V. Goncharov, V.M. Kurtepov, and V.G. Selivanov, *An experiment on acoustic tomography of the western Mediterranean from a moving ship*, Proc. 3rd European Conf. Underwater Acoust. (Herakion) (J.S. Papadakis, ed.), Crete Univ. Press, 1996, pp. 821–826.

[6] E.C. Lo, J.X. Zhou, and E.C. Shang, *Normal mode filtering in shallow water*, J. Acoust. Soc. Am. **74** (1983), 1833–1836.

[7] E.K. Skarsoulis and G.A. Athanassoulis, *Arrival-time perturbations of broadband tomographic signals due to sound-speed disturbances. a wave theoretic approach*, J. Acoust. Soc. Am. **97** (1995), 3575–3588.

[8] F.B. Jensen, W.A. Kuperman, M.B. Porter, and H. Schmidt, *Computational ocean acoustics*, AIP Press, New York, 1994.

[9] G.V. Frisk, *Ocean and seabed acoustics: A theory of wave propagation*, Prentice Hall, 1994.

[10] H.T.Yura, C.C. Sung, S.F. Clifford, and R.J. Hill, *Second–Order Rytov approximation*, J. Optical Society of America **73, No.4** (1983), 500–502.

[11] J.-P. Hermand, *Model-based matched filter processing: A broad-band approach to shallow-water inversion*, Full field inversion methods in ocean and seismo-acoustics (O. Diachok, A. Caiti, P. Gerstoft, and H. Schmidt, eds.), Kluwer, Dordrecht, 1995, pp. 189–194.

[12] J.-P. Hermand and W.I. Roderick, *Acoustic model-based matched-filter processing for fading time-dispersive ocean channels: Theory and experiment*, IEEE J. Oceanic Eng. **OE-18** (1993), 447–465.

[13] J.A. Colosi, S.M. Flatte, and S. Bracher, *Internal-wave effects on 1000-km oceanic acoustic pulse propagation: Simulation and comparison with experiment*, J. Acoust. Soc. Am. **96** (1994), 452–468.

[14] J.A. Mercer and J.R. Booker, *Long-range propagation of sound through oceanic mesoscale structures*, J. Geophys. Res. **88** (1983), 689–699.

[15] K.D. Heaney and W.A. Kuperman, *Frequency interpolation technique for broad-band parabolic equation calculation*, J. Comp. Acoust. **7** (1999), 27–38.

[16] J.B. Keller, *Accuracy and validity of the Born and Rytov approximations*, J. Optical Society of America A **59** (1969), 1003–1004.

[17] K.J. McCann and F. Lee–McCann, *A narrow-band approximation to the acoustic pressure field*, J. Acoust. Soc. Am. **89** (1991), 2670–2676.

[18] M. Abramowitz and I.A. Stegun, *Handbook of mathematical functions with formulas, graphs, and mathematical tables*, Dover Publications, New York, 1965.

[19] M. Born and E. Wolf, *Principles of Optics – Electromagnetic Theory of Propagation, Interference, and Diffraction of Light*, p. 453, Pergamon Press, Oxford, 1980.

[20] M.I. Sancer and A.D. Varvatsis, *A comparison of the Born and Rytov methods*, Proc. IEEE (1970), 140–141.

[21] N.C. Geckinli and D. Yavuz, *Discrete Fourier transform and its applications to power spectra estimation*, Elsevier, Amsterdam, 1983.

[22] M.L. Oristaglio, *Accuracy of the born and Rytov approximations for reflection and refraction at a plane interface*, J. Optical Society of America A **2, No.11** (1985), 2789–2798.

[23] P.J. Sutton, W.M.L. Morawitz, B.D. Cornuelle, G. Masters, and P.F. Worcester, *Incorporation of acoustic normal mode data into tomographic inversions in the Greenland Sea*, J. Geophys. Res. **99** (1994), 12487–12502.

[24] P.M. Morse and H. Feshbach, *Methods of theoretical physics*, McGraw Hill, New York, 1953.

[25] R.N. Bracewell, *The Fourier transform and its applications*, McGraw-Hill, Singapore, 1986.

[26] E.K. Skarsoulis, *Second-order fourier synthesis of broadand acoustic signals using normal modes*, J. Comp. Acoust. **5** (1997), 355–370.

[27] E.K. Skarsoulis, *Fast coupled-mode approximation for broadband pulse propagation in a range-dependent ocean*, IEEE J. Oceanic Eng. **24** (1999), 172–182.

[28] E.K. Skarsoulis, *Waveform perurbation of tomographic receptions due to sound–speed variations*, Acta Acustica **89** (2003), 789–798.

[29] S.M. Flatte and R. Stoughton, *Predictions of internal–wave effect on the ocean acoustic coherence, travel–time variance, and intensity moments for very long–range propagation*, J. Acoust. Soc. Am. **84** (1988), 1414–1424.

[30] S.M. Rytov, Yu.A. Kravtsov, and V.I.Tatarskii, *Principles of statistical radiophysics 4*, Springer – Verlag, Berlin Heeidelberg, 1989.

[31] A. Sommerfeld, *Partial differential equations in physics*, Academic Press, New York, 1949.

[32] J.L. Spiesberger, *Ocean acoustic tomography: Travel time biases*, J. Acoust. Soc. Am. **77** (1985), 83–100.

[33] T.F. Duda, S.M. Flatte, J.A. Colosi, B.D. Cornuelle, J.A. Hildebrand, W.S. Hodgkiss, P.F. Worcester, B.M. Howe, J.A. Mercer, and R.C. Spindel, *Measured wave-front fluctuations in 1000-km pulse propagation in the Pacific Ocean*, J. Acoust. Soc. Am. **92** (1992), 939–955.

[34] U. Send, G. Krahmann, S. Mauuary, Y. Desaubies, F. Gaillard, T. Terre, J. Papadakis, M. Taroudakis, E. Skarsoulis, and C. Millot, *Acoustic observation of heat content across the Mediterranean Sea*, Nature **385** (1997), 615–617.

[35] G.N. Watson, *A treatise on the theory of Bessel functions*, Cambridge University Press, England, 1966.

[36] W.B. Beydoun and A. Tarantola, *First Born and Rytov approximations: Modeling and inversion conditions in a canonical example*, J. Acoust. Soc. Am. **83(3)** (1988), 1045–1055.

[37] W.H. Munk and C. Wunsch, *Ocean acoustic tomography: A scheme for large scale monitoring*, Deep-Sea Res. **26A** (1979), 123–161.

[38] W.H. Munk and C. Wunsch, *Ocean acoustic tomography: Rays and modes*, Rev. Geophys. Space Phys. **21** (1983), 777–793.

[39] W.H. Munk and C. Wunsch, *Biases and caustics in long-range acoustic tomography*, Deep-Sea Res. **32** (1985), 1317–1346.

[40] W.H. Munk and C. Wunsch, *Bias in acoustic travel time through an ocean with adiabatic range dependence*, Geophys. Astrophys. Fluid Dyn. **39** (1987), 1–24.

[41] W.H. Munk, P.F. Worcester, and C. Wunsch, *Ocean acoustic tomography*, Cambridge U.P., New York, 1995.

[42] E. Zauderer, *Partial differential equations of applied mathematics, 2nd edition*, Wiley-Interscience, 1989.